Sapienza
Università di Roma

Department of Structural
and Geotechnical Engineering

Ph.D. Thesis in Structural Engineering
(XXXI)

Ph.D. Candidate:
Giorgia Di Gangi

Structural Analysis and Design of Timber Light-Frame shear walls

Ph.D. Coordinator:
Prof. Franco Bontempi

Tutor:
Prof. Giorgio Monti

Rome, February 2019

Acknowledgments

First and foremost I want to thank people who shared with me tough and exciting times, starting from my family: my very patient boyfriend, my beloved father, mother and brother, who have never stopped encouraging and stimulating me, following my path also during my stay abroad in China.

I am grateful to Prof. Giorgio Monti, who believed in me and shared his enthusiasm and time, giving me the illuminating suggestions that guided the development of the work presented in this thesis.

Furthermore I am grateful to Cristoforo Demartino, who first trasmitted me the passion for programming, and to Giuseppe Quaranta for his precious advices along with patient and constant support to improve my skills and work.

My sincere thanks also go to everybody who supported me during the experimental tests: Prof. Yan Xiao in China, at the laboratory of Nanjing Tech University, and Marco Vailati along with Silvano Silvani in Italy at the laboratory of Sapienza located in Valle Giulia.

My time during my Ph.D. was made enjoyable also thank to many friends and colleagues I spent time with.

Finally, I would like to thank Prof. Natalino Gattesco and Dr. Ingrid Boem (University of Trieste, Italy) for having shared the data of the experimental tests reported in (Gattesco and Boem, 2016).

Contents

Nomenclature

$\tilde{\mu}_f$ Ductility of the bilinearized F-d curve of fastener

$\tilde{\mu}_i$ Bilinearized ductility of the wall weakest connection

$\tilde{\mu}_{SH}$ Bilinearized ductility of the sheathing-to-framing connections

$\tilde{\mu}_v$ Bilinearized ductility of the wall

$(\mathrm{EI}_y)_{eff}$ Effective bending stiffness

α Aspect ratio of the wall panel

α_f Parameter that identifies the resistance decrement of the considered fastener

α_{YS} Opening area ratio according to Yasumura and Sugiyama (1984)

β Ratio of the characteristic embedment strength of members in the assemblage

β_{YS} Wall length ratio according to Yasumura and Sugiyama (1984)

Δ_A Horizontal displacement provided by the rigid-body translation contribution

Δ_d Target displacement amplitude

Δ_H Horizontal displacement provided by the rigid-body rotation contribution

$\Delta_{i,pl}(u_{i,pl})$ Plastic displacement of the wall weakest connection

$\Delta_{i,u}(u_{i,u})$ Ultimate displacement of the wall weakest connection

$\Delta_{i,y}(u_{i,y})$ Yield displacement of the wall weakest connection

Δ_P Horizontal displacement provided by the shear deformation of sheathing panel

Δ_{SH} Horizontal displacement provided by the sheathing-to-framing connections contribution

$\Delta_{v,u}$ Ultimate displacement of the wall

$\Delta_{v,y}$	Yield displacement of the wall
η	Damping factor
γ	Coefficient that represents the energy dissipation distribution along the perimeter horizontal joists
γ_i	Connection efficiency factor
γ_M	Partial safety factor
$\gamma_{R,d}$	Over-strength ratio
γ_s	Shear angle
κ	Coefficient that represents the energy dissipation distribution along the perimeter vertical studs
$\lambda(\alpha)$	Shape parameter depending on the aspect ratio of the wall panel
μ	Ductility ratio of the structure
μ_f	Ductility of a single fastener (nail)
μ_i	Ductility of the wall weakest connection
μ_{SH}	Ductility of the sheathing-to-framing connections
ω	Frequency of the load
ω_n	Natural vibration frequency of the system
ρ_k	Characteristic density of timber or LVL
ρ_m	Mean density of timber or timber-based product
$\tau \cdot l$	Internal lever arm of the wall panel
$\xi_{eq,hyst}$	Equivalent viscous damping correspondent the hysteretic behavior of the structural system
ξ_{eq}	Equivalent viscous damping (hysteretic damping)
ξ_f	Equivalent viscous damping of a single fastener
ξ_{in}	Inherent viscous damping equal to 5%
ξ_{tot}	Total equivalent viscous damping
$\tilde{E}_{Df}$	Dissipated energy under the bilinearized F-d curve of fastener
$\tilde{F}_{f,Rd}$	Yield strength of the bilinearized F-d curve of fastener
$\tilde{F}_{i,Rd}$	Bilinearized strength of the wall weakest connection

$\tilde{F}_{v,Rd}$	Yield strength of the bilinearized F-d curve of the wall
$\tilde{u}_{i,pl}$	Bilinearized plastic displacement of the wall weakest connection
$\tilde{u}_{i,Rd}$	Bilinearized yield displacement of the wall weakest connection
$\tilde{u}_{v,pl}$	Bilinearized plastic displacement of the wall
$\tilde{u}_{v,Rd}$	Yield displacement of the bilinearized F-d curve of the wall
A_0	Asymptotic strength of fastener
A_1	Slip at one half the asymptotic strength of fastener
A_{hyst}	Dissipated energy enclosed in one hysteresis loop
A_i	Cross-section area of the i-th element
$a_i(z_i)$	Distance between the global Y-axis of the whole cross-section and the i-th local y-axis
b_i	Panel width
c	Damping coefficient
c_i	Parameter that takes into account the aspect ratio of the wall panel
d	Diameter of fastener (nail)
D_p	Flexibility of the wall
$E_{b,mean}$	Mean value of the modulus of elasticity parallel to the grain for the sheathing panel
E_{Dd}	Energy dissipated in one elliptical cycle from the equivalent viscous damper
E_{Df}	Maximum energy that can be dissipated by a single fastener
E_D	Energy dissipated in one hysteresis cycle by the structural system
E_i	Mean value of the modulus of elasticity of the i-th element
E_{s0f}	Elastic energy of a single fastener
E_{s0}	Available potential energy to failure of the structural system
$E_{t,mean}$	Mean value of the modulus of elasticity parallel to the grain for timber framing elements
F	Applied horizontal force to the wall panel

$F_{ax,Rk}$ Characteristic withdrawal capacity of fastener

F_d Damping force

$F_{f,Rd}$ Yield strength of fastener

$f_{f,Rd}$ Shear force per unit length of fasteners

$F_{f,Rk}$ Characteristic load-carrying capacity per fastener

$F_{f,ud}$ Ultimate force of fastener

$f_{h,0,k}$ Characteristic embedment strength parallel to the grain of fastener

$f_{h,90,k}$ Characteristic embedment strength perpendicular to the grain of fastener

$f_{h,i,k}$ Characteristic embedment strength of the connected member

f_h Number of perimeter horizontal fasteners (nails)

f_u Characteristic tensile strength of fastener

$F_{v,Rd}$ Racking load-carrying capacity of the wall

$F_{v,ud}$ Ultimate global force of the wall

f_v Number of perimeter vertical fasteners (nails)

$G_{b,mean}$ Mean value of the sheathing panel shear modulus

G_p Shear modulus of the sheathing panel in Casagrande et al. (2016)

h Height of the wall panel

i_a Constant spacing of the angle-brackets

I_i Second moment of area of the i-th element

K_0 Initial stiffness of the SAWS mechanical model

K_1 Post-yield stiffness of the SAWS mechanical model

K_2 Slope for deformations greater than δ_{peak}

k_a Angle-bracket stiffness

k_c Fastener stiffness in Casagrande et al. (2016)

K_{eff} Effective stiffness of the equivalent SDOF system

K_{fi} Stiffness of the i-th fastener per joining plane

k_f^{sec} Secant stiffness at peak strength of fastener

K_H^{sec}	Global secant stiffness of the wall associated to the hold-downs contribution
k_h^{sec}	Secant stiffness at peak strength of hold-down
K_i	Stiffness of the wall weakest connection
K_i^{sec}	Secant stiffness of the wall weakest connection
k_{mod}	Modification factor linked to the load duration and timber moisture content
K_{ser}	Slip modulus for SLS
K_{SH}^{sec}	Global secant stiffness of the wall linked to the sheathing-to-framing connections contribution
K_u	Slip modulus for ULS
K_v^{sec}	Secant stiffness of the wall
l	Width of the wall
L_{eff}	Effective length of the shear wall
m_e	Effective mass of the equivalent SDOF system
$M_{y,Rk}$	Characteristic yield moment of fastener
n_a	Number of angle-brackets
n_{bs}	Number of wall braced sides (1 or 2)
N_d	Tension force on a fastener due to the withdrawal effect during loading
n_h	Number of hold-downs for each corner of the wall
n_s	Number of vertical studs
P_0	Load-intercept of the post-yield stiffness asymptote of the SAWS mechanical model
q	Vertical load on the wall panel
q_μ	Behaviour factor
q_s	Behaviour factor to take into account the over-strength of a structure
r	Opening coefficient according to Yasumura and Sugiyama (1984)
r_a	Angle-bracket strength
$R_{b,d}$	Design strength capacity of the timber member

$R_{c,d}$	Design strength capacity of the connection member
r_f	Fastener (nail) strength in Casagrande et al. (2016)
r_h	Hold-down strength
R_i	Strength of the wall weakest connection
R_W	Strength of the wall in Casagrande et al. (2016)
s_c	Constant nails spacing
s_{is}	Nails spacing on the intermediate vertical studs
s_{ps}	Nails spacing on the perimeter vertical studs
s_r	Nails spacing on the horizontal joists
T	Natural vibration period of the structure
t	Time
T_C	Natural vibration period at the end of the constant acceleration plateau of the elastic and design spectra of the structure
T_e	Effective period of the equivalent SDOF system
t_p	Thickness of the sheathing panel
U_1	Strain energy due to the deformation of fasteners
U_2	Potential energy due to the horizontal load
$u_{f,Rd}$	Yield displacement of fastener
$u_{f,ud}$	Ultimate displacement of fastener
$u_{v,Rd}$	Yield displacement of the wall
$u_{v,ud}$	Ultimate displacement of the wall
V_B	Base shear force

1 | Introduction

1.1 Modern approach for building design

The modern approach in buildings design takes into account different aspects, that could be summarized in the watchword integrated design. As it is reported in the "Whole Building Design Guide" [1], the role that buildings currently plays makes them really complex. The main function is to host communities and their activities in order to ensure "energy efficiency, durability, life-cycle performance, and occupant productivity" as reported in the Energy Policy Act of 2005 (Public Law 109-058) [2]. Moreover, this guide says that the whole-building design has to be adopted to *"... achieve energy, economic, and environmental performance that is substantially better that standard practice."* Thus, the framework through which the designers are moving encompasses both energy and structural aspects, looking for solutions targeting the so-called *green buildings* and taking also care of the safety against accidental events such as earthquakes. The above aspects need to fulfill also aesthetic requirements, respect of the site where buildings are placed and potential features as requested by clients or communities. As regards the structural standpoint, current codes tend to provide rules to consider the construction as combination of structural elements, non-structural elements and equipments. These last ones play, in fact, an important role, especially in hospitals and buildings whose operativity must be ensured even after seismic events. It is also noteworthy the interaction among non-structural components, equipments and bearing elements, in a design that pursues the people's life safety: building has not to collapse, but also the secondary elements have to remain as much as possible in place, to avoid loss of human lives due to local failures as well as to ensure post-event serviceability if needed. For this purpose, it is thus important to conceive buildings from a *holistic* point-of-view. The term *holism* was coined by Jan Christian Smuts, former South African Prime Minister and philosopher: he believed that a system can be observed and understood considering the synergy among its parts and observing their different behaviors. Integrated design approach and integrated team process are, in fact, the two main components of the Whole Building Design approach. Regarding the first point, some targets have to be balanced, such as accessibility, aesthetics, historic preservation, sustainability, flexibility. As for the latter, an interactive approach during the design process is required, involving all the stakeholders and considering all phases of the project. Only implementing this approach it is possible to achieve a high-performance building.

1.2 The concept of green building

The need to design sustainable buildings (also called green buildings) and save as much energy as possible arises from some circumstances that have changed the way to conceive the constructions. Climate change is obviously the main driver to the concepts of sustainability and sustainable construction [3]. These common purposes now involve the international community, counting almost 60 national green building councils, that establish performance goals for their Countries. In the USA, it is emerging a concept of net zero energy (NZE), supporting a wider program called Architecture 2030 Challenge. According to it, buildings have to generate as much energy as possible from renewable sources, reducing the greenhouse gas (GHG) emission, during the construction process or their major renovations (climate neutral operations). Also in Europe, with the European Directive 2010/31/CE [4], the trend is to achieve the so-called nearly Zero-Energy Buildings (nZEBs) within the 2020. The EU target relates to the reduction of CO_2 emissions, to achieve energy efficiency and exploitation of renewable energies. Starting from these needs, a major study about principles that define this kind of buildings, has been conducted by Ecofys for the Buildings Performance Institute Europe (BPIE) [5]. The effects of these intervention strategies consist in an increased demand of resource-efficient buildings, that, in turn, promote the use of renewable energies. In fact, the rapid depletion of natural sources of energy, dependence on fossil fuels and emission of gases, such as human-generated carbon dioxide, methane and others, will deeply affect temperatures and weather patterns in the near future. Thus, the modern Whole Building Design approach has to take into account these aspects, through the implementation of the most advanced technologies and strategies currently available. For example, the so-called system thinking (like the advanced day lighting strategy), reduces the use of fixtures, thereby decreasing daytime peak cooling loads and the use of mechanical cooling system. Buildings can be designed for sustainability also from the point-of-view of the materials selection: an efficient design approach envisages use, reuse and recycling process of materials rather than their disposing, also if most of construction materials are not completely recyclable but rather downcyclable. Furthermore, in order to exploit natural sources, the reduction of potable water use is leading to the reuse of rainwater and graywater, employing them in the air-conditioning system's cooling towers or for flushing toilets. The reclaimed water is also used for irrigation and into reconstructed wetland systems. Starting from these above considerations, it is clear that the surrounding environment needs new and deep attentions. Mainly for this reason, the concept of green building is currently largely widespread. However, it is important to highlight that, to reach the high-performance building requirements, the structural behavior with respect to the static and dynamic actions cannot be neglected. The full integration among energy-acoustic efficiency and structural safety could lead to innovative and interesting solutions, from architectural and structural standpoints. Structural and non-structural elements have to be implemented within the constructions to achieve the following targets:

- insulation and consequent less energy dispersion, providing an internal thermo-hygrometric comfort;
- equipment integration;
- high structural performances in case of seismic events.

1.2.1 Wood and bamboo as environmentally-friendly materials

Timber light-framed constructions are mostly used in North America, New Zealand and Northern Europe. Especially in North America, most housing and commercial structures used wood as the major structural material till the 20th century. These constructions are very attractive for several reasons, including aesthetic pleasure, sustainability and a speedy assembly of the elements. Moreover, they present a fairly good earthquake resistance, due to the high strength-to-density ratio of timber and to the good ductility of joints with metal fasteners, providing limited inertia forces and good energy dissipation, respectively.

Various stud walls systems have been developed over time offering good structural, hygrothermal and acoustical performance, although being economical and simple to build. Frenette et al. [6] developed a multi-criteria framework for the evaluation of the light frame timber wall assemblies (Fig. 1.1). In particular they defined three main performances attributes, namely: *i)* structural integrity, *ii)* durability and *iii)* control of the interior environment. These design goals should be reached by simultaneously reducing overall costs and limiting environmental impact [7].

Figure 1.1. Design goals defined by Frenette et al. [6] for timber light-frame wall assemblies.

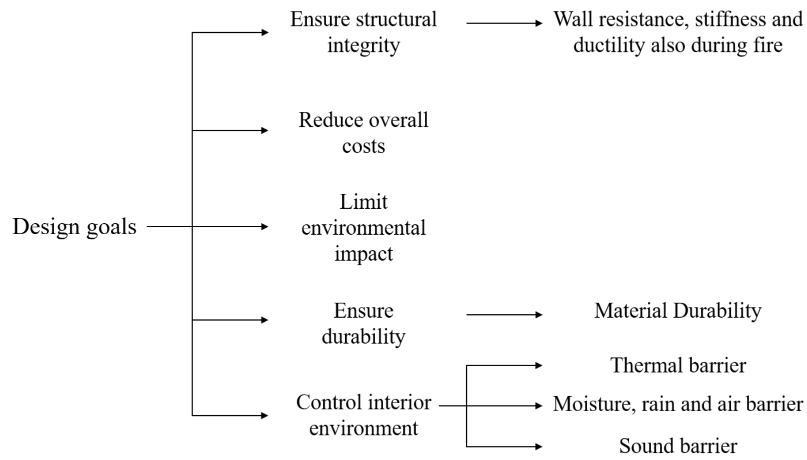

The widespread use of wood is ascribed also to its sustainability in terms of reduced embodied energy needed for the acquisition of raw material, its production, processing, manufacturing, transportation and use in construction site, reduced CO_2 emissions and regeneration of the materials in cycles of 25-50 years. A Canadian Wood Council report [8] shows the comparison in terms of effects on the environment using wood, steel and concrete (Fig. 1.2), highlighting also that wood is a natural insulator, seen its cellular structure that traps air resulting in low conductivity. Moreover, wood can be recycled or reused and is biodegradable, thus fully respecting the concept of *cradle to cradle*: materials has to be designed to return safely to the soil or to flow back to industry to be used again. The series of standard ISO 14000 set out the approach known as Life-cycle assessment (LCA), which is *"the recognized international approach to assess the environmental merits of products or processes"*.

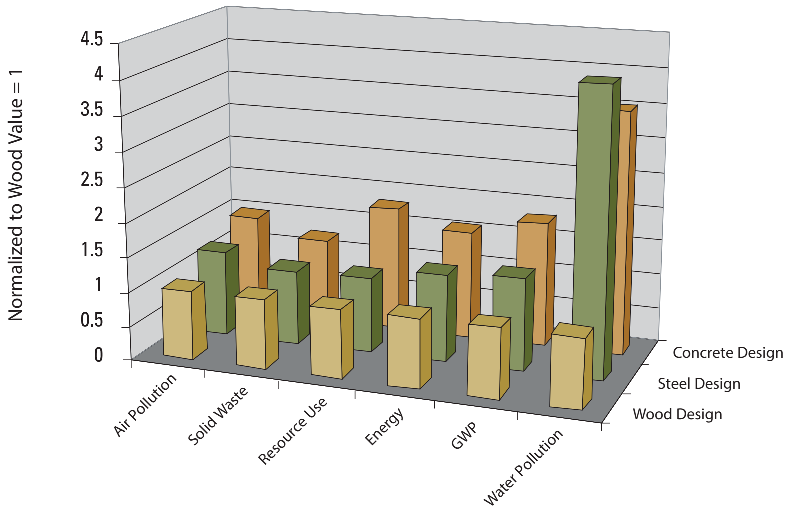

Figure 1.2. Embodied effects in use of wood, steel and concrete (from [8]).

Another environmentally-friendly material is bamboo, which is a grass plant used since long time to build basic habitats as well as complex structures. In tropical zones the bamboos most commonly used for constructions are the Bambusa, Chusquea, Dendrocalamus, Gigantochload and Guadua whereas the group of Phyllostachys are used in temperate zones. Among the positive environmental effects in the use of bamboo as construction materials, there are the biomass production, the reduction of soil erosion because of the dense network of roots that anchors earth and helps to lessen erosion due to rain and flooding, the water retention, the regulation of hydraulic flow (because the retaining water in its stem), temperature reduction due to its leaves. Moreover, because its rapid growth, bamboo can take in more CO_2 than a tree, which is relevant for international greenhouse gas emission allowance trading. Bamboo has been used mostly in rural zones of warm humid climate like Indonesia and India, at the beginning for the construction of scaffolding [9]. For structural applications, laminated bamboo lumber (LBL) has been developed in South America and China [10], which is produced gluing slender strips obtained through a splitter machine.

1.3 Goals and original contributions of the thesis

The thesis aims at investigating the seismic performances of timber light-frame shear walls with focus on the contribution offered by the sheathing-to-framing connections in terms of energy dissipation and ductility. Numerical non-linear analyses under displacement-controlled loading conditions are carried out using an original parametric finite element (FE) model developed within the open-source software OpenSees [11] in order to allow the easy variation of some basic design variables affecting the overall racking capacity of the wall, namely: *i)* aspect ratio, *ii)* nails spacing, *iii)* number of vertical studs and *iv)* cross-section size of the framing elements.

In fact, although many researches dealt with the in-plane behavior of a fully-anchored timber shear wall, few efforts have been spent so far to analyze the mechanical behavior and the energy dissipation attributable to the sheathing-to-framing connections that, with hold-down connections, represent the highest contribution in terms of a wall deformation. There are few parametric analyses that consider different wall configurations [12–14] of a fully-anchored timber shear wall. Several experimental tests have demonstrated that the dissipative behavior of a shear wall is mainly influenced by its connections. Timber has, in general, a poor dissipative capacity and is a brittle material in bending and in tension, unless it is properly reinforced [15]. Conversely, the steel connections ensure a good amount of energy dissipation and cyclic ductility notwithstanding their significant pinching, strength degradation and softening. This evidence is well reflected into many numerical models proposed in literature, where the non-linear wall response is related to the load-deformation relationships of the connections [16–18]. Observing the results of the sensitivity analyses and starting from the study by Casagrande et al. [19] - who model the timber shear wall considering rigid framing elements - an analytical procedure is here proposed to predict the capacity curve of a timber light-frame shear wall. Considering the characteristic non-linear softening-type behavior of timber structures, an analytical expression of the equivalent viscous damping is provided, which allows to assess the ductility of a common timber shear wall configuration. Finally, optimal configurations of a timber light-frame shear wall, considering two values of aspect ratio (2 and 1), are provided to show how the design variables affect the variation of racking capacity and costs.

1.4 Layout of thesis

The thesis is composed by nine chapters and four appendixes.

Some general concepts about the modern approach in buildings design have been provided in CHAPTER 1. Particularly, the focus was on the growing attention paid to the environment at issues in building design, describing the strategies to encourage the use of renewable energies along with the choice of environmentally-friendly materials for constructions, in terms of both needed energy for the production and reuse at the end of their life-cycle (*cradle to cradle* or *cradle to grave*). A comparison among timber and bamboo performances against steel and concrete was thus given. CHAPTER 2 describes the code framework about timber structures, in order to provide the references for the classifications, marking of wood-based products and rules to design timber buildings. It also presents an overview about the classification of the widespread construction systems and basic elements belonging to platform frame constructions.

CHAPTER 3 provides a description of the geometric and mechanical properties of the basic elements is use within platform framing buildings, with details about timber walls with openings. Then, a deeper description of the sheathing-to-framing connections is proposed within CHAPTER 4, where the mechanical behavior according to the EuroCode 5 [20] is described along with an overview of literature proposals in mechanical modeling. Within CHAPTER 5 the basic concepts about Italian seismic hazard are recalled and a review of seismic analysis and design methods is provided, in order to introduce how the mechanical behavior of a timber light-frame shear wall is considered both in the EuroCode 5 and in literature. In particular, the definition of the equivalent viscous damping is provided in order to estimate the damping factor η in use within the Capacity Spectrum Method for reducing the demand of the elastic acceleration spectrum as proposed in the EuroCode 8 (*force-based* design method) [21]. The numerical modeling in presence of rigid or flexible framing elements is described, highlighting how it is possible to extend the design approach of the EuroCode 5 related to the composite timber sections to a wall panel, in line with the studies by Pintarič and Premrov [22].

Within CHAPTER 6 the original parametric FE model is deeply described, by providing details about the identification process carried out to calibrate the mechanical model of one fastener (that represents the sheathing-to-framing connections) and about the validation of the FE model. Sensitivity analyses have been carried out in order to assess the influence of some common design variables affecting the racking load-carrying capacity of the wall as well as to estimate the value of the equivalent viscous damping. Starting from these results, an analytical procedure to predict the response of a timber light-frame shear wall is proposed in CHAPTER 7. The bilinearization of the non-linear backbone curve has been provided for both a single fastener and for the reference walls, imposing the principle of energy equivalency. This approach is widely used for timber structures, in order to account for the typical softening phenomenon, such as [23] and [24]. In these cases, a procedure to define initial stiffness and yield displacement is provided along with that of ultimate displacement, the latter corresponding to a load dropping equal to 80% of the maximum load. As reported in [25], in some cases a significant loss of strength is observed after reaching the racking strength peak, and thus the displacement at the maximum load is used as ultimate displacement. The proposed analytical procedure moves from these shortcomings to improve the identification of yielding and ultimate displacement, by observing in parallel the results in terms of global wall response and local behavior of nails. In particular, two Limit States are defined and the following criterion is adopted: the equivalent viscous damping is computed from the load-displacement curve once the first nail reaches a resistance decrement equal to 65% according to the experimental data in [26]. Thus, the ultimate displacement is not conventionally defined as in the existing approaches, but it is derived from mechanical considerations. The Collapse Limit State can be reasonably considered to occur once the first nail has reached the resistance decrement experimentally observed: in fact, after its failure, the adjacent nails start to fail sequentially. Moreover, in line with EuroCode 5 recommendations, the analogy between the behavior of a single fastener and the wall is exploited, not just to estimate the overall racking load-carrying capacity but also the overall stiffness. Within chapter 8 optimal configurations of a timber light-frame shear wall are shown, in such a way to highlight how the input design variables affect the overall response, providing also considerations about the costs.

chapter 9, collects some comments about the obtained results and proposes some topics for future developments.

Finally, the appendices include:

- the main parts of the TCL code developed in the open-source software OpenSees (Appendix A);
- a practical example on how the shear strength of a single fastener is computed according to the Johansen's theory, as reported in the EuroCode 5 (Appendix B);
- some preliminary results related to experimental tests performed on bamboo specimens, in order to investigate the non-linear behaviour of sheathing-to-framing connections (Appendix C);
- an application of the proposed analytical procedure to the reference configuration wall used to validate the FE model (Appendix D).

2 | Timber Light-Frame buildings

Abstract

A code framework about timber structures, with references for the classifications, marking of wood-based products and rules to design timber buildings, is here provided. An overview of the widespread construction systems is also given, with focus on the basic elements belonging to the one studied in this thesis.

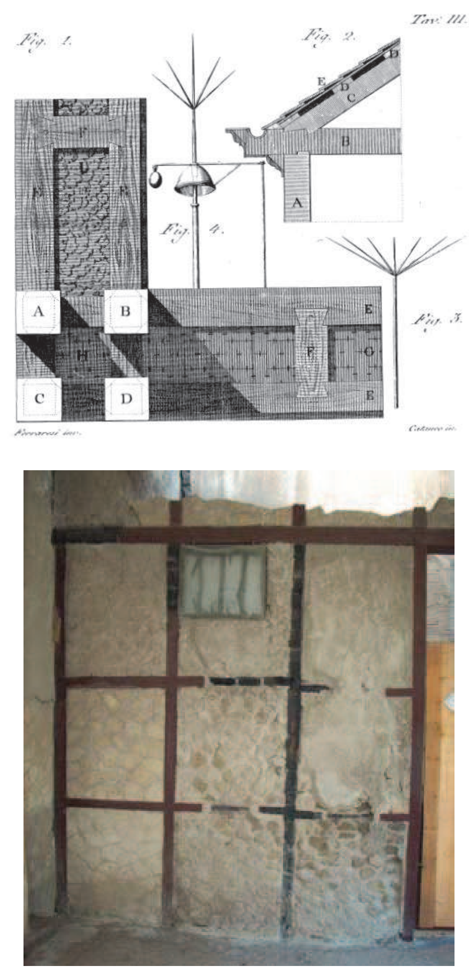

Figure 2.1. The Vivenzio's a-seismic prototype (top [27]) and *opus craticium* wall, Herculaneum (bottom [27, 28]).

2.1 Code framework

The code framework has been often incomplete and wary about the use of timber for buildings. The first law that cited timber was the Royal Decree 18/04/1909, n. 193, which regards framed constructions and the Borbone a-seismic system known as *Casa baraccata*, the Engineer La Vega's invention, based on an ancient wooden constructive tradition adopted in Calabria region (Fig. 2.1). The structural system recalls the characteristics of the *Opus Craticium*, a construction technique already described by Vitruvio and rediscovered during the excavation at Herculaneum on 1740. It is comprised of masonry reinforced by means of a web of timber elements, and it was mostly adopted for the reconstruction after the strong earthquake that struck the Calabrian territory on 1783.

Law n.1684, 25/11/1962 permits only lumber constructions authorized preventively by the Civil Engineering office, whereas law n. 64 2/2/1974 cites timber structures imposing height limits *"where construction systems other than masonry or with reinforced and standard prestressed concrete, steel or combined systems of the aforesaid materials, are used for buildings with four or more floors within and above ground, the suitability of such systems must be proven by a statement issued by the president of the board of public works on the advice of the same council"*. The Ministerial Decree 16/1/1996, says *"The upright ribs and other parts making up the static organism of wooden buildings must be one-piece or connected in such a way that there is no weakening at the joints"*. Notably, this is in contradiction with the EuroCode 8 [21] according to which *"the dissipative zones must be localized in correspondence of the nodes and the connections, while an elastic behavior must be assumed for the wooden members"*.

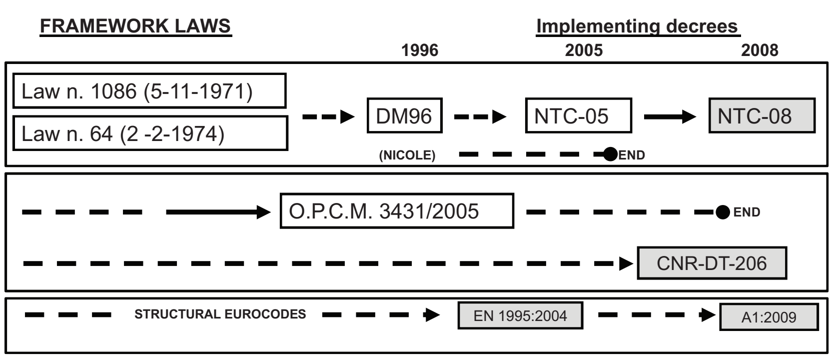

Figure 2.2. Code framework until 2008 (from [29]).

In Italy, the code framework has been modified on December 2011 through the Legislative Decree n. 201, 6/12/2011. At the art. 45, it states: *"If materials or construction systems other than those governed by the technical regulations in force are used, their suitability must be proven by a declaration issued by the President of the Board of Public Works on the* *basis of the opinion of the same Council"*, thereby removing limitations of a regulatory nature for the construction of a multi-storey building in seismic area made entirely by wood. A proposal of national legislation was developed by a special Commission at the National Research Council (CNR) that was named Nicole (Norme tecniche italiane per la progettazione, esecuzione e collaudo delle costruzioni di legno). It serves at preparing a text of Instructions (C.N.R. DT 206) as support for the application of Constructions Technical Standards [30]. A summary of legislative evolution is shown in Fig. 2.2.

The reference European codes for timber structures are:

1. UNI EN 338:2016 [31], UNI EN 14081:2016 [32] (which classify strength classes for solid coniferous wood) and UNI EN 14080:2013 [33] (which classifies glued laminated timber). An example of marking is shown in Fig. 2.3.

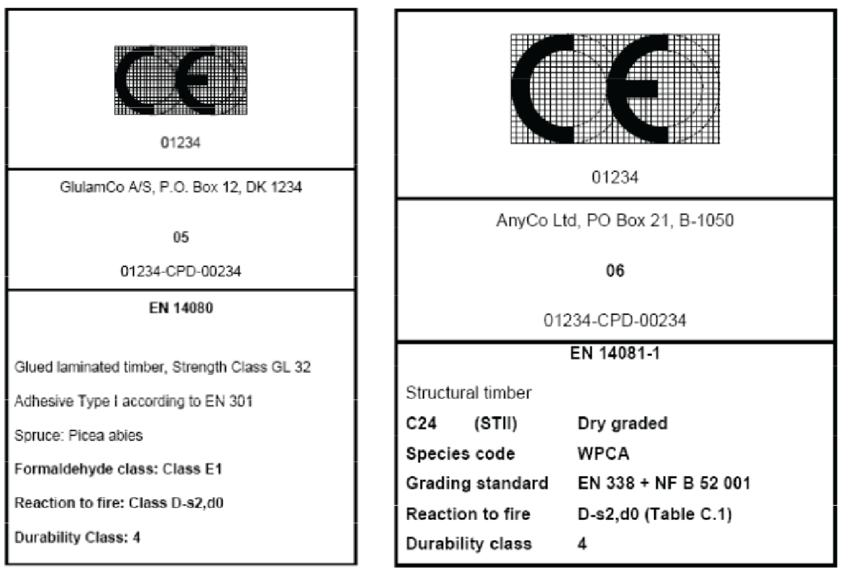

Figure 2.3. CE marking for glued laminated timber (left) and solid timber (right).

1. EN 1995 - EuroCode 5 [20], which provides common rules for the static design;

2. EN 1998 - EuroCode 8, chapter 8 [21], which gives specific rules for seismic design of timber buildings.

EuroCode 8 provides definitions and methods to compute the seismic action as function of the elastic spectrum, the main elastic period of the structure, its regularity, seismic mass and ductility along with dissipative behavior. The verifications are performed in terms of resistance to seismic actions for the Ultimate Limit States (ULS) and of maximum compatible inter-storey drift for Serviceability Limit States (SLS).

The reference Italian code for timber structures is the Construction Technical Code (NTC), Ministerial Decree 2008-01-14, chapter 4.4 and 7.7 for seismic design [30].

2.2 Timber classification

The commercial timber types are divided in two main groups, namely: *i)* softwood and *ii)* hardwood. These terms refer to the botanical origin of timber and do not reflect the actual softness or hardness of wood. Softwood are generally evergreen with needle-like leaves comprising single cells called tracheids, which fulfill the functions of conduction and support. The most diffused European softwood are, for example, spruce, larch, Scots pine and Douglas fir. Whitewood is sold generally for carcassing, inexpensive construction and painted material. The uses of redwood ranges from flooring to cladding, roof joists and picture framing. Larch is generally sold for cladding, decking or marine applications while Cedar is adopted for construction and joinery. As reported in [34], the main characteristics of softwood are:

- quick growth rate (trees can be felled after 30 years) resulting in low-density timber with relatively low strength;
- generally poor durability, unless treated with preservatives;
- they are readily available and comparatively cheaper due to the speed of felling.

Conversely, hardwoods are not evergreen and often lose their leaves at the end of each growing season, and are generally broad-leaved trees (deciduos). Their cell structure is more complex than that of softwoods comprising thick-walled cells, called fibres, (which provide the structural support) and thin-walled cells called vessels (providing the medium for food conduction). The most diffused European hardwoods are oak, beech, ash, alder, birch, maple, poplar, willow.

As reported in [34], the main characteristics of hardwood are:

- slower growing rate than softwoods, which generally results in a timber of high density and strength that takes more time to mature (over 100 years in some instances);
- there is less dependence on preservatives for durability qualities;
- they tend to be expensive in comparison with softwoods due to the time taken to mature and the transportation costs (since they mostly grow in tropical zones).

2.3 Construction systems

Timber has been the first and most important material used to build bearing structures, mainly for its lightness and easy assembly. Nowadays, timber is also appreciated because of its aesthetic pleasure, sustainability and high strength-to-density ratio that ensures a reduction of the inertial forces under dynamic loads. The Sakyamuni Pagoda is an example of ancient structure made in timber. It was built on 1056 with a total of 9 storeys whereas height and base diameter are equal to 67 m and 30 m, respectively (Fig. 2.4). According to historical chronicles, it withstood many destructive earthquakes.

Recent studies revealed that timber creates less pollution than steel or concrete. Moreover, wood-based materials have environmental benefit in terms of *crandle-to-grave* and the *gate-to-grave/reincarnation* when compared to masonry and concrete materials.

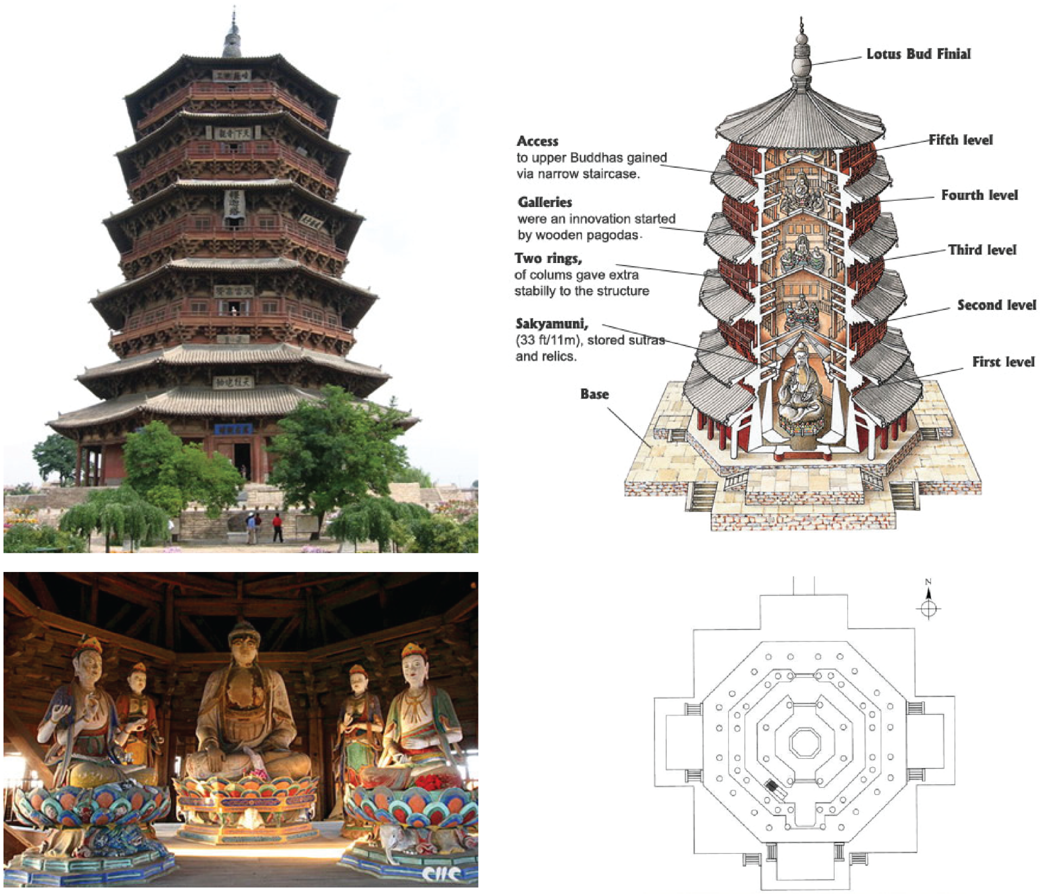

Figure 2.4. Sakyamuni Pagoda, Fogong Temple, Ying County, Shanxi, China 1056.

For ordinary buildings, two types of light-frame configurations are commonly used, namely: balloon and platform framing [35].

2.3.1 Balloon- and platform-frame construction systems

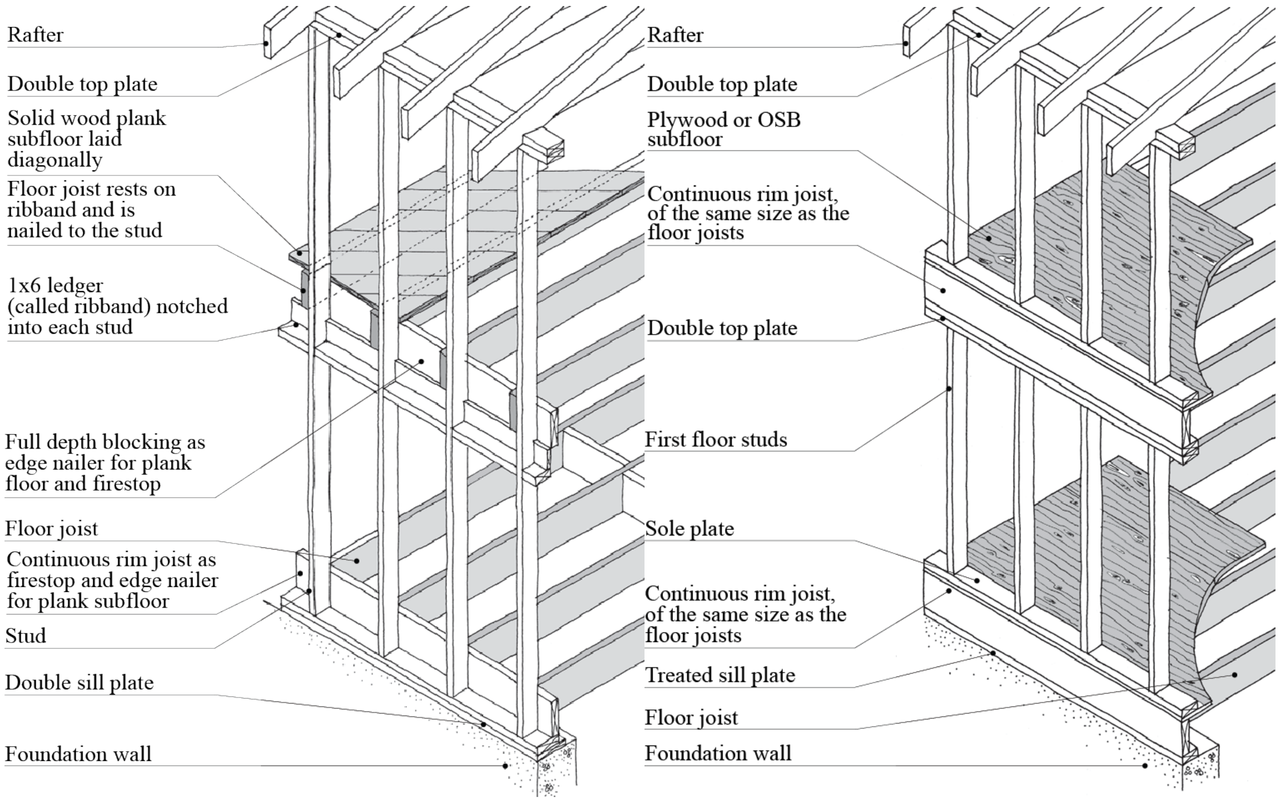

Figure 2.5. A typical balloon frame construction (left); a typical platform frame construction (right) (from [36]).

The definition "balloon frame" was coined as form of contempt for such kind of construction system, which was considered unfit to withstand significant load levels. The previous construction system - realized by heavy timber beams jointed using mortise-and-tenon - was replaced, thereby allowing the construction of buildings without the experience of craftsmanship, which was required at the beginning to build tight joints [36]. The new constructive system was comprised of thin, closely spaced vertical timber members, named studs (or *chords*, according to [13]), connected with horizontal framing members, called joists for floors (or *struts* according to [13]) and rafters for roofs (Fig. 2.5, left).

The connections between the lightweight members, starting from balloon frame, were made by means of simple nails and their installation did not require large efforts anymore. The studs run the full height of the building, from the sill plate at the bottom to the top plate under the rafters. The intermediate floor joists, named *ribband*, are notched into the studs whereas fire-stops are provided at floor lines, thereby interrupting the continuous air space between the studs.

The main shortcoming of this kind of construction system was continuity required for the studs, since the limited availability of long and straight members increases the overall cost. On the other hand, the benefits provided by this type of construction system were associated to its stability. Since the floor joists are supported directly on the studs the cross-grain members, as such as the ribband and fire-stops, do not affect shrinkage and swelling of the frame.

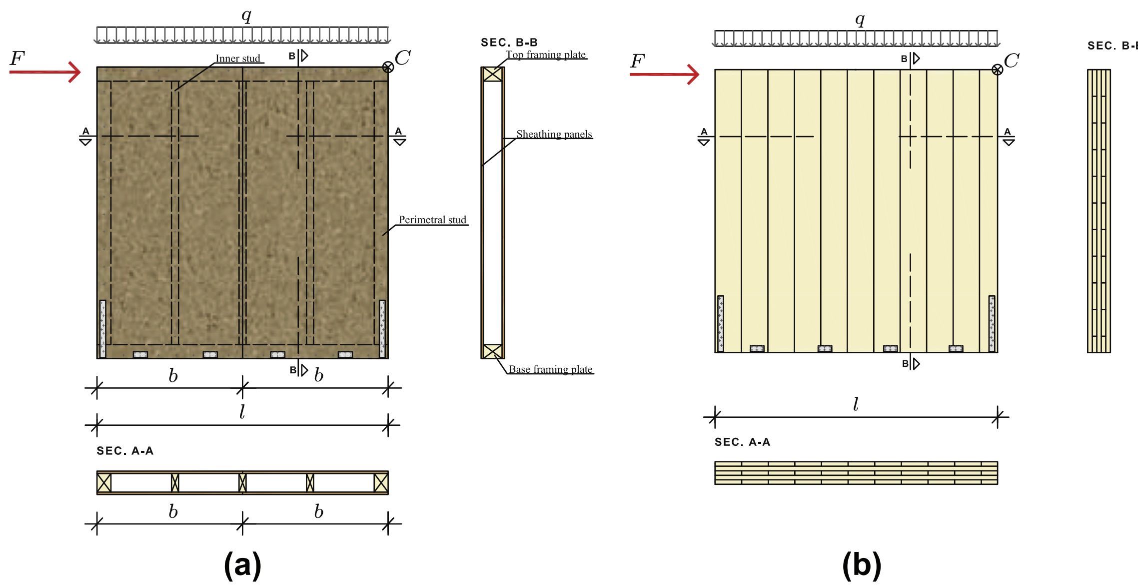

Figure 2.6. Type of walls employed in platform framing buildings: (a) Timber Framed walls; (b) Cross Laminated Timber walls (from [37]).

Conversely, platform framing buildings have discontinuous framing members (studs) connected using plates supporting floor joists for each story, with a shear wall underneath. In this case, fire-stops are automatically provided at each floor level (Fig. 2.5, right). Additionally, building structures with more than two stories is possible but different from the balloon frame because the length of studs imposes some limitations.

As pointed out by Porteous and Kermani [34], platform framed walls can be classified in the following two categories, namely: stud walls and racking walls.

The first category includes walls designed to carry vertical loads only with a sheathing panel that, if inserted, provides only an additional strength to the studs against in-plane and out-of-plane axial buckling. The walls belonging to the second category, instead, are designed to withstand in-plane lateral actions by means of the sheathing-to-framing connections.

The following types of walls are used in platform framed buildings (Fig. 2.6):

- Cross Laminated Timber walls (CLT), which are fabricated with a wood product realized by adhering and compressing wood layers called *lamellas* in perpendicular grain orientations to form a solid panel. Wood layers are glued together;

- Timber Framed walls (TF).

The dimensions of the frame are usually based on the size of the panel used to sheathed it on one or both sides, which is made by different materials like OSB (Oriented Strand Board), plywood, gypsum, GLG (Glued Laminated Guadua) bamboo [38], fibreboard and so on.

The overall system can be subdivided into individual building components that could form either an overall system or be combined in the form of a composite system that have a relationship with the overall system.

Inspired by American experiences and successes, the first systems based on the *platform frame* appeared in Europe around 1930 and were designated as *timber stud construction*. It took place in a totally different manufacturing structure to that of the United States and in a way more suitable to European conditions and quality demands. It was particularly successful in Germany and Switzerland. The most important difference between timber stud construction and timber-frame construction is the way the structure is braced.

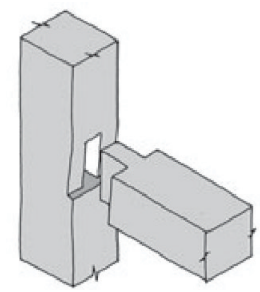

Figure 2.7. Mortise-and-tenon joint (from [36]).

The load-bearing framework of the second one is itself stiffened by the inclusion of inclined braces, whereas in timber stud construction the load-bearing framework is given by attaching solid timber sheathing to the outside or on both sides. Also the connections are different: in the timber stud construction, they are achieved via a direct contact between the timber members (compression), through nailing, lap and halving joints, in some cases using mortise-and-tenon joints (Fig. 2.7).

Modern timber stud construction, together with balloon- and platform-frame constructions, have been superseded in Europe by panel construction due to its far superior quality [39].

2.3.2 Panel construction system

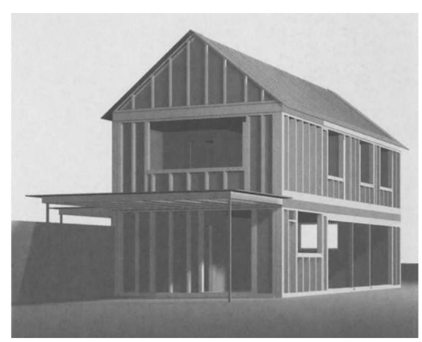

Figure 2.8. View of assembled building without external sheathing (from [39]).

The load-bearing structure in panel construction consists of load-bearing ribs of squared sections and a sheathing that stabilizes the ribs (Fig. 2.8). The individual vertical members carry the vertical load from roof and suspended floors, while sheathing panels resist to the horizontal forces and represent a bracing system for the component.

The feature, and also the advantages, of this type of construction can be summarized as follows:

- design freedoms;

- simple form of construction;

- repetitive details;
- loadbearing ribs of slender, standardised sections;
- building braced by sheathing;
- simple material procurement;
- storey-by-storey assembly;
- connections achieved by direct contact and with mechanical fasteners;
- modular dimension 400-700 mm, preferably 625 mm;
- construction clad both sides;
- short on-site time, different manufacturing depths possible.

2.4 Basic elements

For one- and two-storey buildings, timber sections measuring 60 × 120 mm are sufficient for the structural members. This could therefore be the basic element from which the main structure of the building is constructed. However, thermal insulation thicker than 120 mm is now often required in the external walls. The depth of the section must therefore either be increased from 120 to 160, 180, 200 mm. Alternatively, a second layer of insulation independent from the load-bearing construction must be provided.

As the addition of a second insulating layer also eliminates thermal bridges, this variation is the clear favorite. A hybrid solution, i.e. a deeper load-bearing construction plus a second layer of insulation on the outside, is also possible. In the case of multistorey panel construction, larger sections will be needed for structural reasons anyway.

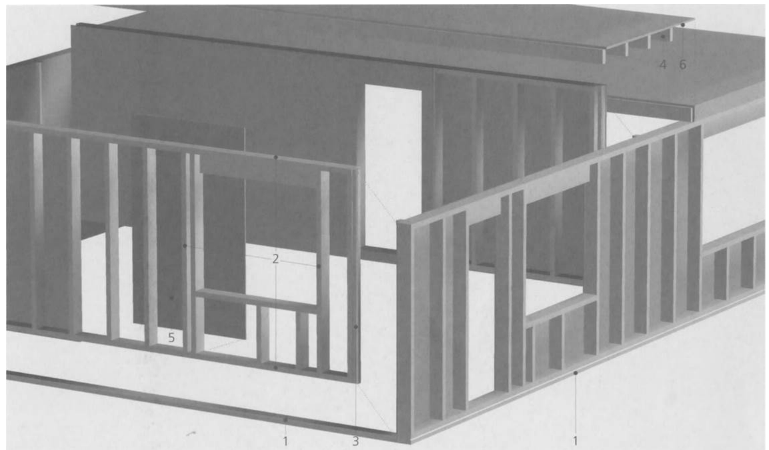

Figure 2.9. The parts of panel construction elements (from [39]).

1 Base plate
2 Bottom and top plates, studs
3 Assembly post
4 Rib, joist
5 Structural wall sheathing
6 Structural floor sheathing

In panel construction, the main components are as follows (Figs. 2.9 and 2.10):

- *Load-bearing ribs:*
  - structural timber (solid timber, compound sections), strength grade C24;
  - species: spruce, fir;
  - moisture content: 12% ± 2%.

  To ensure good dimensional stability, the use of compound (solid) sections is recommended for panel construction.

- *Stiffening wall and floor sheathing*:
  - 3-ply core plywood;
  - OSB, MDF, particleboard;
  - gypsum fibreboard;
  - veneer plywood.

- *Thermal insulation*:
  - mineral - fibreboards;
  - cellulose fibers;
  - wood fibreboards;
  - diverse insulating materials.

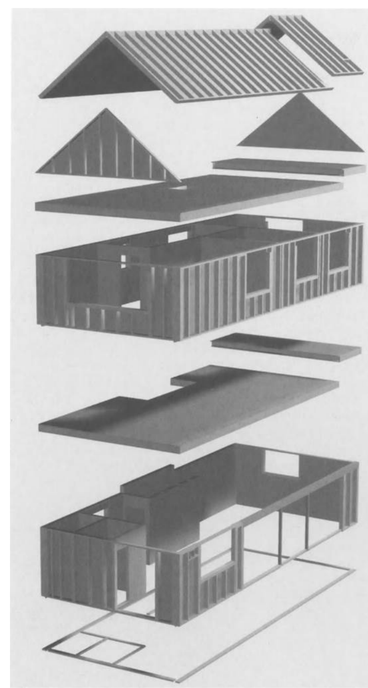

Figure 2.10. Exploded view showing individual structural elements (from [39]).

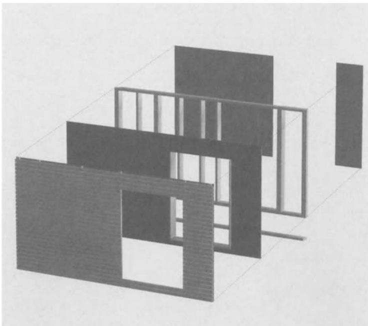

Figure 2.11. Exploded view showing the individual components of a wall (from [39]).

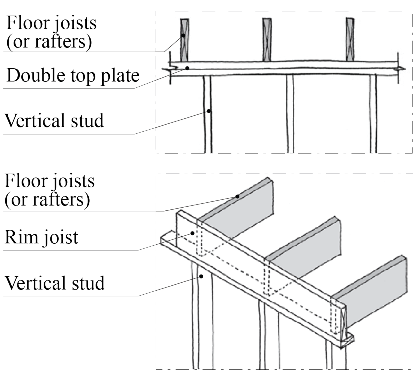

Figure 2.12. A detail of the top part of a wall: (a) double top plate; (b) single top plate (from [36]).

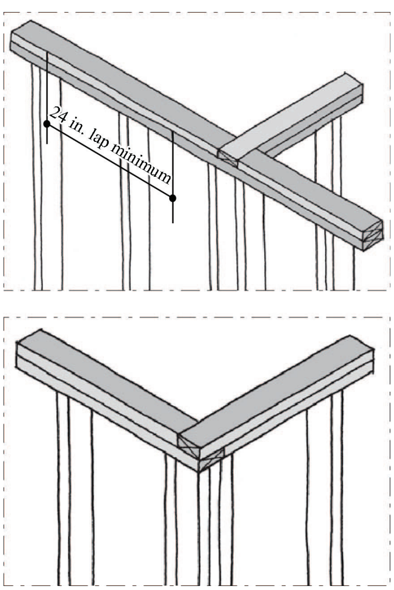

Figure 2.13. The junctions in correspondence of top plate: (top) T-junction; (bottom) wall corner junction (from [36]).

2.4.1 Wall frame

The main feature of the wall assembly is that it includes several parallel and closely spaced members, joined at each end to a continuous cross member that runs perpendicular to the parallel members (Fig. 2.11). These cross members are the top and bottom plates.

The top plate of the wall can consist of one or two members, each of the same size of the studs. Doubling the top plate makes the whole structure stronger, allowing to place the floor joists or rafter anywhere on the top plate (Fig. 2.12).

Whether, instead, the top plate is comprised of just one element, the floor joists and rafters must be aligned with the underlying studs to transfer loads vertically till the foundation. The *double top plate*, in the latter case, does not have a beam-type role.

The double plate is also useful to provide a structural continuity because floor and roof work as diaphragms in a wood frame building. This produces tension as well as compression under wind and earthquake loads. The discontinuity at the joints, due to a single plate, instead, is not able to counteract tension forces. Building codes require a minimum of 24 inches ($\sim$ 61 cm) lap at the joints between the two top plates (Fig. 2.13). For the same reason, the two top plates must be staggered at corners and junctions of the walls.

A sheet metal connector is needed at the joints when a single plate is used: this is why the single top plate is inconvenient (Fig. 2.14). Moreover, a typical arrangements of studs at corners is shown in Fig. 2.15.

A triple top plate is seldom used, if the distance between vertical studs is greater than 24 inches [36].

In the wall assembly, the bottom plate has a twofold designation, namely: sole plate or sill plate. In the first case, the single plate is not in contact with the foundation but is, for example, the bottom plate of the second floor. The sill plate is, instead, connected with the foundation and must either be a preservative-treated wood or a naturally decay-resistant wood specie.

2.4.2 Exterior walls: cross junctions

A shear wall, subjected to horizontal actions, has a resistance mostly influenced by the connections with the foundation and the other structural elements[1]. Therefore, the corner must be stronger than the field of the wall, requiring a minimum of three studs at the corner. Moreover, the provision of three studs is needed to have ad adequate nailing surface to suitably fix the interior gypsum board and exterior sheathing panel.

[1] The deeper study of this behavior is described in Section 5.6.

2.4.3 Exterior walls: openings

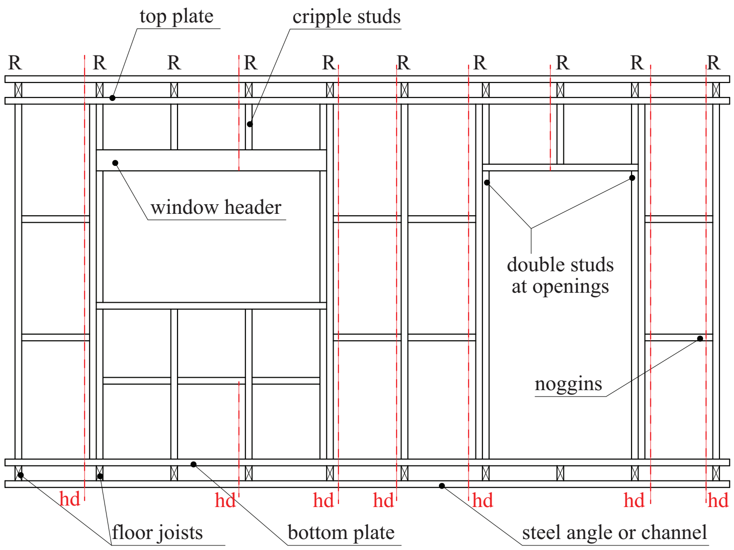

R: rafters
hd: hold-downs

Openings within a shear wall require the use of the so-called *jack studs* on their both sides. They are partial-height studs that support the lintel beam, generally known as *header* (or lintel header). If the size of the opening is very large or the number of floors in the building exceeds two, the use of two or three jack studs may be needed.

A header is typically made of two or three 2-by lumber members[2], depending on the thickness of the wall. The members are face nailed to form a beam. If the wall is framed of 2×4 members, two 2-by lumber members are required, with a $\frac{1}{2}$in.-thick filler (Fig. 2.16). The filler is usually a plywood or an OSB sheet. In a 2×6 wall, three 2-by lumber members are required with two filler sheets. For large openings, trussed headers or glulam headers are used.

2.4.4 Floor frame

The layout of a floor frame plan is comprised of joists that generally are laid in the direction of the shorter span and, when this is not possible, a glulam beam or a wall on the lower floor has to be inserted over long spans. Moreover, when there is a cantilevered floor, the joist must be bear on a support and securely connected at the far end to a wall or a beam. As for the joist framing around openings, also for cantilevered floor joists along opposite end have to be doubled. Further elements are inserted to prevent buckling of joists, called *rims* or *bands joists* that provide lateral restraints.

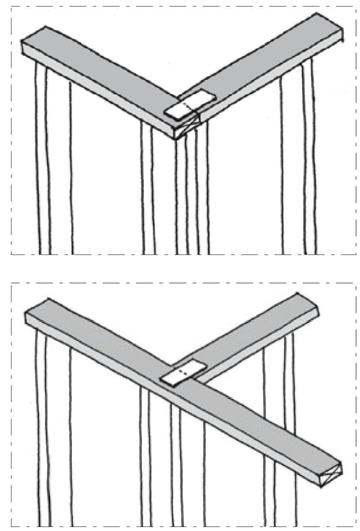

Figure 2.14. Steel metal connector for single top plate (from[36]).

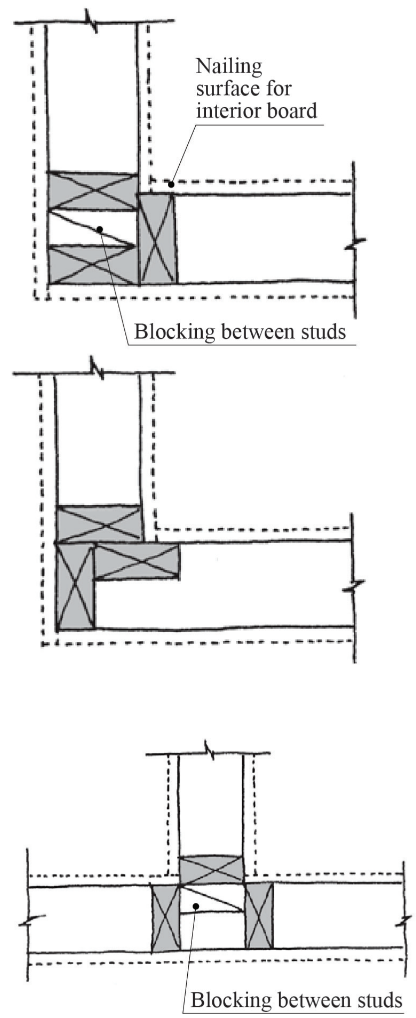

Figure 2.15. Typical arrangements of studs at corners (from [36]).

[2] The *2-by* notation is used to identify the widespread lumber thickness size used in constructions, equal to 2 in.

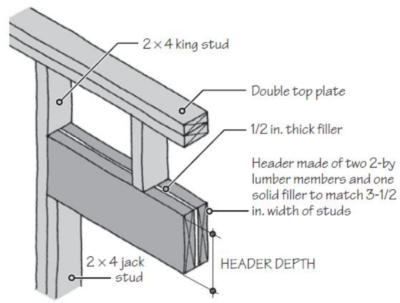

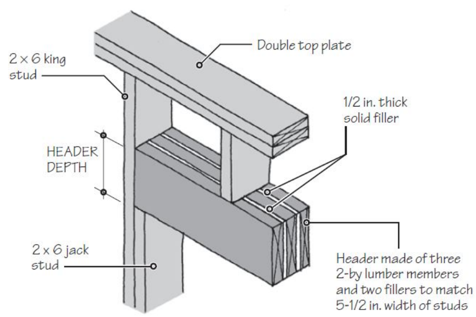

Figure 2.16. Headers made with 2-by lumber members: (top) 2 x 4 stud wall; (bottom) 2 x 6 stud wall (from [36]).

2.4.5 Roof frame

Generally, the roof is sloped and has gable, hip or shed shape. The slope is expressed as rise-to-run ratio, where run is kept constant and equal to 12. The greater the rise, the greater the roof slope, which allows to divide roofs in two types:

- low-slope roof with a rise-to-run ratio less than 3:12;
- steep roof with a rise-to-run ratio greater than 3:12.

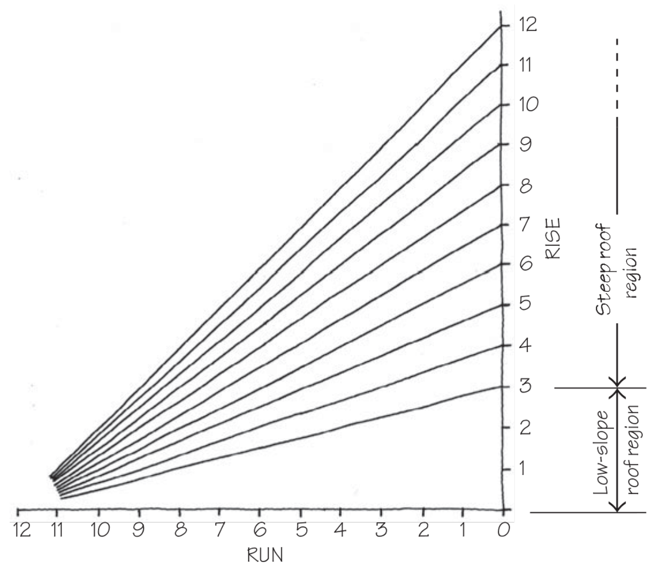

The roof frame could be comprises of trusses, shop-fabricated, or rafter-and-ceiling joist assemblies, site-fabricated. For the latter, the connection between two rafters is made through a continuous ridge board, which does not have structural function except to align the rafter ends in a straight line at the top and generally it is 2-by member element in LVL. Each rafter pair is tied together at the bottom to resist outward thrust created by the gravity loads on the roof. Then, to transmit load vertically at the supports, each rafter is cut to have a horizontal bearing on the supporting walls (Fig. 2.17) and the notch is known as *bird's mouth*. Moreover, to prevent the separation of rafters due to uplift loads link to wind-load, collar ties are often located within the upper one-third of the attic.

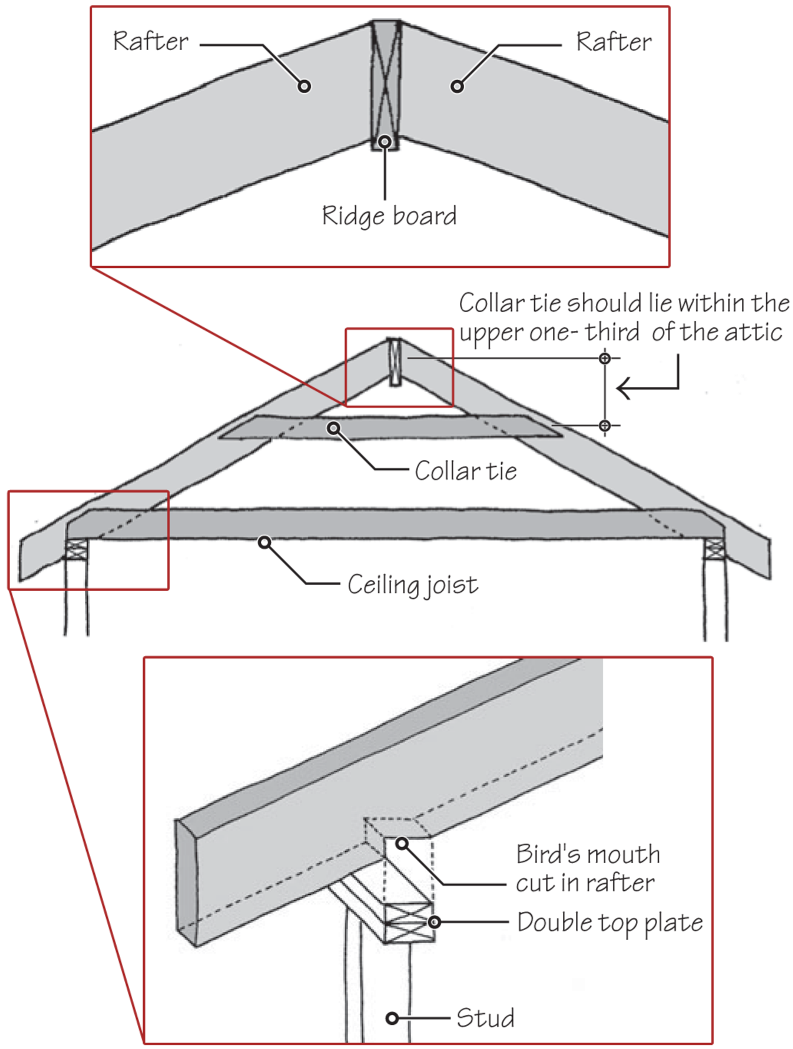

Figure 2.17. The element that comprise the roof frame: (top) ridge board; (middle) collar tie (bottom) bird's mouth (from [36]).

3 | Timber Light-Frame shear walls: geometry and mechanics of basic elements

Abstract

A brief description of the main geometric and mechanical properties of the basic elements employed in timber light-frame shear walls is here provided. Further details and a deeper description of the sheathing-to-framing connections is then reported in the next section, in order to introduce their main mechanical characteristics along with the mechanical models used in literature and within the EuroCode 5. These characteristics will be used in the next sections to define the parametric FE model and to develop the analytical procedure aiming at predicting the global load-displacement curve of a timber light-frame shear wall.

3.1 Frame

A typical size of the framing elements cross-sections used in timber light-frame shear walls is about 38 mm × 89 mm and 38 mm × 140 mm for internal and external wall studs, respectively [7]. Also 80 mm × 160 mm, 120 mm × 160 mm, 120 mm × 200 mm, 140 mm × 160 mm and 160 mm × 200 mm sizes are used in Italy and in Alpine area Countries [26]. Further details about sizes of engineered wood products can be found in [34, §1.7].

The most common center-to-center spacing of vertical members is 12 inches (∼30.5 cm), 16 inches (∼38 cm), 19.2 inches (∼48.8 cm, seldom used) and 24 inches (∼61 cm), according to the loads that act on the structure. The dimensions are also determined by the size of the sheathing panel adopted to brace, both one and two sides of the wall. The strength capability of timber is a function of several parameters, including species type, density, size of members, moisture content, duration of the applied load and various strength reducing characteristics like the presence of defects, knots, fissures etc. The design properties of timber are determined non-destructively, often with visual strength grading or by machine strength grading criteria. The interested reader can refer to [34, §1.5.1 and §1.5.2] for details about them. Timber are

Strength class		Characteristic strength properties (N/mm²)						Stiffness properties (kN/mm²)				Density (kg/m³)	
		Bending	Tension 0	Tension 90	Compression 0	Compression 90	Shear	Mean modulus of elasticity 0	5% modulus of elasticity 0	Mean modulus of elasticity 90	Mean shear modulus	Density	Mean density
		($f_{m,k}$)	($f_{t,0,k}$)	($f_{t,90,k}$)	($f_{c,0,k}$)	($f_{c,90,k}$)	($f_{v,k}$)	($E_{0,mean}$)	($E_{0.05}$)	($E_{90,mean}$)	(G_{mean})	(ρ_k)	(ρ_{mean})
Softwood and poplar species	C14	14	8	0.4	16	2.0	1.7	7.0	4.7	0.23	0.44	290	350
	C16	16	10	0.5	17	2.2	1.8	8.0	5.4	0.27	0.50	310	370
	C18	18	11	0.5	18	2.2	2.0	9.0	6.0	0.30	0.56	320	380
	C20	20	12	0.5	19	2.3	2.2	9.5	6.4	0.32	0.59	330	390
	C22	22	13	0.5	20	2.4	2.4	10.0	6.7	0.33	0.63	340	410
	C24	24	14	0.5	21	2.5	2.5	11.0	7.4	0.37	0.69	350	420
	C27	27	16	0.6	22	2.6	2.8	11.5	7.7	0.38	0.72	370	450
	C30	30	18	0.6	23	2.7	3.0	12.0	8.0	0.40	0.75	380	460
	C35	35	21	0.6	25	2.8	3.4	13.0	8.7	0.43	0.81	400	480
	C40	40	24	0.6	26	2.9	3.8	14.0	9.4	0.47	0.88	420	500
	C45	45	27	0.6	27	3.1	3.8	15.0	10.0	0.50	0.94	440	520
	C50	50	30	0.6	29	3.2	3.8	16.0	10.7	0.53	1.00	460	550
Hardwood species	D30	30	18	0.6	23	8.0	3.0	10.0	8.0	0.64	0.60	530	640
	D35	35	21	0.6	25	8.4	3.4	10.0	8.7	0.69	0.65	560	670
	D40	40	24	0.6	26	8.8	3.8	11.0	9.4	0.75	0.70	590	700
	D50	50	30	0.6	29	9.7	4.6	14.0	11.8	0.93	0.88	650	780
	D60	60	36	0.6	32	10.5	5.3	17.0	14.3	1.13	1.06	700	840
	D70	70	42	0.6	34	13.5	6.0	20.0	16.8	1.33	1.25	900	1080

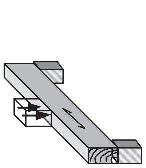

Bending parallel to grain: f_m and E_0
Shear: f_v and G

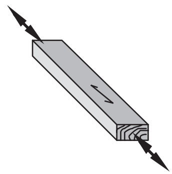

Tension or compression parallel to grain: $f_{t,0}$, $f_{c,0}$ and E_0

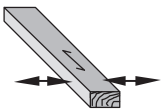

Tension or compression perpendicular to grain: $f_{t,90}$, $f_{c,90}$ and E_{90}

Subscripts used are:0, direction parallel to grain; 90, direction perpendicular to grain; m, bending; t, tension; c, compression; v, shear; k, characteristic.

Table 3.1. Strength and stiffness properties and density values for structural timber strength classes, (in accordance with Table 1, of EN 338:2003) (from [34]).

thus grouped into strength classes since from 1984 [40], today collected in [31] and labelled with letter C and D according to their botanical origin, softwood or hardwood respectively (ref. to Sec. 2.2 for details). The number of each class refers to its characteristic bending strength in N/mm^2.

The characteristics properties (see Tab. 3.1) are defined as the population 5^{th}-percentile values obtained from tests results with a duration of approximately 5 minutes at the equilibrium moisture content relating to a temperature of 20°C and a relative humidity of 65%. The interested reader can refer to [34, §1.5.3.1] for further details.

3.1.1 Headers for openings

Lumber is usually available in lengths of 8 ft, 10 ft, 12 ft (∼244 cm, ∼305 cm, ∼366 cm), and so on, up to a maximum length of 26 ft (∼792 cm).

A special precut length that is commonly used for studs is 7 ft (∼213 cm height) $8\frac{5}{8}$ in. (∼13 cm thick) (Fig. 3.1). The use of these studs saves on-site labor and gives a clear interior height (finished floor to ceiling) of 8 ft (∼244 cm). The 8-ft clear height is common in multifamily dwellings, hotels, townhouses, and so on. If 2 × 12 headers are used with these studs, the opening height obtained is 6 ft (∼183 cm height), which is the standard lintel height for residential doors and windows. Another commonly used special precut length of studs is 104 in. (∼264 cm), which gives a floor-to-ceiling height of 9 ft (∼274 cm). Note that 8-ft and 9-ft floor-to-ceiling heights conform to gypsum board panel sizes.

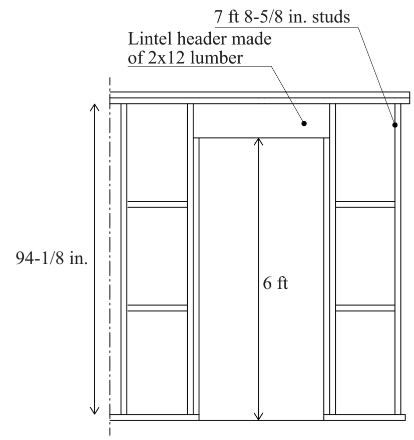

Figure 3.1. The use of oversize headers.

3.2 Sheathing panels

Wood panels can be used as either structural or non-structural elements. The first case is related to the sheathing panels of walls, floors and roofs. The latter case deals with exterior siding and interior paneling.

In general, wood panels are divided into the following three classes:

- *Veneered panels*, that consist of plywood panels;
- *Nonveneered panels*, consisting of Oriented StrandBoard (OSB) and particle board panels. The second type is mostly used for shelving and furniture making;
- *Composite panels*, consisting of two parallel face veneers with a non-veneer core. Their use in contemporary structural applications is limited.

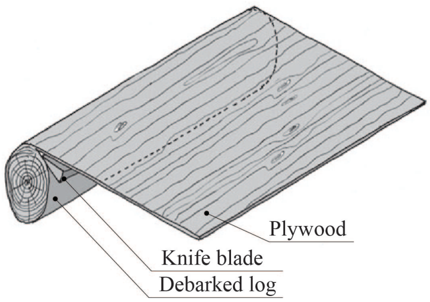

Figure 3.2. Method of making plywood veneers commonly in use (from [36]).

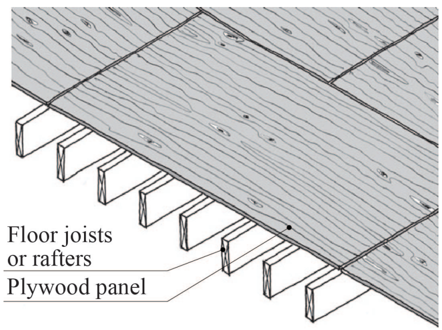

Figure 3.3. Installation of plywood panels: they must be oriented with their long direction perpendicular to the supporting members and a gap of 3.2 mm must be left all around panels to accommodate moisture expansion (from [36])

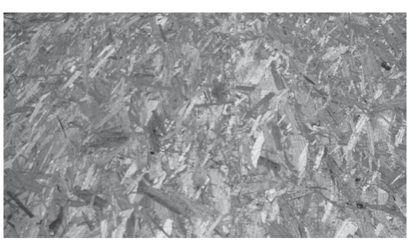

Figure 3.4. Surface appearance of OSB panel (from [36]).

3.2.1 Plywood panels

This kind of panels is made by gluing wood veneers under heat and pressure.

Veneers are generally produced by a machine that holds a debarked log at two ends in a lathe and rotates the log against a stationary knife blade extending throughout the length of the log (Fig. 3.2). The veneer so obtained is subsequently cut to desired sizes, the defects in veneers, such as knot holes and splits, are cut away or repaired where necessary. The veneers are then dried and glued together so that the grain direction in each veneer is oriented at a right angle to the grain direction of the adjacent veneer.

The most commonly used plywood panel nominal size is 4 ft x 8 ft ($\sim$122 cm × $\sim$244 cm), with thickness varying from $\frac{1}{4}$in. to 1 inch. (0.635 to 2.54 cm). Its actual dimension is $\sim$104.5 cm × $\sim$211 cm, which allows to install the panel all around for moisture expansion (Fig. 3.3).

These panels are generally obtained from softwood, and are graded in five grades (from A - the highest - to D - the lowest) based on the defects size such as knots and splits [36]. Each panel has a different grade for the two different sides: it must be exposed on the side with the highest veneer grade. The main feature of the plywood panels used for sheathing is that, differently from those used for furnitures, they are unsanded. The core of the plywood is generally of rotary-sliced softwood veneers or particle board.

3.2.2 Oriented StrandBoard (OSB) panels

These panels are comprised of wood strands and the name is due to the alternate layers of strands, oriented at right angles to each other (Fig. 3.4). They are made by gluing the layers under heat and pressure, and have the same dimensions as plywood panels (4 ft x 8 ft =$\sim$122 cm × $\sim$244 cm). The process used to arrange side-by-side the veneers of hardwood and softwood is called veneer matching.

This type of panel is preferred because of lower costs and high shear strength, as consequence of the lack of core voids (which is the most important factor in the racking resistance of a shear wall), especially along its long direction. Thus, it is used for floor, roof and wall sheathing in a typical wood frame building.

There are some limitations in the use of OSB panels, namely: *i)* they are used only for structural applications, it is no possible neither to stain it, nor to paint it, differently from plywood; *ii)* they cannot be sanded smooth; *iii)* there are some problems with edge swelling if they remain wet for prolonged periods; *iv)* they cannot be treated with preservatives.

The OSB panels are also known as Sterling board or Sterling OSB in

United Kingdom and are composed of wood strands, flakes or wafer sliced from small-diameter round timber logs. The strands are oriented in the long panel direction, with inner layers comprising randomly oriented wood strands. The strength is mainly linked to the multi-layered make-up and cross-orientation of the strands, which are bonded with an exterior-type adhesive (comprising 95% wood and 5% resin and wax) under heat and pressure.

The widespread use of OSB in place of plywood is due to its cost-effective, environmentally friendly and dimensionally stable panel, which may have various thicknesses (from 8 to 25 mm) and sizes (up to 2.4 wide×4.8 m long).

The code that provides information on the mechanic values is EN 12369-1:2001 [34] complying with EN 300:1997 [34] for use in designing structures to EC5:

- OSB/2 is a general purpose load-bearing panel for use in dry conditions only (service class 1);
- OSB/3 is a load-bearing structural panel for use in humid conditions (service classes 1 or 2);
- OSB/4 is a heavy-duty load-bearing structural panel for use in humid conditions (service classes 1 and 2).

The grades intended for use in design and construction of load-bearing or stiffening buildings, like walls, flooring, roofing and I-beam, are grade OSB/3 and OSB/4. The minimum characteristics values for OSB are summarized in Tab. 3.2.

3.3 Connections for wood-based buildings

Traditionally, different types of interlocking joints were adopted to connect wood members. Nowdays, wood joints are built by simply nailing the members together or by nailing them through sheet metal connections as well as screws and bolts in some cases.

3.3.1 Nails

A nail is made of low or medium carbon steel wire that is heat treated to increase its stiffness. If a higher impact resistance is needed, then a higher carbon content is used. Whether no further treatment for corrosion is used, the nail is called *brite nail*. In exterior siding and decks, hot-dip galvanized are used, because cheaper than stainless steel nail.

For increased holding power, nails are phosphate or vinyl coated. Vinyl-coated nails produce heat due to friction when the nail is driven, which increases the bond between the wood and the nail by melting

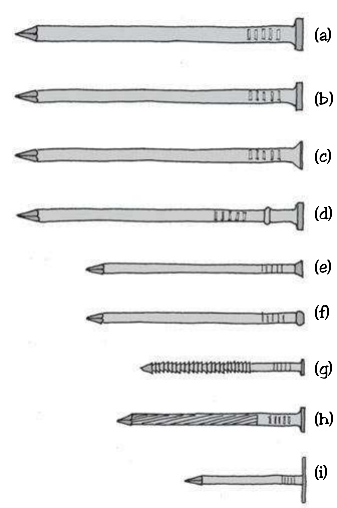

Figure 3.5. Types of nails in wood frame constructions commonly in use (from [36]).

the vinyl. They have a thinner shank and are easier to drive into wood and are, therefore, called *sinker nails*.

For framing connections common nails are generally used. A brief classification is shown in Fig. 3.5.

The *(a)* type is the *common nail*, its thick shank gives greater strength; *(b)* is called *box nail* and is used for attaching wood siding and shingles and its thin shank reduces wood splitting; *(c)* is the *sinker nail*, its tapered head sinks into wood and it is generally vinyl coated; *(d)* is called *duplex nail* and is used in scaffolding and concrete form work for temporary nailing; *(e)* is the *casing nail*, used for wood trim, window frames, casing and decks; *(f)* is called *finish nail* and is used for finer carpentry and finishing; *(g)* is the *ring shank nail*, used for attaching floor sheathing and gypsum wallboard, with its ring shank gives greater holding power; *(h)* is called *fluted shank nail* and is used for attaching wood to masonry or concrete; this is the case when high carbon steel is used to give greater impact resistance; *(i)* is the *roofing nail*, which is used for attaching roof shingles thanks to its large head [36].

The classification of nails is made using the so-called Penny system: the length of common nails in the United States is designated using the system originated in England, when 1 poundweight of 10d and 12d nails cost 10 pence 12 pence, respectively. A summary is reported below (Fig. 3.6 and Tab. 3.3).

Table 3.2. Strength, stiffness properties and density values for OSB boards complying with EN 300:1997 (based on EN 12369-1:2001) (from [34]).

Section properties	Characteristic strength (N/mm^2)								Characteristic Density (kg/m^3)	Mean modulus of rigidity (N/mm^2)		Mean modulus of elasticity (N/mm^2)					
	Bending		Compression		Tension		Panel shear	Planar (rolling) shear		Panel shear	Planar shear	Bending		Tension		Compression	
Thickness (mm)	$f_{m,0,k}$	$f_{m,90,k}$	$f_{c,0,k}$	$f_{c,90,k}$	$f_{t,0,k}$	$f_{t,90,k}$	$f_{v,k}$	$f_{r,k}$	ρ_k	$G_{v,mean}$	$G_{r,mean}$	$E_{m,0,mean}$	$E_{m,90,mean}$	$E_{t,0,mean}$	$E_{t,90,mean}$	$E_{c,0,mean}$	$E_{c,90,mean}$
OSB/2: load-bearing boards for use in dry conditions; OSB/3: load-bearing boards for use in humid conditions																	
> 6–10	18.0	9.0	15.9	12.9	9.9	7.2	6.8	1.0	550	1080	50	4930	1980	3800	3000	3800	3000
> 10–18	16.4	8.2	15.4	12.7	9.4	7.0	6.8	1.0	550	1080	50	4930	1980	3800	3000	3800	3000
> 18–25	14.8	7.4	14.8	12.4	9.0	6.8	6.8	1.0	550	1080	50	4930	1980	3800	3000	3800	3000
OSB/4: heavy-duty load-bearing boards for use in humid conditions																	
> 6–10	24.5	13.0	18.1	14.3	11.9	8.5	6.9	1.1	550	1090	60	6780	2680	4300	3200	4300	3200
> 10–18	23.0	12.2	17.6	14.0	11.4	8.2	6.9	1.1	550	1090	60	6780	2680	4300	3200	4300	3200
> 18–25	21.0	11.4	17.0	13.7	10.9	8.8	6.9	1.1	550	1090	60	6780	2680	4300	3200	4300	3200

The 5% characteristic values for stiffness (i.e. G_k and E_k) should be taken as 0.85 times the mean values given in this table. Other properties not given in this table shall comply with the requirements given in EN 300 for the grades OSB/2, OSB3 or OSB/4.

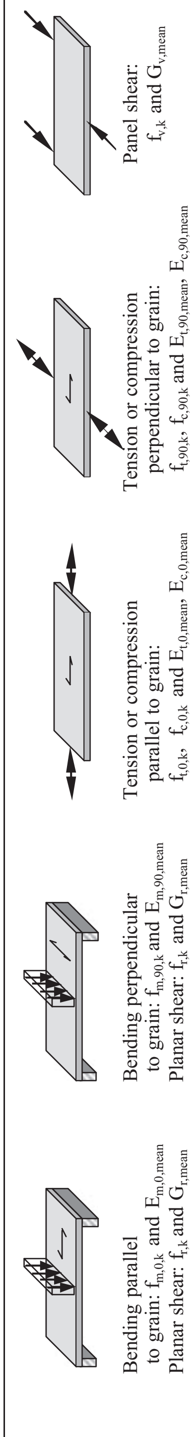

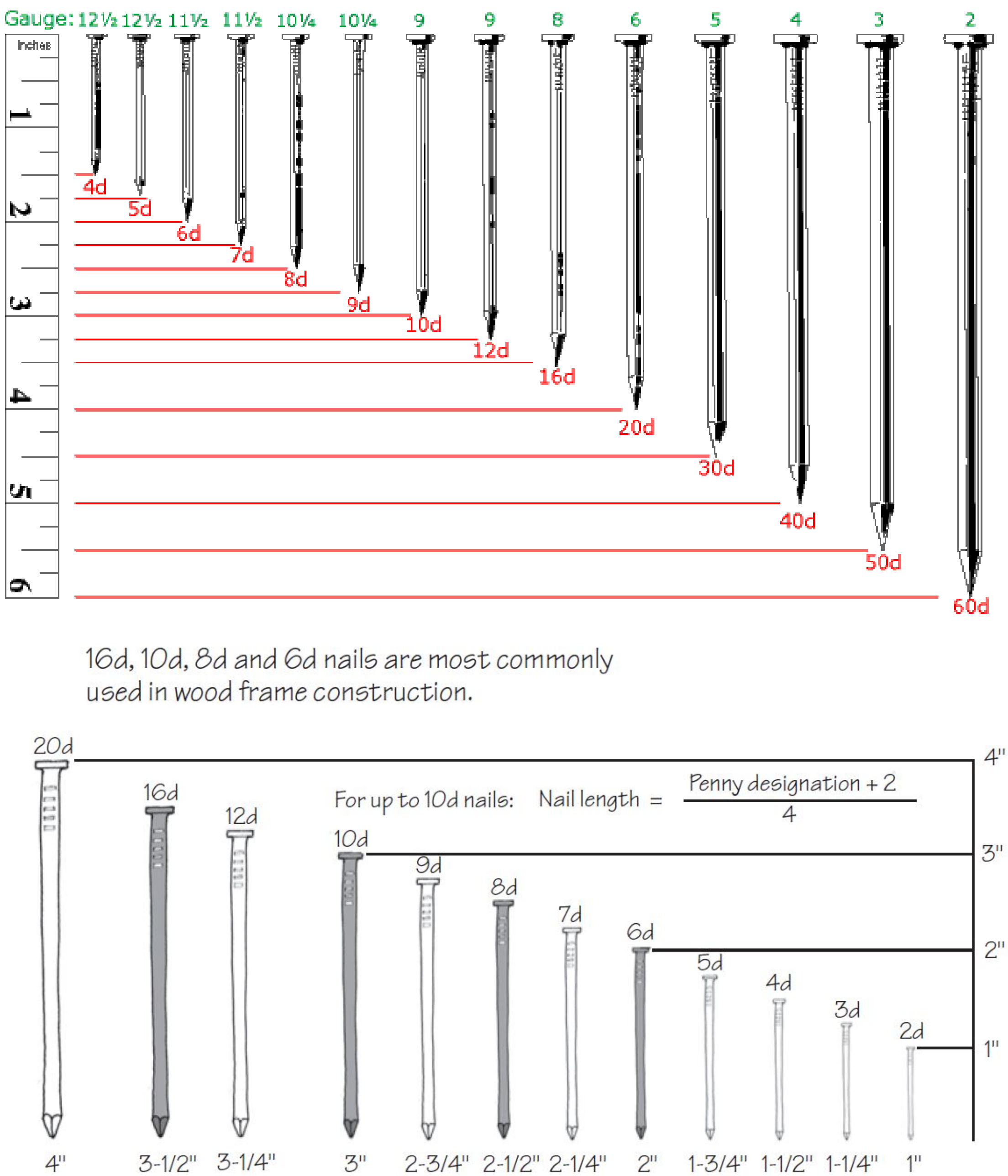

Figure 3.6. The nails sizes, according to "Penny" system: (top) sizes bigger than 20d are included; (bottom) from 2d to 20d (from [36, 41])

Nail (Penny) Size	Shank Diameter		Shank Length		Head Diameter
	Nominal [inches]	Nominal [mm]	Nominal [inches]	Nominal [mm]	Apprx. [inches]
2D	0.072	1.83	1″	25.4	3/16″
	0.083	2.11	1″	25.4	13/64″
3D	0.083	2.11	1.25″	31.8	13/64″
4D	0.109	2.77	1.5″	38.1	1/4″
5D	0.109	2.77	1.75″	44.5	1/4″
6D	0.12	3.05	2″	50.8	17/64″
8D	0.134	3.40	2.5″	63.5	9/32″
10D	0.148	3.76	3″	73.2	5/16″
12D	0.148	3.76	3.25″	82.6	5/16″
16D	0.165	4.19	3.5″	88.9	11/32″
20D	0.203	5.16	4″	101.6	13/32″
30D	0.22	5.59	4.5″	114.3	7/16″
40D	0.238	6.05	5″	127.0	15/32″
60D	0.238	6.05	6″	152.4	17/32″
	0.284	7.21	6″	152.4	17/32″

Table 3.3. Classification of nails (from [41])

The best behavior of nails is obtained if they are subjected to shear (i.e., when the load is perpendicular to the length of the nails) or when they are in compression. The withdrawal resistance is instead needed when the load is parallel to the length of the nails, trying to pull the connected members apart. Three types of nailed connections are used in wood frame constructions:

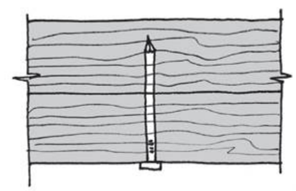

Figure 3.7. Face nailing.

- Face-nailed (Fig. 3.7);
- End-nailed (Fig. 3.8);
- Toe-nailed (Fig. 3.9).

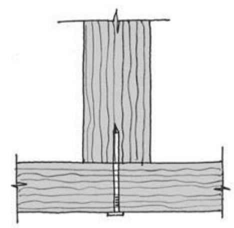

Figure 3.8. End nailing.

The first one is the strongest and has the highest withdrawal resistance. This one is function of the orientation of nails, considering the grain of wood in the holding member (which contains the tip of the nail). If the axis of nail is parallel to the grain, then the resistance is very small: this is why it is neglected. If the axis of nail is perpendicular to the grain, then the resistance is the highest. The end-nailed connection is the weakest and toe-nailed connection is used when it is not possible to have access to end nailing.

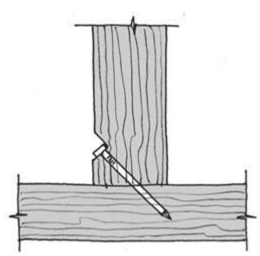

Figure 3.9. Toe nailing (from [36]).

There are two methods to drive nails into the framing members: *i)* hand-driven nailing (manual hammering) and *ii)* power-driven nailing. The latter is made through pneumatic or electric nailing guns, and is preferred because less tiring than the first method. The nails used are different in terms of dimensions: those for power-driven nailing are thinner and smaller than the corresponding pennyweight size of hand-driven nails.

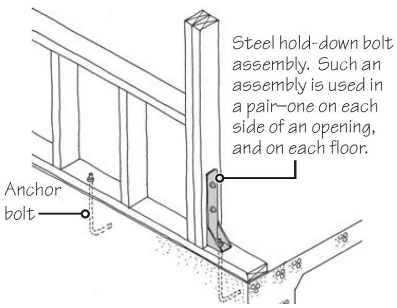

Figure 3.10. Hold-down assembly (from [36]).

3.3.2 Hold-downs

Hold downs are steel brackets placed at the bottom rails of a timber shear wall for the connection with the foundation and the upper/lower storey of a building (Fig. 3.10). Their role is to control the uplift due to the overturning in-plane action applied to the wall, which induces its rigid rotation. As well explained in [37], when the vertical load provides a stabilizing moment that contrasts the overturning moment, no tensile forces act on hold-downs and the friction block F_q is defined as follows:

$$M_{ovt} = Fh \geq M_{stb} = \frac{ql^2}{2} \tag{3.1}$$

$$F_q = \frac{ql^2}{2h} \tag{3.2}$$

Conversely, if the applied horizontal load is greater than the vertical load, the hold-downs devices are in tension and the wall deformation is linked not just to the sheathing-to-framing connections contribution but also to the rigid rotation contribution. Hold-down devices are attached to the external timber studs by means of nails that transfer the force along the vertical flange. The tensile force generated increases at each row of nails, achieving the maximum one in correspondence of the lowest row. Then, they are anchored to the foundation or upper/lower walls by means of screws and bolts that create an eccentricity, thus a moment that induces a rotation of the device. This is why the vertical plate is usually reinforced by vertical steel flanges in order to increase the resistance, or by means of the so-called *thick washer* [42].

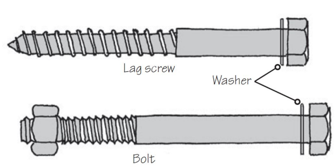

Figure 3.11. Lag screws and bolts (from [36]).

3.3.3 Screws and bolts

Building codes[1] require a minimum of $\frac{1}{2}$in.-diameter (1,27 cm) steel bolts that must be embedded at least 7 in. ($\sim$18 cm) into foundation concrete or masonry. The maximum spacing between bolts is 6 ft ($\sim$183 cm) in low-wind and nonseismic locations. The anchor bolts are required to be larger and located closer together in high-wind and seismic zones. Each sill plate length must have at least two bolts. Additionally, a bolt is required within 12 in. ($\sim$31 cm) of the end of a sill plate length. To reduce air infiltration, a compressible, fibrous felt may be placed between the sill and the foundation: this helps to seal the

[1] At the beginning: the International Conference of Building Official (ICBO, 1922); the Southern Building Code Congress International (SBCCI, 1940); the Building Officials and Code Administrators (BOCA, 1915). They merged and jointly founded the International Code Council (ICC) in 1994. Finally, the International Building Code (IBC) published in its first edition in 2000 and the International Residential Code (IRC).

gaps between the sill plate and the uneven surface of the foundation. In termite-infested areas, the use of a continuous termite shield is a good practice, in addition to using a preservative-treated sill plate.

These type of connections have a much higher withdrawal resistance than nails and are commonly used in cabinet work, furniture and for fastening door and windows in a shear wall, and to build connections to the foundation through the hold-down and the angle-brackets. A lag screw has the shank of a screw but the head of a bolt (Fig. 3.11).

4 | Timber Light-Frame shear walls: sheathing-to-framing connections

Abstract

A review about the classification of nails used for sheathing-to-framing connections and the pertinent literature is provided in this section, along with the definition of the main properties that influence the overall behavior of a timber light-frame shear wall. A summary of the mechanical models developed in the literature aims at introducing the SAWS mechanical model implemented within the parametric FE model developed by means of OpenSees, in order to simulate the behavior of a single nail.

4.1 Fasteners classification

Timber connections can be divided in two main groups, according to the mechanical transfer of load [34]:

- Metal dowel type fasteners, in which the load is transferred by dowel action (e.g., nails, screws, dowel and bolts, staples, etc.);
- Bearing-type connectors, in which the load is primarily transferred by bearing onto the timber near the surface of the member (e.g., punched metal plate, split-ring, etc.).

In timber-framed construction, nailing is the most common method used to link members. Nails are available in many types and forms. They are usually pointed and headed, bright, smooth. The wire used for their manufacturing has a circular cross-sectional area with a minimum tensile strength equal to 600 N/mm^2. Nails can be plain or enamelled, etched, electroplated, galvanized or polymer-coated, and are commonly used in framing, walls, decks, floors, roofs [34]. The performance of a nail, both under lateral and withdrawal loading, may be enhanced by mechanically deforming the nail shank to form annular ringed- or helical threaded-shank nails, so as to provide higher withdrawal resistance than plain shank nails of the same size.

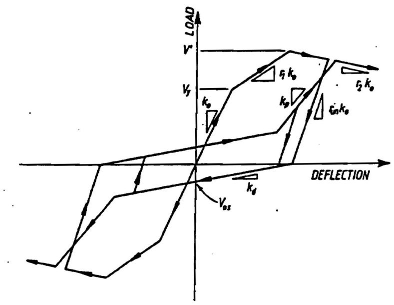

(a)

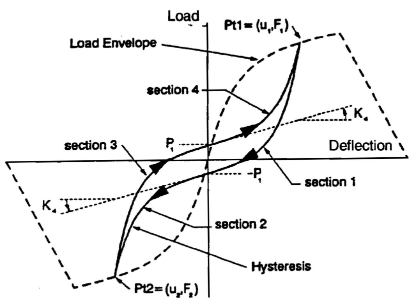

(b)

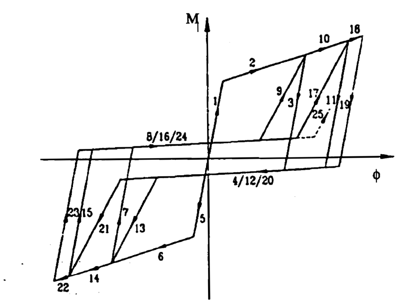

(c)

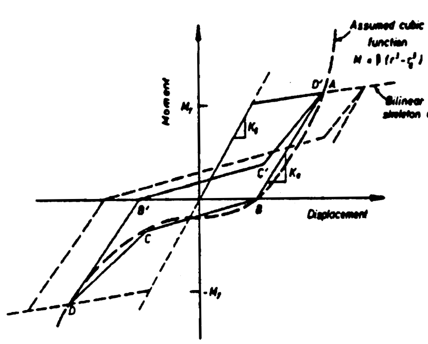

(d)

Figure 4.1. Hysteresis model proposed by: (a) Stewart (1978), (b) Dolan (1989), (c) Ceccotti and Vignoli (1990) and (d) Kivell et al. (1981) for nailed sheathing-to-framing connections (from [43]).

4.2 Background

The racking capacity of a shear wall is mainly governed by sheathing-to-framing connections, which are able to ensure a great amount of plastic deformation, thereby governing the overall shear wall behavior and the energy dissipation mechanism. As well known, yielding of nails is the ductility source in a typical timber light-frame shear wall [12]. An extended overview of nailed joints' performances has been provided by Ehlbeck [44].

Stewart [45] (Fig. 4.1, a) tested shear walls with plywood sheathing under cyclic quasi-static, sinusoidal and arbitrary dynamic loading conditions, by varying nails spacing, plywood thickness and hold-down details. Dolan [46] (Fig. 4.1, b), performed monotonic and cyclic racking tests as well as free vibration tests, and confirmed also that the larger is the nail density, the greater is the stiffness.

Numerous phenomenological hysteretic models have been proposed in the '80ies to describe the non-linear load-slip relationship of nailed connections. Among the available hysteretic models, the one proposed by Bouc and modified by Wen [47] is especially suitable for such kind of applications. Here, the hysteretic restoring force is given by a non-linear first order differential equation. Baber and Wen [48] extended the original Bouc-Wen model to take into account stiffness and/or strength degradation. Another significant improvement of the original Bouc-Wen model is due to Baber and Noori [49], who added pinching capability. Fig. 4.2 (top) shows the hysteresis cycles as function of the parameters β, γ, n that appear in the classical Bouc-Wen model. The figure 4.2 (bottom, left) illustrates the strength and stiffness degradation as function of the parameter A, which governs the tangent stiffness and the ultimate hysteretic strength. On the other hand, Fig. 4.2 (bottom, middle and right) highlights the strength and stiffness degradation governed by the strength and stiffness degradation parameters ν and η respectively.

Other researchers investigated the wood joints behavior, since it defines the overall response of a shear wall. For instance, Ceccotti and Vignoli [50] (Fig. 4.1, c) developed a hysteresis model for moment-resisting semi-rigid wood joints that accounts for pinching and stiffness degradation. Kivell et al. [51] proposed an idealized hysteresis model based on a modification of the Takeda model, by defining the end points of the lines by a cubic function that passes through the maximum deflections (Fig. 4.1, d). This model, then, has been employed for dynamic analyses of two timber portal frames with nailed beam-to-column connections. Lee [52] considered the model proposed by Polensek and Laursen [53] and performed dynamic analyses of wood wall and floor systems using the finite element method. The control

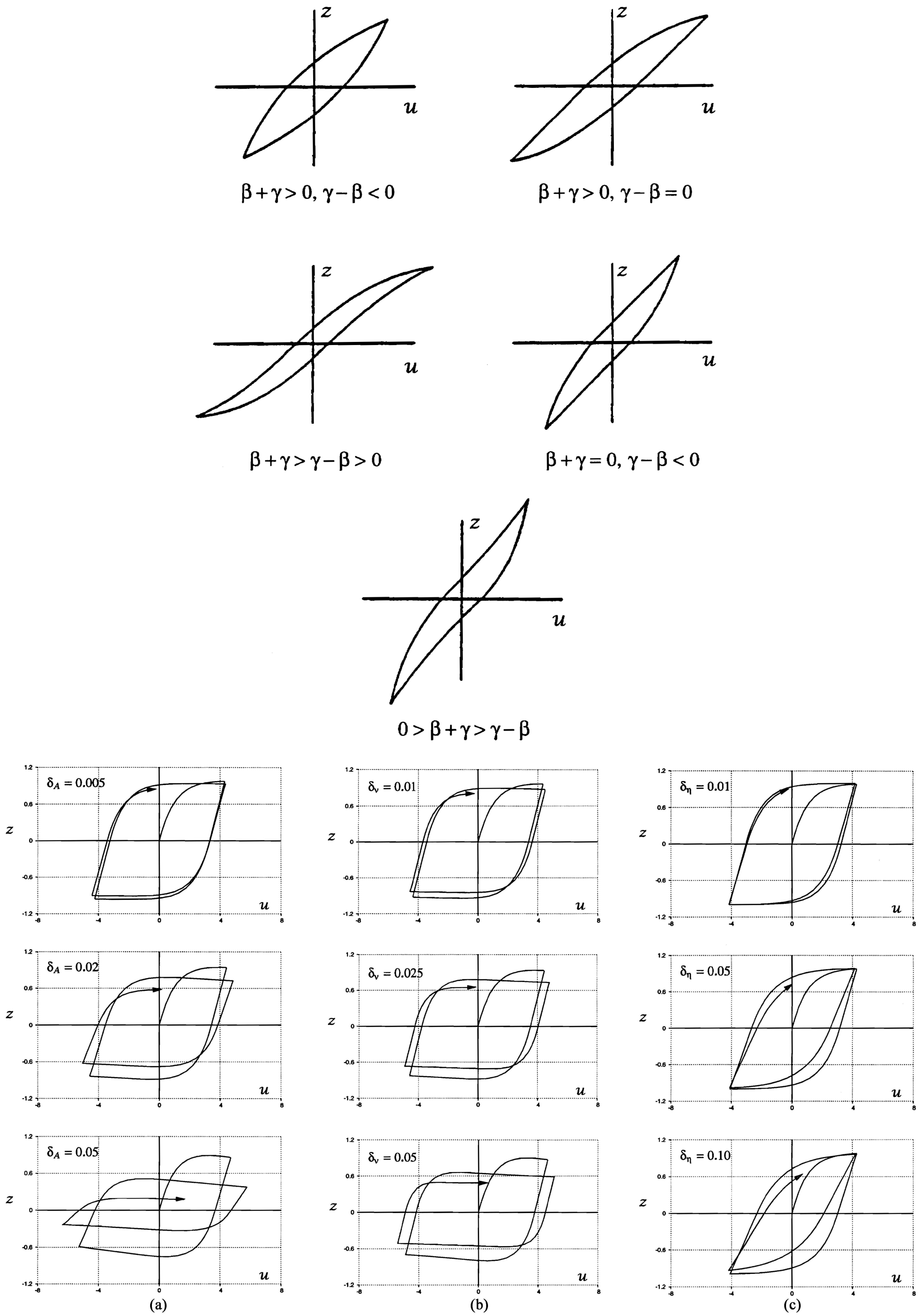

Figure 4.2. The Bouc-Wen Baber Noori hysteresis model shape, varying the mechanical parameters (from [43]).

points are here obtained using a statistical fit of test data. Finally, Chou [54] tested nailed plywood-to-wood connections under cyclic loading and investigated the experimental hysteresis cycles. Moreover, he assessed the mechanisms of load transfer through nailed joints, by conducting sensitivity studies to investigate the effect of material properties on the joint damping and stiffness. His model has a limited use in dynamic analyses of wood structural systems because the non-linear response has been approximated by a linear step-by-step approach, thus considering the sum of different linear responses under small increments of load [43].

For the sake of completeness, it is also worth mentioning the hysteresis models proposed by Sakamoto and Ohashi [55], Kamiya [56] and Miyazawa [57] (Fig. 4.3).

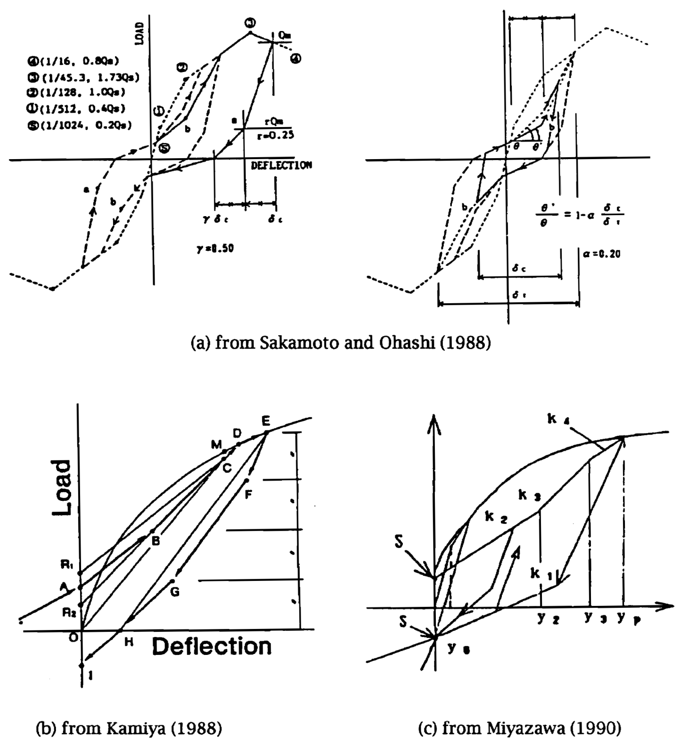

Figure 4.3. The hysteresis models proposed by the Japanese researchers (from [43]).

4.3 Mechanical behavior according to the EuroCode 5

The design rules in the EuroCode5 [20] have been developed to ensure that failure of nails subjected to lateral loading occur in a ductile rather than a brittle manner. The term *dowel* is used for a fastener that transfers load between connected members by a combination of flexure and shear and bearing in timber (embedment strength). The ductile failure theory used for connections assumes that fastener and timber or timber-based material behave as essentially rigid plastic materials. This assumption considerably simplifies the analysis. By virtue of this assumption, Johansen [58] derived the strength equations for connections formed using metal dowel type fasteners in timber, that have been slightly modified by other researchers to enhance the connection strength. These connection strength equations (Tab. 4.1) are dependent on the geometry of the connection, the embedment strength of the timber and the bending strength of the fastener, under the hypothesis that it is not withdraw from the connected members. The load-carrying capacity per shear plane per fastener $F_{v,Rk}$ is taken as the minimum value provided by these capacity equations, and is associated to the first failure mode.

One or two shear planes per fastener occur in single and double shear connections, respectively (Fig. 4.4).

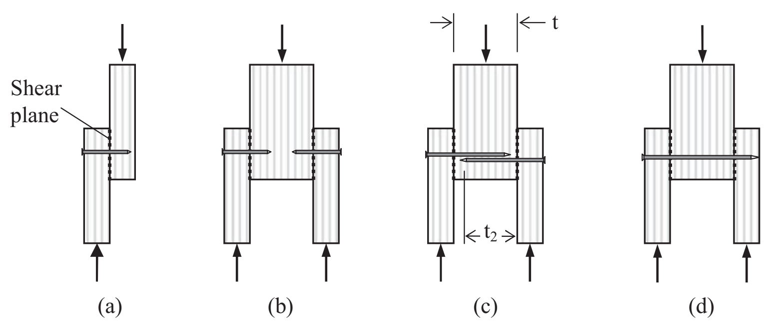

Figure 4.4. Metal dowel type fasteners loaded laterally in single and double shear (from [34]): (a) and (b) single shear with one shear plane per fastener; (c) single shear with overlapping nails; (d) double shear with two shear planes per fastener.

Particularly, the equations given for double shear connections only apply to symmetrical assemblies. The characteristic load-carrying capacity per fastener is:

$$F_{v,Rk(double-shear)} = 2 \cdot F_{v,Rk} \tag{4.1}$$

and throughout the thesis it will be identified as $F_{f,Rk}$, whereas the subscript $_v$ will be used to identify the shear wall, as in the EuroCode 5.

The characteristic fastener yield moment $M_{y,Rk}$ and the characteristic embedment strength of the connected i-th member $f_{h,i,k}$ are used in the mentioned equations listed within Tab. 4.1 .

The basic Johansen's yield equations for connections in single or double-shear can be derived using a static analysis or by means of virtual work approach commonly used in plastic analyses.

4.3.1 Characteristic yield moment of fastener

The yield moment was taken as the moment at the elastic limit of the fastener, and in the Johansen's original equations was derived from the product between yield strength and elastic modulus of the fastener, Connections in single and double shear

Failure modes

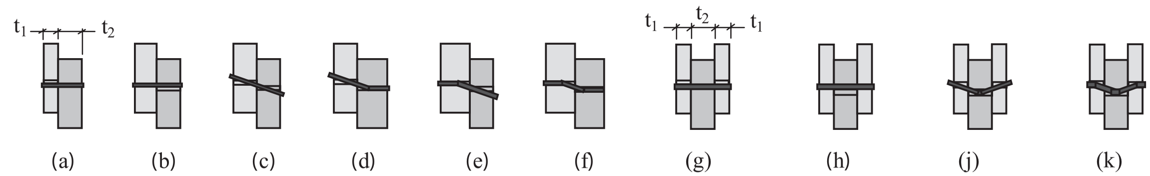

$F_{v,Rk} = f_{h,1,k} \cdot t_1 \cdot d$	mode (a)
$F_{v,Rk} = f_{h,2,k} \cdot t_2 \cdot d$	mode (b)
$F_{v,Rk} = \frac{f_{h,1,k} \cdot t_1 \cdot d}{1+\beta} \left[\sqrt{\beta + 2\beta^2 \left[1 + \frac{t_2}{t_1} + \left(\frac{t_2}{t_1}\right)^2 \right] + \beta^3 \left(\frac{t_2}{t_1}\right)^2} - \beta \left(1 + \frac{t_2}{t_1}\right) \right] + \frac{F_{ax,Rk}}{4}$	mode (c)
$F_{v,Rk} = 1.05 \frac{f_{h,1,k} \cdot t_1 \cdot d}{2+\beta} \left[\sqrt{2\beta(1+\beta) + \frac{4\beta(2+\beta)M_{y,Rk}}{f_{h,1,k} \cdot t_1^2 \cdot d}} - \beta \right] + \frac{F_{ax,Rk}}{4}$	mode (d)
$F_{v,Rk} = 1.05 \frac{f_{h,1,k} \cdot t_2 \cdot d}{1+2\beta} \left[\sqrt{2\beta^2(1+\beta) + \frac{4\beta(1+2\beta)M_{y,Rk}}{f_{h,1,k} \cdot t_2^2 \cdot d}} - \beta \right] + \frac{F_{ax,Rk}}{4}$	mode (e)
$F_{v,Rk} = 1.15 \sqrt{\frac{2\beta}{1+\beta}} \sqrt{2M_{y,Rk} \cdot f_{h,1,k} \cdot d} + \frac{F_{ax,Rk}}{4}$	mode (f)
$F_{v,Rk} = f_{h,1,k} \cdot t_1 \cdot d$	mode (g)
$F_{v,Rk} = 0.5\, f_{h,2,k} \cdot t_2 \cdot d$	mode (h)
$F_{v,Rk} = 1.05 \frac{f_{h,1,k} \cdot t_1 \cdot d}{2+\beta} \left[\sqrt{2\beta(1+\beta) + \frac{4\beta(2+\beta)M_{y,Rk}}{f_{h,1,k} \cdot t_1^2 \cdot d}} - \beta \right] + \frac{F_{ax,Rk}}{4}$	mode (j)
$F_{v,Rk} = 1.15 \sqrt{\frac{2\beta}{1+\beta}} \sqrt{2M_{y,Rk} \cdot f_{h,1,k} \cdot d} + \frac{F_{ax,Rk}}{4}$	mode (k)

Table 4.1. Characteristic load-carrying capacity per fastener per shear plane for timber-timber and timber-timber based connections (from [34]).

while in the subsequent developments the elasto-plastic strength has been used. For smooth round nails, it is computed as follows [20, eq. 8.14]:

$$M_{y,Rk} = 0.3 \cdot f_u d^{2.6} \, [Nmm] \tag{4.2}$$

while for square nails it is:

$$M_{y,Rk} = 0.45 \cdot f_u d^{2.6} \, [Nmm] \, . \tag{4.3}$$

where f_u is the characteristic tensile strength of the fastener.

4.3.2 Interface properties: embedment strength

The characteristic embedment strength of timber or timber-based material is the average compressive strength under the action of a stiff straight fastener loaded as shown in Fig. 4.5.

For a timber piece with thickness t (mm), loaded with a nail with diameter d (mm) under the maximum load F_{max}(N), the embedment strength f_h is computed as follows:

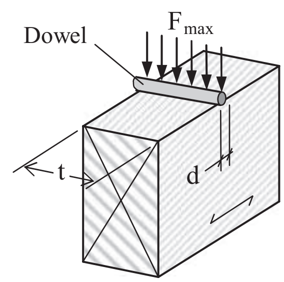

Figure 4.5. Embedment strength of timber or timber-based material (from [34]).

$$f_h = \frac{F_{max}}{d \cdot t} \left[N/mm^2 \right] \tag{4.4}$$

It is not a material property but it depends on several factor, including the type of fastener being used. To simplify the Johansen's equations, the ratio of the characteristic embedment strength of members, $f_{h,1,k}$ and $f_{h,2,k}$ is considered:

$$\beta = \frac{f_{h,2,k}}{f_{h,1,k}} \tag{4.5}$$

Timber framing elements

The embedment strength for timber and for LVL connections using nails up to 8 mm in diameter is computed as follows [20, eqs. 8.15 and 8.16]:

- without pre-drilled holes

$$f_{h,k} = 0.082 \cdot \rho_k d^{-0.3} \tag{4.6}$$

- with pre-drilled holes

$$f_{h,k} = 0.082 \cdot (1 - 0.01d) \cdot \rho_k \tag{4.7}$$

where d is the diameter of the nail (mm), ρ_k is the characteristic density of timber or LVL (kg/m^3). When using timber-to-timber or LVL and nails with the diameter greater than 8 mm, the embedment strength

$f_{h,\alpha,k}$ is dependent on the direction of the applied load (angle α) relative to the grain and it is determined using Hankinson's equations [59]:

$$f_{h,\alpha,k} = \frac{f_{h,0,k} \cdot f_{h,90,k}}{f_{h,0,k} \cdot sin^2\alpha + f_{h,90,k} \cdot cos^2\alpha} \tag{4.8}$$

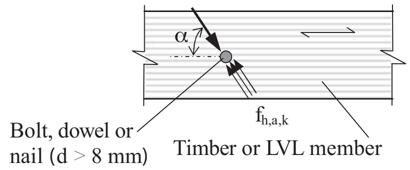

Figure 4.6. Embedment strength for a nail with $d > 8\ mm$ (from [34]).

where $f_{h,0,k}$ is the characteristic embedment strength parallel to the grain and $f_{h,90,k}$ is the characteristic embedment strength perpendicular to the grain (Fig. 4.6).

Sheathing panels

The embedment strength for panel-to-timber connections with nails having a head diameter of at least 2d and where the panel is in particleboard or OSB is computed as follows [20, eq. 8.22]:

$$f_{h,k} = 65 \cdot d^{-0.7} t^{0.1} \tag{4.9}$$

where t is the panel thickness (mm). When using nails with a diameter greater than 8 mm, for panel-to-timber connections loaded at any angle to the face grain, the embedment strength, $f_{h,\alpha,k}$, is computed as follows [20, eq. 8.37]:

$$f_{h,\alpha,k} = f_{h,k} = 50 \cdot d^{-0.6} \cdot t^{0.2} \tag{4.10}$$

4.3.3 Interface properties: withdrawal strength

For the original Johansen's yield equations, friction forces between members and characteristic withdrawal resistance of the fasteners are ignored. Conversely, they have to be properly taken into account for failure modes that involve yielding of the fasteners. Two type of frictions can be recognized:

1. friction that develop if the members are in contact on assembly;
2. friction that arises when the fastener yields and pulls the members together, in case of lateral load-induced deformation of the fasteners.

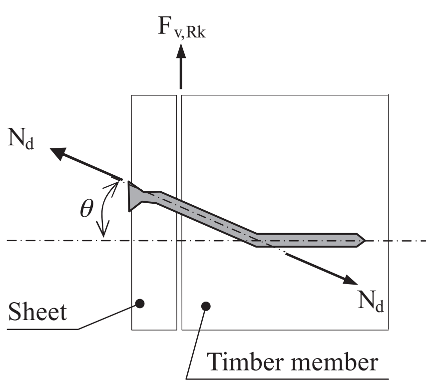

Figure 4.7. Failure mode for fastener in single shear (from [34]).

As shown in Fig. 4.7, for the latter form of friction the fastener yields and timber members allow it to rotate by an angle θ. The coefficient of friction between timber framing element and sheathing panel is μ. Thus, the fastener is subjected to bending along with to a tension force N_d, due to the withdrawal effect during loading. This force has a vertical component $N_d sin\theta$ and a horizontal component $N_d cos\theta$, the latter compressing the sheet onto the timber thereby inducing an additional vertical resistive force $\mu N_d cos\theta$. The force in the fastener is computed as follows:

$$F_{f,Rk} = N_d(sin\theta + cos\theta) + F_{fy,Rk} \tag{4.11}$$

where $F_{fy,Rk}$ is the Johansen's yield load for the joint. The component $N_d sin\theta$ is accounted in failure modes equations by means of the quantity $F_{ax,Rk}/4$, where $F_{ax,Rk}$ is the fastener's characteristic withdrawal capacity. The final expression of the load carrying capacity of a fastener is:

$$F_{f,Rk} = \mu \cdot F_{fy,Rk} + F_{ax,Rk}/4 \tag{4.12}$$

The values used for the friction factor are 5% when the fastener partially yields (e.g., modes (d) and (e)) and 15% when it fully yields (e.g., mode (f)), and the factor 1.05 or 1.15 incorporates this effect in equations related to these failure modes. The latter contribution is commonly called rope effect, and is equal to:

- 15% for round nails;
- 25% for square nails;
- 50% for other nails;
- 100% for screws;
- 25% for bolts;
- 0% for dowels.

As reported in [20, §8.2.2(2)] *"If $F_{ax,Rk}$ is not known then the contribution from the rope effect should be taken as zero"*.

4.4 Mechanical model of fastener

4.4.1 Definition of lateral stiffness at the SLS and ULS into the EuroCode 5

When members of a structural system are jointed by means of mechanical fasteners, their slipping under lateral load has to be considered. The amount of slip varys depending on the fastener type and embedment strength of timber members. The stiffness of a fastener is defined as the ratio of the lateral load per shear plane divided the slip, and the EuroCode 5 provides equations to compute the slip modulus K_{ser} for SLS and K_u for ULS (Fig. 4.8).

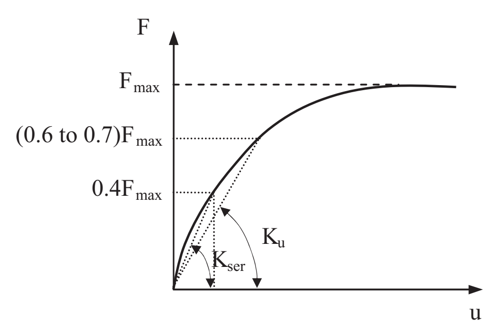

Figure 4.8. Typical load-slip behavior of a nailed connection (from [34]).

The term K_{ser} is assumed to be the secant modulus of the load-displacement curve at a load level of appproximately 40% of the maximum load, and it is computed differently according to the type of fastener as shown in Tab. 4.2 where d is the diameter of the fastener (mm) whreas ρ_m is the mean density of the timber or timber-based product used in the structural system.

Table 4.2. Values for K_{ser} for fasteners in timber-to-timber and wood-based panel-to-timber connections (from [20, Table 7.1]).

Type of fastener used	Serviceability limit state slip modulus K_{ser}
Nails	
Without pre-drilling	$\rho_m^{1.5} d^{0.8}/30$
With pre-drilling	$\rho_m^{1.5} d/23$
Staples	$\rho_m^{1.5} d^{0.8}/80$
Screws	$\rho_m^{1.5} d/23$
Bolts with or without clearance†	$\rho_m^{1.5} d/23$
Dowels	$\rho_m^{1.5} d/23$

† The clearance should be added separately to the deformation.

If the connection joins member of different densities, ρ_{m1} and ρ_{m2}, then the total mean density can be computed as follows [20, eq. 7.1]:

$$\rho_m = \sqrt{\rho_{m1} \cdot \rho_{m2}} \tag{4.13}$$

For ULS, the slip modulus K_u is assumed to be the secant modulus of the load-slip curve at a load between 60% and 70% of the maximum capacity, and is computed as follows:

$$K_u = \frac{2}{3} K_{ser}. \tag{4.14}$$

The main limit of this approach is that the equations provided by the EuroCode 5 (Tab. 4.2) do not take into account important parameters such as type of nail, thickness of the timber and timber-based elements, failure mode, type of steel [60].

4.4.2 Mechanical models in literature

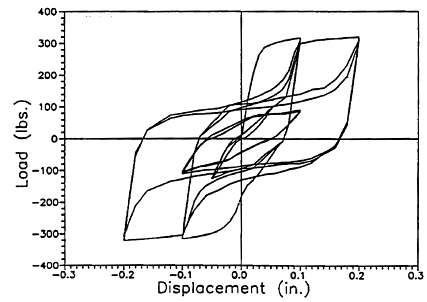

Figure 4.9. Hysteresis model proposed by Foschi and associates (UBC 1993) for wood joints with dowel-type fasteners (from [43]).

The most famous mechanical model, which is also used in this work, has been originally proposed by Foschi [61] for a nail considered as an elasto-plastic beam on a non-linear foundation, that is the wood support, keeping track of the gap between the beam and the support during load cycling (Fig. 4.9). This model has been validated by means of cyclic testing of nails driven into spruce wood. These experimental tests have been also used to estimate the model parameters [43].

The model is expressed as follows:

$$F_n = (P_0 + K_1\delta)\left[1 - exp\frac{-K_0\delta}{P_0}\right] \tag{4.15}$$

where K_0 and K_1 are the initial and post-yield stiffness of the connection, respectively, whereas P_0 is the load-intercept of the post-yield stiffness asymptote (Fig. 4.10)

Dolan [46] modified the Foschi's equation by adding the post-capacity degradation slope:

$$F_n = (P_0 + K_1\delta)\left[1 - exp\frac{-K_0\delta}{P_0}\right] - K_2(\delta - \delta_{peak}) \tag{4.16}$$

where K_2 is used to define the slope for deformations greater than δ_{peak} (Fig. 4.10).

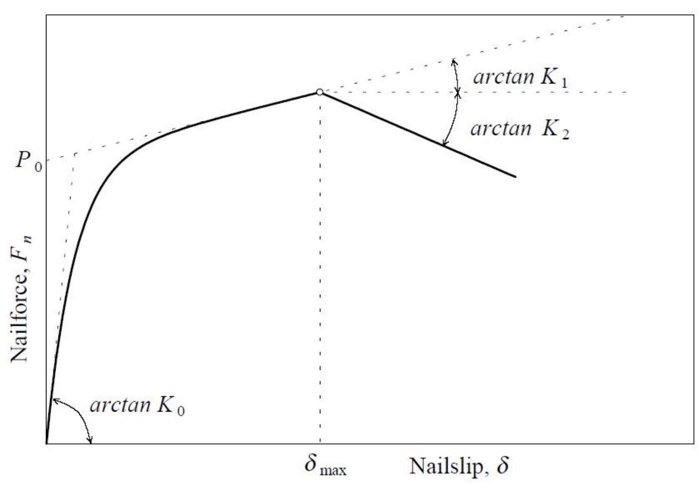

Figure 4.10. Modified Foschi load-slip curve by Dolan 1989 (from [12]).

The experimental study on a single fastener by Patton-Mallory and McCutcheon [62] have shown that the asymptotic fastener curve fitting (Fig. 4.11) produces the best predictions of shear wall performance up to the peak loads:

$$F_n = \frac{A_0\delta}{A_1 + \delta} \tag{4.17}$$

where A_0 represents the asymptotic strength of the connection whereas A_1 is the slip at one half the asymptotic strength.

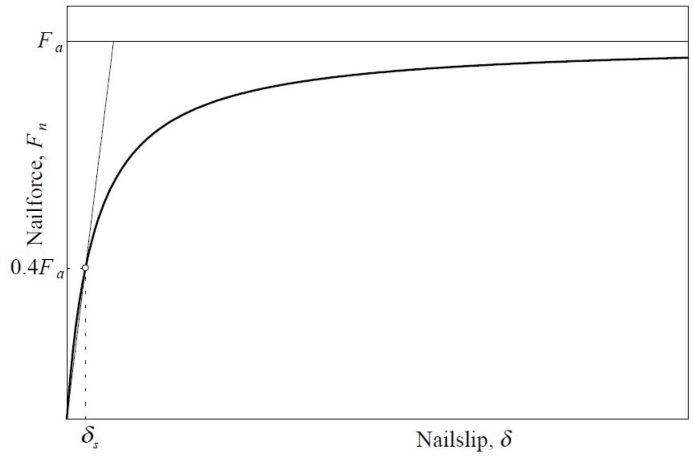

Figure 4.11. Asymptotic approximation of load-slip curve (from [12]).

5 | Timber Light-Frame shear walls: review of seismic analysis and design methods

Abstract

Once the elements of a timber light-frame shear wall are described, a state of art review about the mechanical behavior of the assembly is here presented. The review of seismic analysis and design methods used in literature and in the EuroCodes is provided in order to introduce the strategy adopted to develop the FE model and the analytical procedure for predicting the wall behaviour. The assessment of the equivalent viscous damping and the estimation of the damping factor η are intended in order to exploit both the force-based and the Direct Displacement Based Design design methods. The theory about the mechanical behaviour considering both rigid and flexible framing elements is described, then showing how it is employed within the EuroCode 5.

5.1 Seismic Hazard

Seismic risk is determined by the combination of *hazard*, *vulnerability* and *exposure* and is the measure of the expected damage in a given time interval, taking into account seismicity, building resistance and anthropization. Generally speaking, hazard is defined in terms of frequency and intensity of the seismic phenomena; the vulnerability is expressed as the fragility of the considered construction while the exposure can be quantified using several socio-economic parameters. More precisely, the seismic hazard is defined as the probability that an earthquake can exceeds a given intensity (typically the peak ground acceleration Pga within a given area and in a certain time interval).

In Italy, during the 19th century, with the development of seismological sciences, researches about causes and geographical distribution of earthquakes began to be available. The spread of seismic instruments from the late 19th century and monitoring networks in the 20th century gave the definitive impulse to map the seismic hazard over the national territory.

The studies about the seismic hazard have been employed, especially in recent years, for territorial and regional analyses targeted at the zonations (Fig. 5.1) (basic hazard for the seismic classification) or microzonations (Fig. 5.2) (local hazard). In the latter case, hazard assessment is intended to identify the areas on a municipal scale that, in case of a seismic event, may be subjected to amplification phenomena.

The seismic vulnerability is the propensity of a structure to suffer damage levels, given a seismic event with a certain intensity. Today, the regulations for buildings in earthquake zones are conceived in such a way that new or retrofitted buildings are not damaged by low-intensity earthquakes, do not experience severe structural damages under earthquakes with medium intensity and do not collapse during strong earthquakes, even though they may suffer serious damages. The Limit States (LS) defined by most of the existing codes are the following:

- Serviceability Limit States, in which the damage must be limited and structures relevant for civil protection must remain operational (probability of exceedance during the reference period are 81% for Operativity LS and 63% for Damage LS);

- Ultimate Limit States, in which the main concern is the protection of the human lives (probability of exceedance during the reference period are 10% for Life Safety LS and 5% for Collapse LS).

5.2 Direct Displacement Based Design (DDBD)

The procedure so-called Direct Displacement Based Design (DDBD) is based on the concept of the substitute structure proposed by Shibata and Sozen [65], i.e. the real structural system is represented by an equivalent SDOF, a substitute linear system with an appropriate stiffness and viscous damping combination that best reproduces the response of the inelastic system at the performance level under investigation (Fig. 5.3).

The fundamental concept is to design a structure in order to achieve a performance level under the design seismic action. The steps that have to be followed are well described in [66]:

1. selection of a target displacement (Δ_d) of the structure based on the performance level to be reached;

2. calculation of the viscous damping factor to be used to reduce the elastic response spectra, which is strictly related to the structure ductility;

3. the effective period of the structure can be estimated for the target displacement and the reduced design spectrum corresponding to the obtained equivalent viscous damping level;

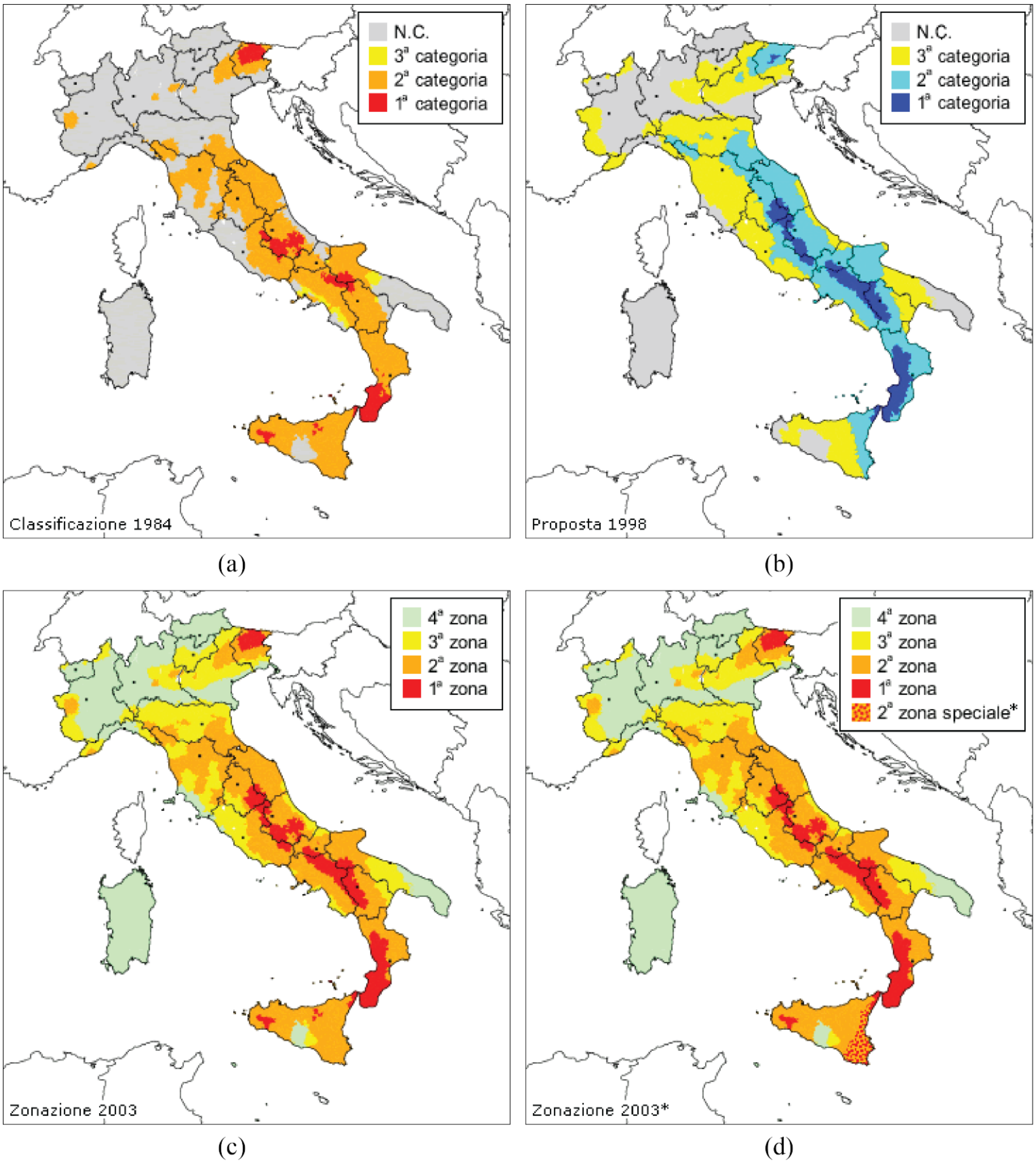

Figure 5.1. Italian seismic zonation evolution: (a) Decree MLP 14/07/1984; (b) 1998; (c) OPCM 3274, 20/03/2003; (d) Seismic zones until 2004, March, with variations for Regions (from [63]).

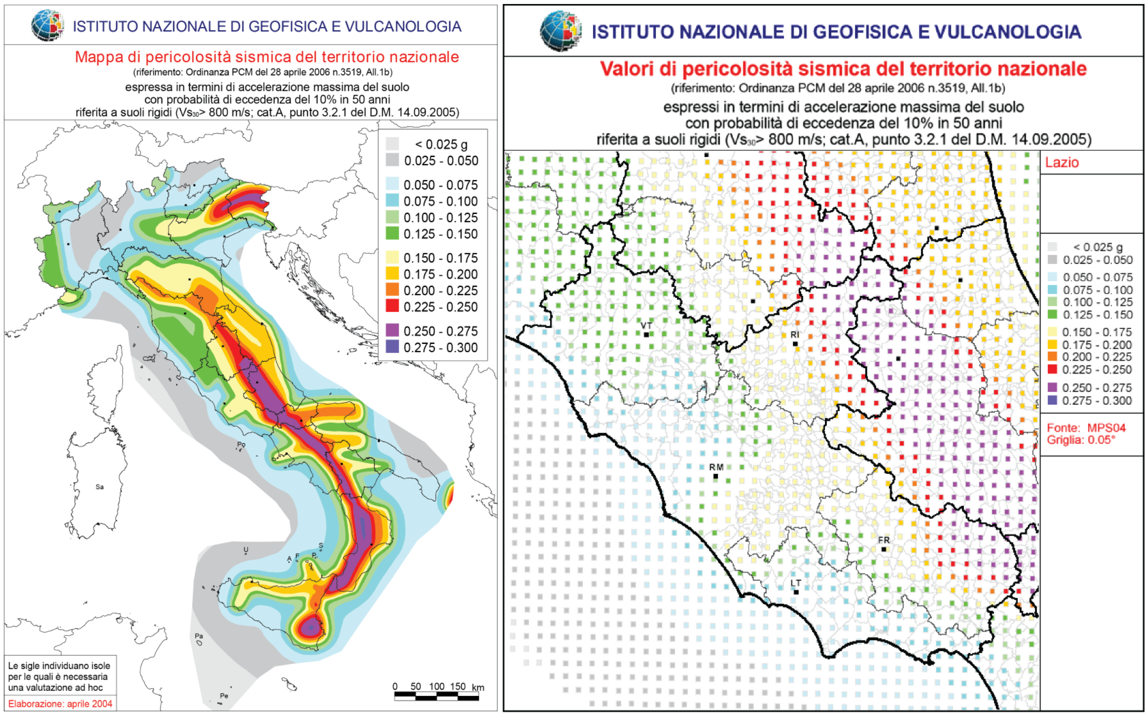

Figure 5.2. Italian microzonation (from [63]).

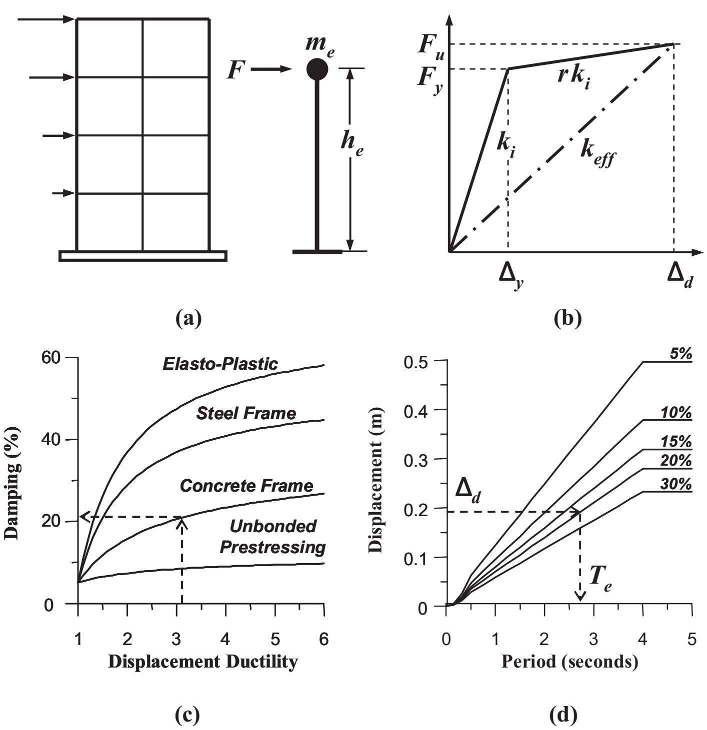

Figure 5.3. Fundamentals of Direct Displacement-Based Design (from [64]).

4. from the effective period, it is possible to obtain the effective stiffness of the equivalent single-degree-of-freedom (SDOF) system as follows:

$$K_{eff} = 4\pi^2 m_e / T_e^2 \tag{5.1}$$

where m_e is the effective mass of the structure participating in the fundamental mode of vibration (Fig. 5.4).

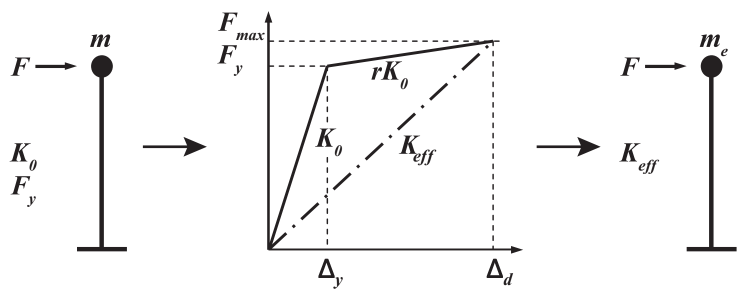

Figure 5.4. The process to define the substitute structure.

Thus, the design lateral force is obtained as follows:

$$F = V_B = K_{eff} \cdot \Delta_d \tag{5.2}$$

where Δ_d is the target displacement amplitude.

5.3 Equivalent viscous damping

The first proposal to model the inelastic behavior of a structural system by means of a parameter proportional to velocity has to be ascribed to Jacobsen [67], who approximated the non-linear frictional behavior to a power of velocity. This has been used initially to compute the response of a SDOF system when subjected to sinusoidal loads. Then, other researchers such as Housner [68] carried out some investigations to extent the concept to other hysteretic systems.

The total equivalent viscous damping, ξ_{tot}, is considered in many equations proposed by different authors such as Rosenblueth and Herrera [69] and Iwan [70], which is obtained by adding the inherent viscous damping, ξ_{in} (assumed equal to 5%):

$$\xi_{tot} = \xi_{in} + \xi_{eq} \tag{5.3}$$

where ξ_{in} is the initial damping due to the energy dissipation of the structure in the elastic range. Additionally, ξ_{eq}, also indicated as ξ_{hyst}, corresponds to the equivalent viscous damping ratio that represents energy dissipation attributable to the hysteretic behavior of the structural system.

The equivalent viscous damping ξ_{eq}, as suggested by EN 12512 [71], is a quantity that can be used to calculate the reduced design seismic actions so as to allow for the energy dissipation ensured by the structure [66]. It is obtained equating the energy dissipated by a viscous damper and the one dissipated from non-linear behavior:

$$\xi_{eq} = \frac{1}{4\pi} \cdot \frac{\omega_n}{\omega} \cdot \frac{E_D}{E_{s0}} \tag{5.4}$$

where $E_D = \int F_d du$ is the energy dissipated in one hysteresis cycle, F_d is the damping force and E_{s0} is the available potential energy to failure, also known ad the maximum strain energy of system [72] or stored energy [67]. In order to use this approach, both systems are assumed to be subjected to a harmonic excitation:

$$m\ddot{u} + c\dot{u} + ku = p_0 sin\omega t \tag{5.5}$$

where ω is the frequency of the load and t is the time. The solution of this differential equations has two parts, and the one that represents the stationary vibrations (steady-state vibrations) is taken into account as follows:

$$u(t) = u_0 sin\left(\omega t - \phi\right) \tag{5.6}$$

$$\phi = tan^{-1} \frac{2\xi\left(\frac{\omega}{\omega_n}\right)}{1 - \left(\frac{\omega}{\omega_n}\right)^2}$$

The stored energy is represented as the area inside the hatched triangle in the first quadrant (Fig. 5.7):

$$E_{s0} = \frac{ku_0^2}{2} \tag{5.7}$$

Starting from eq. (5.6), the velocity can be obtained as follows:

$$\dot{u} = \omega u_0 cos\left(\omega t - \phi\right) \tag{5.8}$$

The energy dissipated by the damper is:

$$\begin{aligned} E_{Dd} &= \int c\dot{u}dx = \int c\dot{u}^2 dt = \\ &= c\omega^2 u_0^2 \int_0^{\frac{2\pi}{\omega}} cos^2\left(\omega t - \phi\right) dt = \pi c\omega u_0^2. \end{aligned} \tag{5.9}$$

Noting that, at resonance, $\omega = \omega_n = \sqrt{\frac{K}{M}}$ and $C = 2\xi\sqrt{KM}$:

$$E_{Dd}(\omega_n) = 2\xi\pi K u_0^2 \tag{5.10}$$

$$\dot{u} = \pm\omega u_0 \sqrt{1 - sin^2\left(\omega t - \phi\right)} = \pm\omega\sqrt{u_0^2 - u^2} \tag{5.11}$$

Rearraging the expression of the damping force, the ellipse equation is obtained (Fig. 5.5):

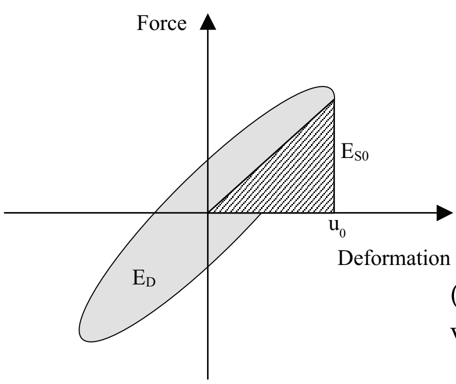

Figure 5.5. Dissipated and stored force for inherent damping (from [66]).

$$\left(\frac{F_d}{c\omega u_0}\right)^2 + \left(\frac{u}{u_0}\right)^2 = 1 \tag{5.12}$$

Hence, the inherent viscous damping is obtained substituting eq. (5.7) in eq. (5.10) obtaining the following expression of the inherent viscous damping:

$$\xi_{in} = \frac{E_{Dd}}{4\pi E_{s0}} \tag{5.13}$$

The equivalent viscous damping, corresponding to the hysteretic damping, is similarly computed as follows (Fig. 5.6):

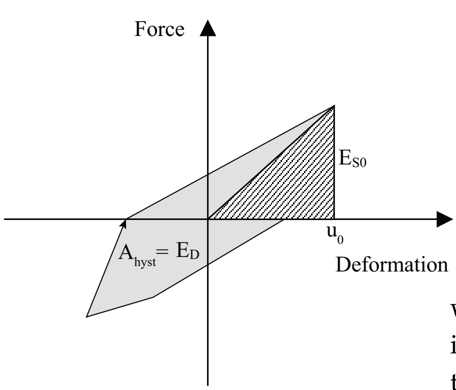

Figure 5.6. Definition of E_D and E_{S0} to determine the equivalent viscous damping of a structure (from [66]).

$$\xi_{eq,hyst} = \frac{A_{hyst}}{2\pi F_{max} u_0} \tag{5.14}$$

where $A_{hyst} = E_D$ is the area enclosed in a hysteretic loop which has its characteristics and shape according to the considered structural system.

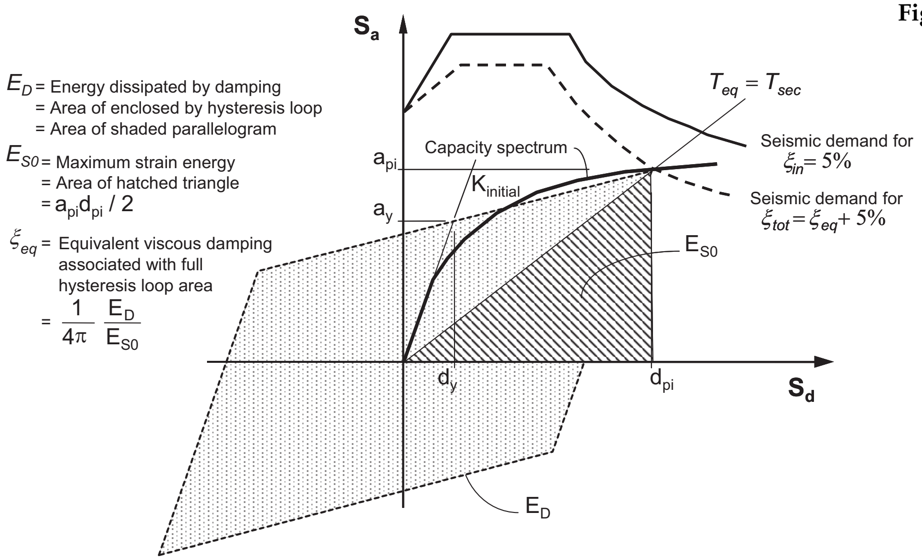

Figure 5.7. Definition of E_D and E_{S0} to determine the equivalent viscous damping of a structure, in ADRS domain (from [73]).

The reduced spectrum is then obtained by using the damping correction factor η, which is computed as follows [21]:

$$\eta = \sqrt{\frac{10}{5 + \xi_{tot}}}. \tag{5.15}$$

5.4 Inelastic demand spectra: Capacity Spectrum and N2 Methods

Usually, the dissipative capacity or ductility of a structure is analyzed by reducing the elastic spectrum, defined according to the hazard at the site. This is usually done by applying two different methods, namely: the Capacity Spectrum Method [74, 75] and the N2 method [76]. The first method takes into account the hysteretic behavior of the structure, applying a suitable damping factor obtained as described in Sec. 5.3. Conversely, with the latter the inelastic spectrum is obtained from the elastic one by using the behaviour factor q_μ, which is computed as follows:

$$\begin{cases} q_\mu = 1 + (\mu - 1)\,\frac{T}{T_C} & T < T_C \\ q_\mu = \mu & T \geq T_C \end{cases} \tag{5.16}$$

where $\mu = \delta_u / \delta_y$ represents the ductility ratio of the structure, T is its natural vibration period and T_C is the value of the natural vibration period at the end of the constant acceleration plateau of the elastic and design spectra. Note that q_μ is different from the q-factor defined by the EuroCode 8 [21] and Italian code [30], which also takes into account the over-strength of the structure q_s as follows:

$$q = q_\mu q_s. \tag{5.17}$$

For the considered typology of structure ("nailed wall panels with nailed diaphragms, connected with nails and bolts"), its upper limit value is equal to 5 [21, table 8.1].

5.5 Ductility of timber structures

The concept of ductility for timber structures is crucial, because reaching large displacements without losing too much strength is hard for timber, unless proper reinforcements are implemented. The definitions of ductility can be grouped as relative and absolute (Fig. 5.8).

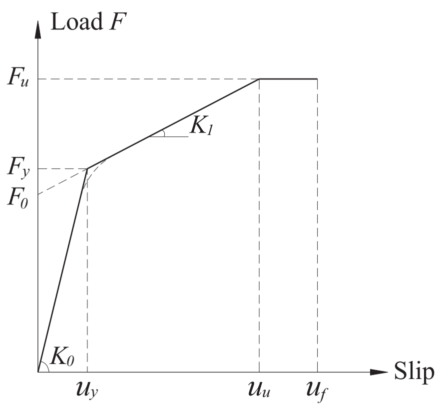

Figure 5.8. Definition of ductility by Stehn and Björnfot (from [15]).

The relative definitions are the following:

$$D_f = \frac{u_f}{u_y} \tag{5.18}$$

$$D_u = \frac{u_u}{u_y} \tag{5.19}$$

$$C_u = \frac{u_u - u_y}{u_u} \tag{5.20}$$

$$C_f = \frac{u_f - u_y}{u_f} \tag{5.21}$$

$$D_{f/u} = \frac{u_f}{u_u} \tag{5.22}$$

$$D_{s/u} = \frac{K_0}{F_1} u_u \tag{5.23}$$

$$D_{s/f} = \frac{K_0}{F_1} u_f \tag{5.24}$$

whereas the absolute definitions are the following:

$$D_{uy} = u_u - u_y \tag{5.25}$$

$$D_{fy} = u_f - u_y \tag{5.26}$$

$$D_{fu} = u_f - u_u \tag{5.27}$$

$$E_u = \int_{u=0}^{u=u_u} f(F,u)du \tag{5.28}$$

$$E_f = \int_{u=0}^{u=u_f} f(F,u)du \tag{5.29}$$

Some of definitions need the computation of the so-called yield slip u_y, which is determined in several ways according to different documents and codes, as discussed in [77]. The ductility definition can be obtained by means of experimental curve or approximate one, for example using the method proposed by Foschi [78] or the Equivalent Energy Elastic-Plastic (EEEP) method [24, 79], which often results in unrealistic values according to Muñoz et al. [77]. For this method, the elastic stiffness is equal to $0.4F_u/u_{0.4F_u}$ whereas the failure displacement is defined where the resistance force drops to $0.8F_u$, being F_u the peak resistance.

For timber shear walls, a linear-elastic analysis is adopted for the design of timber framing elements. Specifically, a linear elastic analysis is performed for the calculation of the load effects in the structural members and for the strength evaluation of their cross-sections. This is the only design method currently recommended in the EuroCode 5 [20]. As well described in [15], fully plastic analysis methods by means of limit analysis theorems for direct assessment of the ultimate load can be applied in timber structures made of members connected with ductile, rigid and semi-rigid connections: the plasticity is concentrated in the connections whereas the timber framing members are inherently brittle and should be over designed (Capacity Based Design [80], Fig. 5.9).

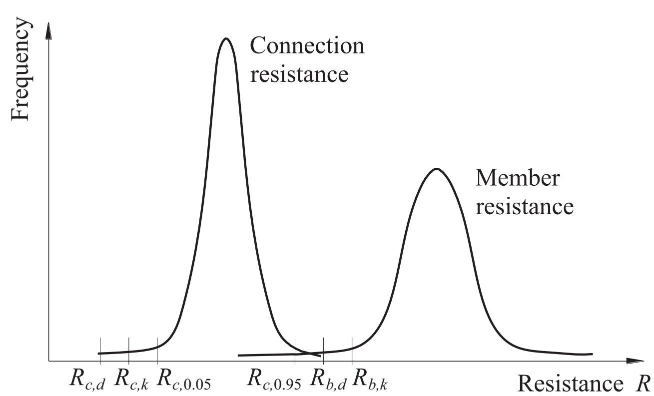

Figure 5.9. The over-strength concept.

To ensure the plasticization of the ductile elements (connections) an over-strength factor should be defined as follows:

$$R_{b,d} \geq \gamma_{Rd} \cdot R_{c,d} \tag{5.30}$$

where $R_{b,d} = k_{mod} \cdot R_{b,k}/\gamma_M$ indicates the design strength capacity of the timber member, $R_{c,d} = k_{mod} \cdot R_{c,k}/\gamma_M$ identifies the design strength capacity of the connection member, k_{mod} is the modification factor linked to the load duration and timber moisture content, and γ_M is the partial safety factor of member. The over-strength ratio, $\gamma_{R,d}$, is given by:

$$\gamma_{Rd} = \frac{R_{c,0.95}}{R_{c,d}} = \frac{R_{c,0.95}}{R_{c,0.05}} \cdot \frac{R_{c,0.05}}{R_{c,k}} \cdot \frac{R_{c,k}}{R_{c,d}} = \gamma_{sc} \cdot \gamma_{an} \cdot \gamma_M \tag{5.31}$$

where $R_{c,0.95}$ and $R_{c,0.05}$ identify the 95^{th} and 5^{th} percentile of the connection strength distribution, respectively. The characteristic values $R_{c,k}$ and $R_{b,k}$ are determined based on theoretical considerations, e.g. using the European yielding model (EYM) [58] for connections with dowel-type fasteners and considering the characteristic embedding strength of timber and yield moment of fastener for connection, whereas characteristic bending strength of timber for the beam member.

5.6 Mechanical behavior and modeling of Timber Light-Frame shear walls: state of art

A large deal of researches on timber shear walls has been performed in the last decades. In fact, researches on mechanical performances dates back to 1927 [81].

As pointed out by Porteous and Kermani [34], platform framed walls can be classified in two categories:

- stud walls;
- racking walls.

The first category includes walls that are intended for carrying vertical loads only with a sheathing panel that, if inserted, provides additional strength only to the studs against in-plane and out-of-plane axial buckling. Conversely, the walls belonging to the second category are designed to withstand also in-plane lateral actions by means of the sheathing-to-framing connections.

Generally, a light-framed timber shear wall is an integrated system that should withstand different static, quasi-static and dynamic loads (i.e., vertical loads, horizontal actions induced by wind and earthquake, thermal loads, etc., Fig. 5.10).

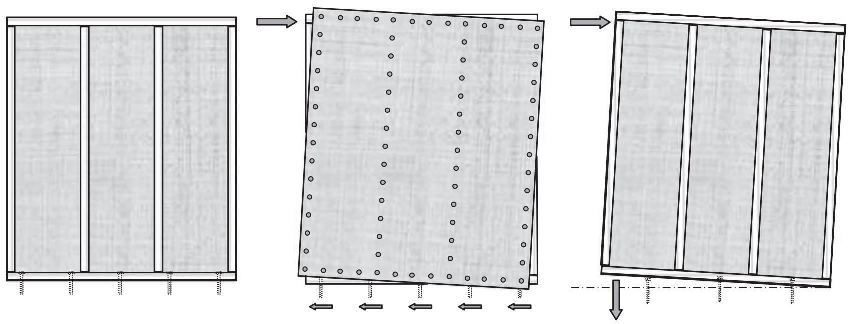

Figure 5.10. Wall diaphragm resisting loads (from [34]).

It is built by assembling vertical studs and horizontal joists, which are connected at their ends with internal constraints that, typically, are considered acting as hinges. The frame is then braced with a sheathing panel on one or both sides connected by means of metal fasteners (e.g., nails, screws or staples). A typical configuration of this wall is shown in Fig. 5.12. Further layers are usually included to provide good thermal insulation performances as well as fire and vapor resistance. The dimensions of the frame depend on the size of the panel used to sheath it, which can be made using different materials like Oriented Strand Board (OSB), ply-wood, gypsum, Glued Laminated Guadua (GLG) bamboo [38], ply-bamboo, fibreboard, and so on. Commonly, as pointed out by Wang et al. [7], the size of a shear wall is 1.22 m × 2.44 m or 2.44 m × 2.44 m, whereas the framing elements (joists and studs) cross-sections are about 38 mm × 89 mm and 38 mm × 140 mm for internal and external wall studs, respectively. Also 80 mm × 160 mm, 120 mm × 160 mm, 120 mm × 200 mm, 140 mm × 160 mm and 160 mm × 200 mm sizes are used in Italy and in Alpine area Countries [26]. The cross-section size of external framing elements is often chosen to accommodate minimum building requirements for thermal insulation.

Generally, common nails with thick shank that gives greater strength, are employed for framing connections. The sizes mostly used are 6D, 8D and 10D, according to the Penny system classification used in the United States. The nails are placed both on the perimeter studs (typically with spacing equal to 50, 75, 100 mm) and on the intermediate studs, where they are two or three times spaced with respect to the nails placed on the perimeter studs.

Källsner and Girhammar [82] pointed out that their presence on the intermediate studs does not increase substantially the racking capacity of the wall, but avoids buckling phenomena of the sheathing panel. According to the connection mode with the foundation, the racking walls are often classified in two main categories [12]:

- fully anchored walls;

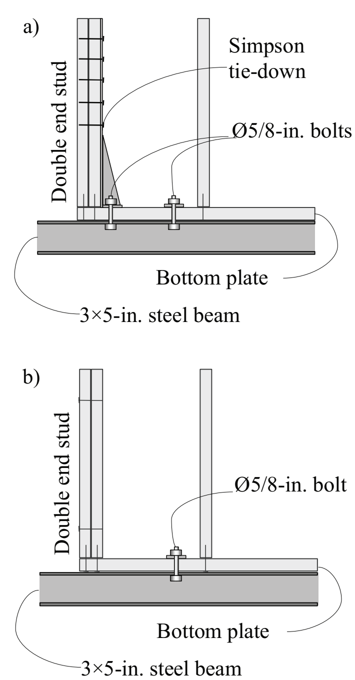

Figure 5.11. Overturning restraint details: a) fully-anchored walls; b) partially-anchored walls (from [12]).

- partially anchored walls.

The walls belonging to the first category are prevented from lifting, when subjected to a lateral load whereas, for the second category, resistance against lifting is ensured by the fixing between the sheathing and the bottom joist as well as between the bottom joist and the support structure (Fig. 5.11).

In a typical timber framed building, timber shear walls are considered to be subjected to horizontal loads, also known as racking loads.

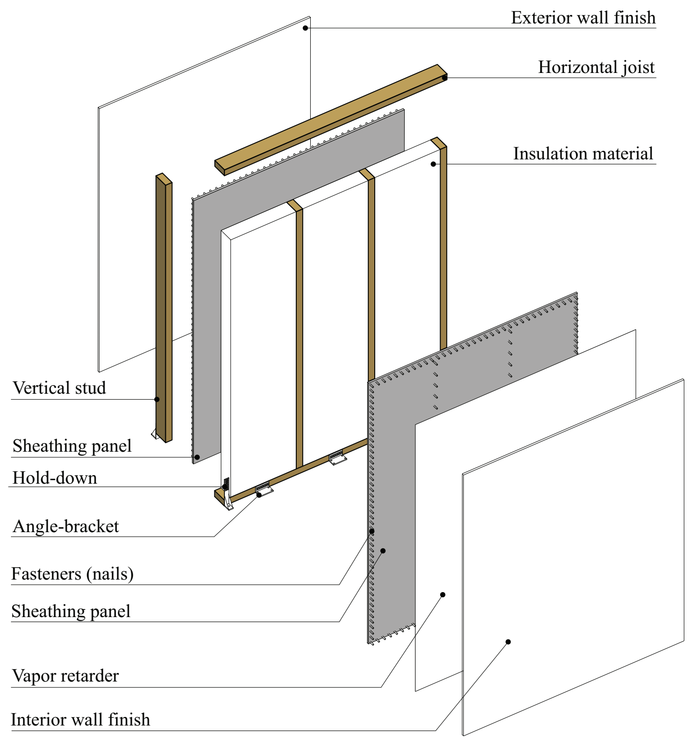

Figure 5.12. A typical configuration of a fully anchored timber shear wall braced on both sides, with further layers to improve thermal performances and fire-vapor resistances.

A large number of studies on the racking resistance, stiffness and ductility using experimental, numerical and analytical methods demonstrated the good mechanical performances of light frame wall assemblies. Particularly, the experimental tests demonstrated that the structural behavior of the shear wall is mainly influenced by the connections, such as sheathing-to-framing joints [83–85], base [86] and stud-joist joints [84]. Metal fasteners (e.g. nails, screws or staples) are used to connect the timber frame with the sheathing panel, which is subjected to in-plane shear force.

The uplift of the shear wall subjected to a horizontal upper force, due to its rigid rotation, is controlled by hold-downs, while its rigid translation is prevented by the angle-brackets [37, 83] (Fig. 5.12).

5.6.1 Modeling considering rigid framing elements

As regards the response of wall components, it has been pointed out by Folz and Filiatrault [87] that elastic in-plane shear forces only can be considered in the sheathing panel, while the framing members can be assumed approximately as rigid elements. This is motivated by the fact that bending of the framing members contributes to a small extent to the global wall response [16, 17, 88, 89]. On the other hand, several experimental tests have also demonstrated that the dissipative behavior of a shear wall is mainly influenced by its connections. In fact, timber has, in general, a poor dissipative capacity as it is a brittle material in bending and in tension, unless it is properly reinforced [15]. Conversely, the steel connections ensure a good amount of energy dissipation and cyclic ductility notwithstanding their significant pinching, strength degradation and softening. This evidence is well reflected into many numerical models proposed in the literature, where the nonlinear wall response is related to the load-deformation relationships of the connections [16–18]. In general, framing elements are modeled with beam elements whereas sheathing panels with plane-stress elements, assuming an elastic behavior in compression and an elastic-brittle behavior in tension [26]. Sheathing-to-framing connections and base connections are usually modeled with non-linear springs.

Part of the model proposed by Källsner and Girhammar [82] is based not just on the assumption that framing members and sheet are rigid but also that *i)* there is no contact between adjacent sheets or between sheets and surrounding structure, to allow the rotation of the panel, *ii)* framing joints act as hinges, *iii)* sheathing-to-framing joints have linear elastic load-slip characteristics up to the failure, the same constant slip modulus and stiffness (independent from the force direction and from the mutual orientation of sheets and framing members), *iv)* displacements of the wall are small compared to the width and height of the sheets and *v)* edge distances of sheathing-to-framing joints are small compared to width and height of the sheets. In order to determine the forces acting on each fastener, they consider the relative displacement between sheets and framing members (Figs. 5.13 5.14).

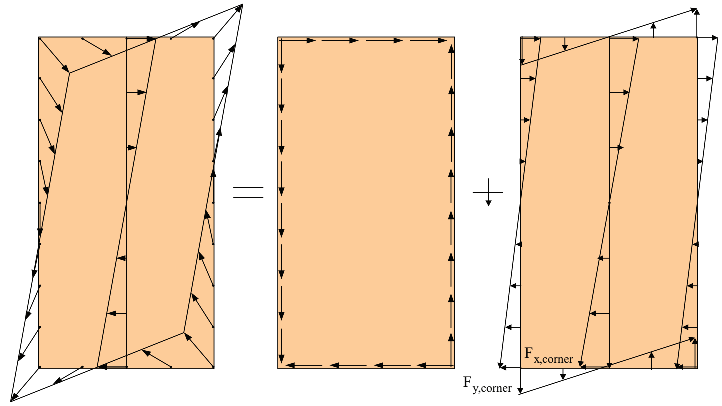

Figure 5.13. Force distribution on the sheet according to Källsner and Girhammar elastic model (from [82]).

The minimization of the potential energy (U) with respect to the unknown quantities to be determined (namely, frame and sheet angle of rotations, initial horizontal and vertical displacements of the sheet) is considered. The strain energy due to the fasteners deformation is:

$$U_1 = \sum_{i=1}^{n} \frac{1}{2} k (u_i^2 + v_i^2) \tag{5.32}$$

while the potential energy due to the horizontal load is:

$$U_2 = -F\gamma h \tag{5.33}$$

and thus the energy function of the problem is:

$$U = U_1 + U_2 = \frac{1}{2} k \sum_{i=1}^{n} \left[[u_0 + (\varphi - \gamma)\, y_i]^2 + (v_0 - \varphi x_i)^2 \right] - F\gamma h \tag{5.34}$$

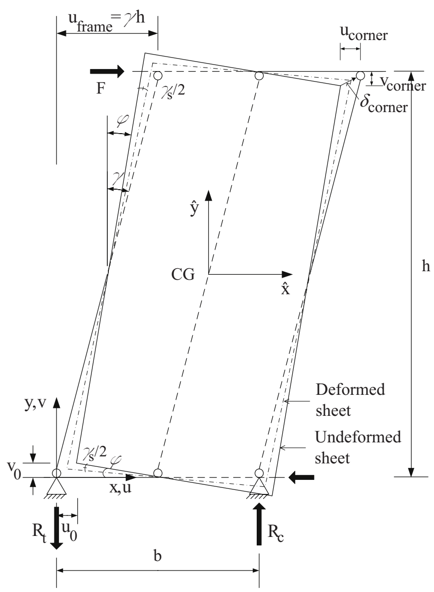

Figure 5.14. Static model of a fully anchored shear wall in loaded state (from [82]).

Rewriting the angles of rotation as a function of a new coordinate system placed in the fasteners centre of gravity ■, the force components acting on each nail can be obtained. Hence, it is found that the maximum force occurs in the fasteners placed in the corners, $F_{corner} = F_{max}$. As a consequence, the load-bearing capacity of the wall unit can be written as follows:

$$F = \frac{F_{f,Rd}}{h\sqrt{\left[\frac{\hat{x}_{corner}}{\Sigma_{i=1}^{n}\hat{x}_i^2}\right]^2 + \left[\frac{\hat{y}_{corner}}{\Sigma_{i=1}^{n}\hat{y}_i^2}\right]^2}} \tag{5.35}$$

where

$$\sum_{i=1}^{n} \hat{x}_i^2 \approx \frac{1}{6}\left(1 + 3\frac{s_r}{s_{ps}}\frac{h}{b}\right)\frac{b}{s_r} b^2 \tag{5.36}$$

$$\sum_{i=1}^{n} \hat{y}_i^2 \approx \frac{1}{12}\left(6 + 2\frac{s_r}{s_{ps}}\frac{h}{b} + \frac{s_r}{s_{is}}\frac{h}{b}\right)\frac{b}{s_r} h^2 \tag{5.37}$$

Källsner and Girhammar [82, eqs. 14a,b] provide approximate formulations to compute the distributed shear flow on the fasteners, which are assumed as discretely located along the sheet edges. This allows to obtain the horizontal load-carrying capacity of the wall as follows:

$$F \approx 0.984 \frac{b}{s_r} F_{f,Rd} \approx \frac{b}{s_r} F_{f,Rd} \tag{5.38}$$

where s_r is the nails spacing on the horizontal joists (rails), equal to that on the perimeter vertical studs $s_{ps}= s_{is}/2$, where s_{is} is the nails spacing on the internal studs. It is a common expedient to smear the fasteners continuously along the framing members, thus modeling the shear forces of the fasteners as a shear force per unit length $f_{f,Rd} = F_{f,Rd}/s_r$, and transforming summations in line integrals.

In [37], the elastic horizontal displacement of a timber light-frame shear wall subjected to a horizontal force can be obtained by adding four main deformation contributions, linked to the elements that comprise the whole system:

$$\Delta = \Delta_{SH} + \Delta_H + \Delta_A + \Delta_P \tag{5.39}$$

where Δ_{SH} is the contribution of sheathing-to-framing connections, Δ_H is the contribution attributable to the base connections (hold-downs) that control the uplift of the wall due to its rigid rotation, Δ_A is the contribution associated to the base connections (angle-brackets) that control the slipping of the wall due to its rigid translation, Δ_P is the contribution of the sheathing panel shear deformation. The flexural deflection of the timber frame as a cantilever is neglected.

Considering the components of each contribution, eq. (5.39) becomes:

$$\Delta = \underbrace{\frac{\lambda(\alpha) \cdot F \cdot s_c}{l \cdot n_{bs} \cdot k_c}}_{①} + \underbrace{\left[\frac{h}{\tau \cdot l \cdot k_h} \cdot \left(\frac{F \cdot h}{\tau \cdot l} - \frac{q \cdot l}{2}\right)\right]}_{②} + \underbrace{\frac{F \cdot i_a}{k_a \cdot l}}_{③} + \underbrace{\frac{F \cdot h}{l \cdot G_p \cdot n_{bs} \cdot t_p}}_{④}$$

For ① (Fig. 5.15):

F: is the applied horizontal force;

α: is the aspect ratio of the panel, i.e. height-to-width ratio;

λ: is a parameter depending on the aspect ratio, expressed by a linear regression as $\lambda(\alpha) = 0.81 + 1.85 \cdot \alpha$. This parameter has been defined to extend the results presented in [82] to different aspect ratios of a wall panel;

s_c : is the nails spacing, which is considered constant along the vertical perimeter studs and horizontal perimeter joists as $s_c = s_{ps} = s_p$;

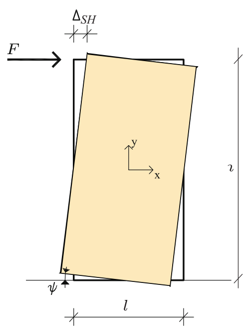

Figure 5.15. Sheathing-to-framing connections contribution (from [37]).

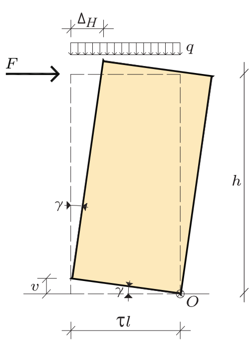

Figure 5.16. Rigid-body rotation contribution (from [37]).

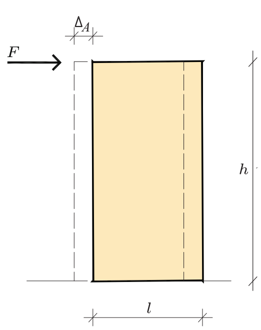

Figure 5.17. Rigid-body translation contribution (from [37]).

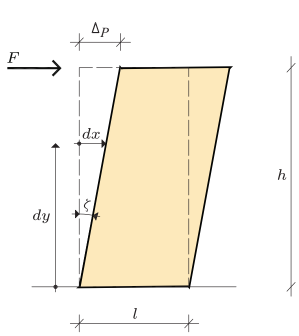

Figure 5.18. Contribution of shear deformation of the sheet (from [37]).

l: is the width of the wall;

n_{bs}: is the number of braced sides;

k_c : is the fastener stiffness.

For ② (Fig. 5.16):

F: is the applied horizontal force;

h: is the height of the wall;

$\tau \cdot l$: is the internal lever arm, i.e. the effective length of rotation;

q: is the vertical load, when considered;

k_h : is the hold-down stiffness.

For ③ (Fig. 5.17):

F: is the applied horizontal force;

i_a/l : is the number of angle-brackets n_a if their spacing i_a is constant, otherwise the contribution is computed as $\Delta_A = F/k_a \cdot n_a$;

k_a : is the angle-bracket stiffness.

For ④ (Fig. 5.18):

F: is the applied horizontal force;

h: is the height of the wall;

l: is the width of the wall;

G_p: is the shear modulus of the sheathing panel;

n_{bs}: is the number of braced sides;

t_p: is the thickness of the sheathing panel.

The rheological model that well represents the behavior of a timber shear wall is a series of springs, each one with the stiffness contribution of each source:

①$K_{SH} = \frac{n_{bs} \cdot k_c \cdot l}{\lambda(\alpha) \cdot s_c} = \frac{n_{bs} \cdot k_c}{\lambda(\alpha) \cdot \frac{s_c}{l}}$ (sheathing-to-framing connections);

②$K_H = \frac{n_h k_h \cdot \tau^2 l^2}{h^2}$(hold-down connections);
where n_h is the number of hold-downs for each corner of the wall;
③$K_A = \frac{k_a \cdot l}{i_a}$(angle-bracket connections);
④$K_P = \frac{G_P \cdot n_{bs} \cdot t_P \cdot l}{h}$(shear deformation of the sheathing panel).
Thus the global stiffness of the wall, K_{tot}, is obtained as follows:

$$\frac{1}{K_{tot}} = \frac{1}{K_{SH}} + \frac{1}{K_H} + \frac{1}{K_A} + \frac{1}{K_P} \tag{5.40}$$

and, since the shear deformation of the panel K_P is usually much greater than the one of the sheathing-to-framing connections K_{SH}, the two contributions are summarized as follows:

$$\frac{1}{K_{SP}} = \frac{1}{K_P} + \frac{1}{K_{SH}} \simeq \frac{1}{K_{SH}} \tag{5.41}$$

The sheathing-to-framing connections strength, according to [19], can be computed starting from the European Standard for timber structures [20] also considering the number of braced sides as follows:

$$R_{SH} = n_{bs} \cdot r_f \cdot \frac{\sum b_i \cdot c_i}{s} \tag{5.42}$$

where n_{bs} is the number of the wall braced sides (1 or 2), r_f is the fastener strength (named $F_{f,Rd}$ along thesis), b_i is the panel width and

$$c_i = \begin{cases} 1 & \alpha < 2 \\ \frac{\alpha}{2} & 2 < \alpha < 4 \\ 0 & \alpha > 4 \end{cases} \tag{5.43}$$

where $\alpha = \frac{h}{b}$ is the aspect ratio (AR) of the panel.

The contribution in terms of racking capacity due to the rigid-body rotation (controlled by hold-downs) is activated if a tensile force acts on them. This occurs if the horizontal force applied on the top of the wall produces an overturning moment greater than the stabilizing moment attributable to the vertical load. The strength can be computed directly from the hold-down strength as follows:

$$R_H = n_h \cdot \frac{r_h \cdot \tau \cdot l}{h} \tag{5.44}$$

where r_h is the hold-down strength, l is the wall width, n_h is the number of hold-downs for each corner of the wall and $\tau \cdot l$ is the internal lever arm, i.e. the effective length of rotation, usually between 0.95-1 [19].

The last contribution, due to the rigid-body translation controlled by angle-brackets, is expressed as follows:

$$R_A = \frac{r_a \cdot l}{i_a} = r_a \cdot n_a \tag{5.45}$$

where r_a is the angle-bracket strength, l is the wall length, n_a is the number of angle-brackets and i_a is a constant spacing of the devices.

The wall strength is thus defined as the minimum value of the strengths associated by each contribution:

$$R_W = min(R_H + F_q; R_A; R_{SH}) \tag{5.46}$$

Also for the wall ductility, the plastic displacement of the rheological model to be considered is the plastic displacement of the weakest contribution. Therefore, as reported in [19, eq. 34], the plastic displacement of the wall is equal to the plastic displacement of the weakest connection $\mathit{\Delta}_{i,pl}$ which is, in turn, correlated to its yield displacement $\mathit{\Delta}_{i,y}$ and ductility μ_i as follows:

$$\mathit{\Delta}_{i,pl} = \mathit{\Delta}_{i,u} - \mathit{\Delta}_{i,y} = \frac{R_i}{K_i} \cdot (\mu_i - 1) \tag{5.47}$$

The wall ductility is defined as the ratio between the wall ultimate displacement $\Delta_{v,u}$ (which is the sum of the yield displacement $\Delta_{v,y}$ and the plastic displacement of the weakest connection $\Delta_{i,pl}$) and the wall yield displacement $\Delta_{v,y}$. Rearranging the equations in [19, eqs. 31-35], the wall ductility μ_v is obtained from the following simplified equation [19, eq. 37]:

$$\mu_v = 1 + \frac{K_v}{K_i} \cdot (\mu_i - 1) \tag{5.48}$$

where K_v is the wall stiffness and K_i the stiffness of the weakest connection.

Finally, Casagrande et al. [19] have observed that the ductility ensured by the sheathing-to-framing connections contribution μ_{SH} is not influenced significantly by the fastener spacing and it increases with the panel aspect ratio α. This will be also confirmed by the sensitivity analyses performed in the present study. Moreover, the contribution of shear deformation to storey displacements increases if the base of the shear wall is significantly larger than its height, as pointed out in [90]. Conversely, if the base is about 30% of the height, then the flexural behaviour is dominant.

The analytical relationship between the sheathing-to-framing connection ductility μ_{SH} and the fastener ductility μ_f is given in [19] as:

$$\mu_{SH} = \rho(\alpha) \cdot \mu_f + \nu(\alpha) \tag{5.49}$$

where the parameters ρ and v were obtained by means of an interpolation of the curves wall ductility vs. fastener ductility:

$$\begin{cases} \rho = -0.054 \cdot \alpha^2 + 0.350 \cdot \alpha + 0.305 \\ v = 0.068 \cdot \alpha^2 - 0.415 \cdot \alpha + 0.753 \end{cases} \tag{5.50}$$

In order to assess the ductility ensured by the sheathing-to-framing connections, mechanical considerations will be given in the present work on the basis of the results carried from the sensitivity analyses. This, in order to define the global ductility of the wall and to compute the ultimate displacement of a timber light-frame shear wall.

5.6.2 The relevance of flexible framing elements and shear contribution of the sheathing panel in numerical modeling

Källsner and Girhammar [82] provided some guidelines to compute the racking capacity taking into account the flexibility of framing members.

No forces develop perpendicularly to framing members and a different moment of inertia of the shear wall is obtained by changing eq. (5.36) and eq. (5.37) as follows:

$$\sum_{i=1}^{n} \hat{x}_i^2 \approx \left(\frac{h}{s_{ps}} - 1\right) \frac{b^2}{2} \approx \frac{h}{s_{ps}} \frac{b^2}{2} \tag{5.51}$$

$$\sum_{i=1}^{n} \hat{y}_i^2 \approx \left[\frac{b}{s_r} + 1\right] \frac{h^2}{2} \approx \frac{b}{s_r} \frac{h^2}{2} \tag{5.52}$$

Considering the shear force per unit length, the racking capacity can be rewritten as follows:

$$F \approx 0.707 \cdot f_{f,Rd} \cdot b \tag{5.53}$$

where b is the width of the panel.

The influence of the shear deformation in the sheathing panel can be estimated by introducing the shear angle γ_s. The shear deformation increases the potential energy of the system and this contribution can be expressed as:

$$U_3 = \frac{1}{2} G_p \cdot \gamma_s^2 bht \tag{5.54}$$

where b, h, t are the width, height and thickness of the sheet, respectively. Also the potential energy associated to the external horizontal force F changes as follows:

$$U_4 = -F\gamma_s h \tag{5.55}$$

By adding these two new contributions to the potential energy U (eq. 5.34) and determining its minimum value, the shear angle can be obtained and, consequently, the top rail displacement of the shear wall can be estimated as:

$$u_{frame} = \frac{F}{k}\left[h^2\left(\frac{1}{\sum_{i=1}^{n}\hat{x}_i^2} + \frac{1}{\sum_{i=1}^{n}\hat{y}_i^2}\right) + \frac{h}{b}\frac{k}{G_p \cdot t}\right] \tag{5.56}$$

whereas both the horizontal load-bearing capacity and the fastener forces are not affected by this further contribution.

5.6.3 Mechanical behavior with openings

Wall openings as windows and doors can reduce the shear wall lateral resistance because the discontinuity of load transfer induces concentration of stresses around openings. The U.S. building code [91] provides the following solutions to design wood-frame shear walls with openings:

1. The shear capacity adjustment factor C_0 proposed by [92, 93], considering the maximum opening height and the percentage of full-height sheathing but not the force transfer around the openings;

2. The force Transfer Around Openings (FTAO), in which shear walls with openings are designed and detailed to transfer loads around openings by means of nails, metal straps that reinforce also corners of openings [94].

According to the first method, Yasumura and Sugiyama [93] proposed a simplified approach to calculate the stiffness of timber-framed wall including the opening.

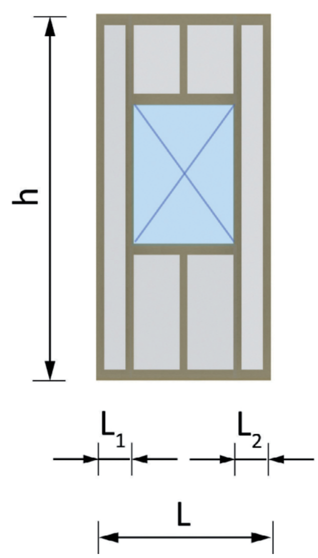

Figure 5.19. Definition of parameters for the computation of opening coefficient r (from [95]).

The effective shear strength and stiffness ratio is computed as follows:

$$F = \frac{r}{3-2r} \tag{5.57}$$

where r is the opening coefficient computed as follows:

$$r = \frac{1}{1+\left(\frac{\alpha_{YS}}{\beta_{YS}}\right)} \tag{5.58}$$

in which $\alpha_{YS} = A_0/h \cdot L$ is the opening area ratio and $\beta_{YS} = \sum L_i/L$ is the wall length ratio, whereas A_0 is the sum of opening areas and L, L_i, h are defined in Fig. 5.19.

Also the experimental tests conducted by [96, 97] have shown neglecting wall openings is not fully appropriate. An analytical formulation to compute the non-dimensional reduction coefficient of the stiffness $k_r(r)$ and load bearing capacity $f_r(r)$ of timber-framed wall with openings clad with fibre-plaster boards depending on the coefficient r is proposed in [98]:

$$k_r(r) = 0.5621 \cdot r^3 + 0.6505 \cdot r^2 - 0.2016 \cdot r + 0.0018 \tag{5.59}$$

$$f_r(r) = 0.7636 \cdot r^2 + 0.3075 \cdot r - 0.0118 \tag{5.60}$$

5.7 Mechanical behavior and modeling of Timber Light-Frame shear walls according to the EuroCode 5

5.7.1 Rigid framing elements: the in-plane racking resistance using method A

For the estimation of the racking strength, the European Standard for timber structures [20, § 9.2.4.2] (Fig. 5.20) provides a relationship between the fastener strength $F_{f,Rd}$ and the strength of a single wall panel $F_{v,Rd}$, obtained by means of the limit analysis static theorem assuming a constant action on each fastener.

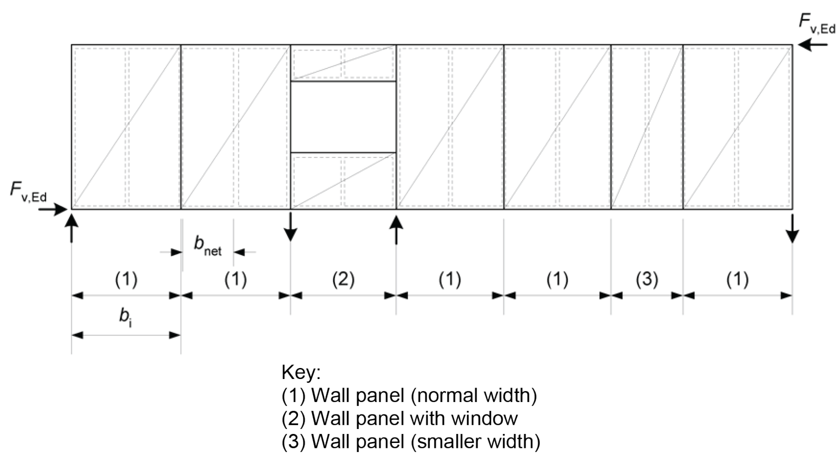

Figure 5.20. Example of the assembly, as proposed in EuroCode 5 [20].

This contribution, in fact, does not just depend on the behavior of the single fastener, but it is also influenced by the disposition of nails along the panel edges. In case of no more than 3 studs for each panel of the assembly, it is expressed as follows:

$$F_{v,Rd} = F_{f,Rd} \cdot \frac{\sum b_i \cdot c_i}{s} \tag{5.61}$$

where b_i is the i-th wall panel width, s is the fastener spacing, assumed constant along the perimeter sheet and

$$c_i = \begin{cases} 1 & b_i \geq b_0 \\ \frac{b_i}{b_0} & b_i < b_0 \end{cases} \tag{5.62}$$

where $b_0 = \frac{h}{2}$ and h is the height of the wall.

5.7.2 Flexible framing elements: the shear wall as a composite timber section

The analytical models described in Sec. 5.6.1 do not account for the effective bending and shear deformability of the timber-framed wall and often the shear stiffness is computed numerically, taking into account the nails spacing. As shown in [22], the braced frame can be considered as a cantilever beam rigidly supported, where the effective bending stiffness $(EI_y)_{eff}$ is determined with the so-called *γ-method*. The flexibility is computed using the stiffness coefficient of the fastener, named connection efficiency factor in the EuroCode 5 [20]. Composite sections jointed mechanically using nails are described in EuroCode 5 [20, Annex B: Mechanically jointed beams, § B.2], and includes webs and flanges made of different materials (Oriented Strain Board, plywood, particleboard etc. for webs; structural timber, LVL or glued laminated timber for flanges). For composite sections, the conventional bending theory cannot be used to determine the bending stiffness because of the effect of the slip, when mechanical fasteners are used. As suggested in [34], this can be achieved by modeling the behavior of each fastener in the connection and analyzing the section using the finite element method. An alternative slightly less accurate method is based on the application of the conventional bending theory to each element assuming a compatibility condition in the curvature and displacement of adjacent column elements at each interface, simulating the slip effect by assuming that the fastener resistance in these zones can be represented by linear spring elements.

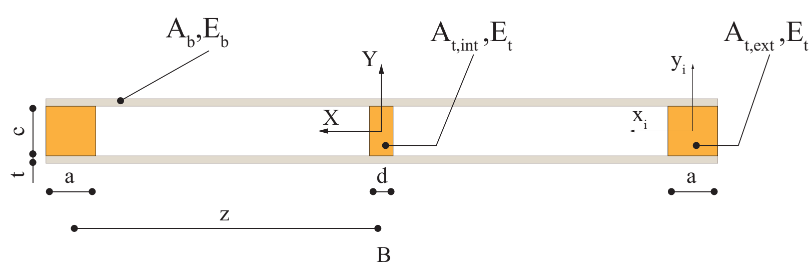

Figure 5.21. Cross-section of a typical timber-framed wall with a two-sided sheathing board.

Thus, through the application of the bending theory and using a linear elastic theory, a reasonable estimation of the bending stiffness can be obtained as follows:

$$(EI_y)_{eff} = \sum_{i=1}^{3}(E_i I_i + \gamma_i E_i A_i z_i^2) \qquad (5.63)$$

where E_i is the mean value of the elastic modulus of the i-th element, A_i is the cross-section area of the i-th element, I_i is the moment of inertia of the i-th element about its axis of bending. Moreover, γ_i is the connection efficiency factor, computed as follows [20, eq. B.5]:

$$\gamma_i = [1 + \pi^2 E_i A_i s_{fi} / (K_{fi} l^2)]^{-1} \tag{5.64}$$

where s_{fi} is the spacing of the fastener in connection i.

If a flange consists of two elements connected to a single web or the web consists of two elements connected to a single flange (Fig. 5.22), then s_{fi} is $1/2$ the fastener spacing per unit length used for each joining planes.

In other words, the stiffness used for the connection is twice the fastener stiffness in each joining planes. K_{fi} is the stiffness of the fastener i per joining plane (Tab. 4.2) and, for ULS, it is equal to $K_{fi,u}$, l is the length of the column, a_i is the distance between the local y_i-axis and the global Y-axis of the whole section. The effective bending stiffness for a section, such as the one shown in Fig. 5.22, is computed as follows:

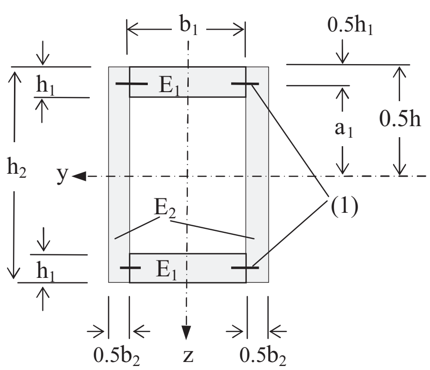

Figure 5.22. Profiles to which rules of EuroCode 5 apply (from [34]).

$$(EI_y)_{eff} = 2E_1 \frac{b_1 h_1^3}{12} + E_2 \frac{b_2 h_2^3}{12} + 2(\gamma_1) E_1 (b_1 h_1) \left(\frac{h_2}{2} - \frac{h_1}{2} \right)^2 \tag{5.65}$$

with $\gamma_1 = \left[1 + \pi^2 E_1 (b_1 h_1) \left(\frac{s_1}{2K_1} \right) \frac{1}{l^2} \right]^{-1}$.

According to [22], the effective bending stiffness for a timber light-frame shear wall may be computed as follows (Fig. 5.21):

$$\begin{aligned} (EI_y)_{eff} &= \Sigma_{i=1}^{n} \left(E_i I_{yi} + \gamma_{yi} E_i A_i z_i^2 \right) = \\ &= E_{b,mean} \frac{tB^3}{6} + E_{t,mean} \left(\frac{a^3 c}{6} + \frac{d^3 c}{12} + 2\gamma_{y,ext} A_{t,ext} z_{ext}^2 \right) \end{aligned} \tag{5.66}$$

where $E_{b,mean}$ and $E_{t,mean}$ are the mean values of the elastic modulus parallel to the grain for the sheathing panel and timber framing elements, respectively, n is the total number of elements in the considered cross-section, $a - c - d$ are the dimensions of the framing elements cross-sections, and z_i is the distance between the global Y-axis of the whole cross-section and the local y_i-axis of the i-th element (Fig. 5.21).

In order to take into account the presence of more than 3 vertical studs, the following equation is proposed:

$$\begin{aligned} (EI_y)_{eff} &= E_{b,mean} \frac{tB^3}{6} + \\ &+ E_{t,mean} \left[\left(\frac{a^3 c}{6} + 2\gamma_{y,ext} A_{t,ext} z_{ext}^2 \right) + \Sigma_{i=1}^{n} \left(\frac{d^3 c}{12} + \gamma_{y,int} A_{t,int} z_{int}^2 \right) \right] \end{aligned} \tag{5.67}$$

where, for every configuration, n is the number of intermediate studs and the mid-one has z_i equal to zero. The stiffness coefficient of fasteners γ_y, for both perimeter and intermediate studs, is defined in accordance with EuroCode 5 as follows:

$$\gamma_y = \frac{1}{1 + \frac{\pi^2 A_t E_{t,mean} s}{L_{eff}^2 2 K_{fi}}} \tag{5.68}$$

where K_{fi} is the slip modulus per shear plane per fastener, computed as reported in Tab. 4.2; A_t is the cross-section area of the i-th (perimeter or intermediate) framing element, s is the (perimeter or intermediate) spacing of fasteners and $L_{eff} = 2H$ is the effective length of the timber light-frame shear wall, assumed as a cantilever beam, and H is its overall height.

The main limit of the previous definitions of slip modulus is the lack of important parameters such as type of fastener, thickness of timber elements and failure mechanism [60].

Finally, the formulation for the wall stiffness k_p as cantilever beam, taking into account the effective bending and shear flexibility of the elements and considering the sheathing panel shear stiffness defined by [37], is given by:

$$k_p = K_{SH}^{sec} = \frac{1}{D_p} = \left(\frac{H^3}{3\left(EI_y\right)_{eff}} + \frac{H}{n_{bs} G_{b,mean} t B} \right) \tag{5.69}$$

where D_p is the flexibility of the wall and H is its height whereas $G_{b,mean}$ is the mean values of the sheathing panel shear modulus.

5.7.3 Mechanical behavior with openings

A further solution to design wood-frame shear walls with openings is provided by the building code in force in U.S. [91], named as *segmented shear wall design method*: adopted in Canadian code [99] and EuroCode 5 [20, § 9.2.4.2 (6)], it considers only full-height wall segments to compute the racking capacity, ignoring contributions from panels above and below the openings (Fig. 5.23).

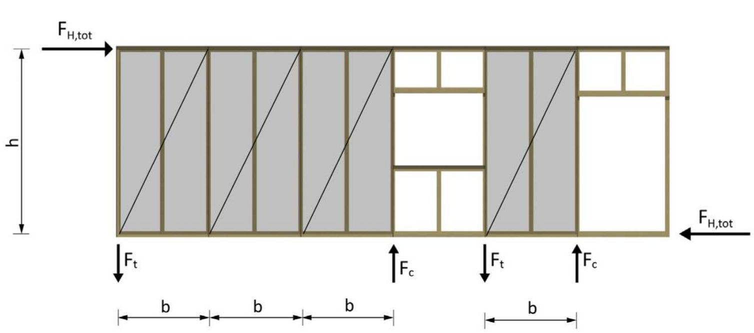

Figure 5.23. Design assumption of Canadian code and EuroCode 5 for timber-framed walls with openings (from [95]).

6 | Parametric numerical model of a Timber Light-Frame shear wall

Abstract

An original parametric numerical model has been developed within OpenSees in order to investigate the mechanical response of a timber light-frame shear wall. In particular, it is employed for a parametric investigation of the influence of several design variables, namely: i) aspect ratio, ii) nails spacing, iii) number of vertical studs and iv) framing elements cross-section size. Moreover, the effects of sheathing-to-framing connections on both the racking capacity and the energy dissipation are evaluated. The global FE model is first validated using experimental data available in the literature. Then, the results of the non-linear cyclic numerical simulations are used to estimate the hysteretic damping, which, in turn, is required to calculate the correction factor η *in use within the Capacity Spectrum Method.*

6.1 Parametric numerical model without openings

The original FE model developed in this work has been implemented in the open-source software OpenSees [11]. To the best authors' knowledge, this is the first parametric numerical model of a timber shear wall developed in OpenSees. Among the FE models available in the literature, it is worth mentioning the one developed by Doudak et al. [100] by means of the commercial finite element software SAP2000. This model also considers the presence of openings, like the one developed by Yasumura [101] with CASTEM 2000. Further models have been proposed by Rinaldin et al. [102] using Abaqus and SAP2000 and by Humbert et al. [84] using the free software Code_Aster. A simplified numerical model has been developed by Casagrande et al. [19] to evaluate the elastic response of light-frame and cross laminated timber shear walls. Another numerical model has been elaborated by Anil et al. [90] by means of Abaqus. On the other hand, Gattesco and Boem [26] performed experimental tests on different configurations of timber light-frame shear walls in order to validate their numerical model developed in Abaqus. Typically, the framing members are modeled as rigid [37] and a quick modification of the common geometric parameters is often not facilitated in the existing models by means of software such as SAP2000. This makes model development a time consuming task.

In this perspective, the parametric FE model proposed in this work has been implemented in the TCL environment to allow a rapid numerical definition of the geometric parameters affecting the racking capacity of the shear walls, namely: *i)* panel size (in terms of aspect ratio), *ii)* horizontal and vertical nails spacing, *iii)* number of vertical studs and *iv)* framing elements cross-section size. All the parameters related to the strength class of the selected timber species can be inputted easily. Once these parameters are defined, the number of nodes and elements are updated automatically.

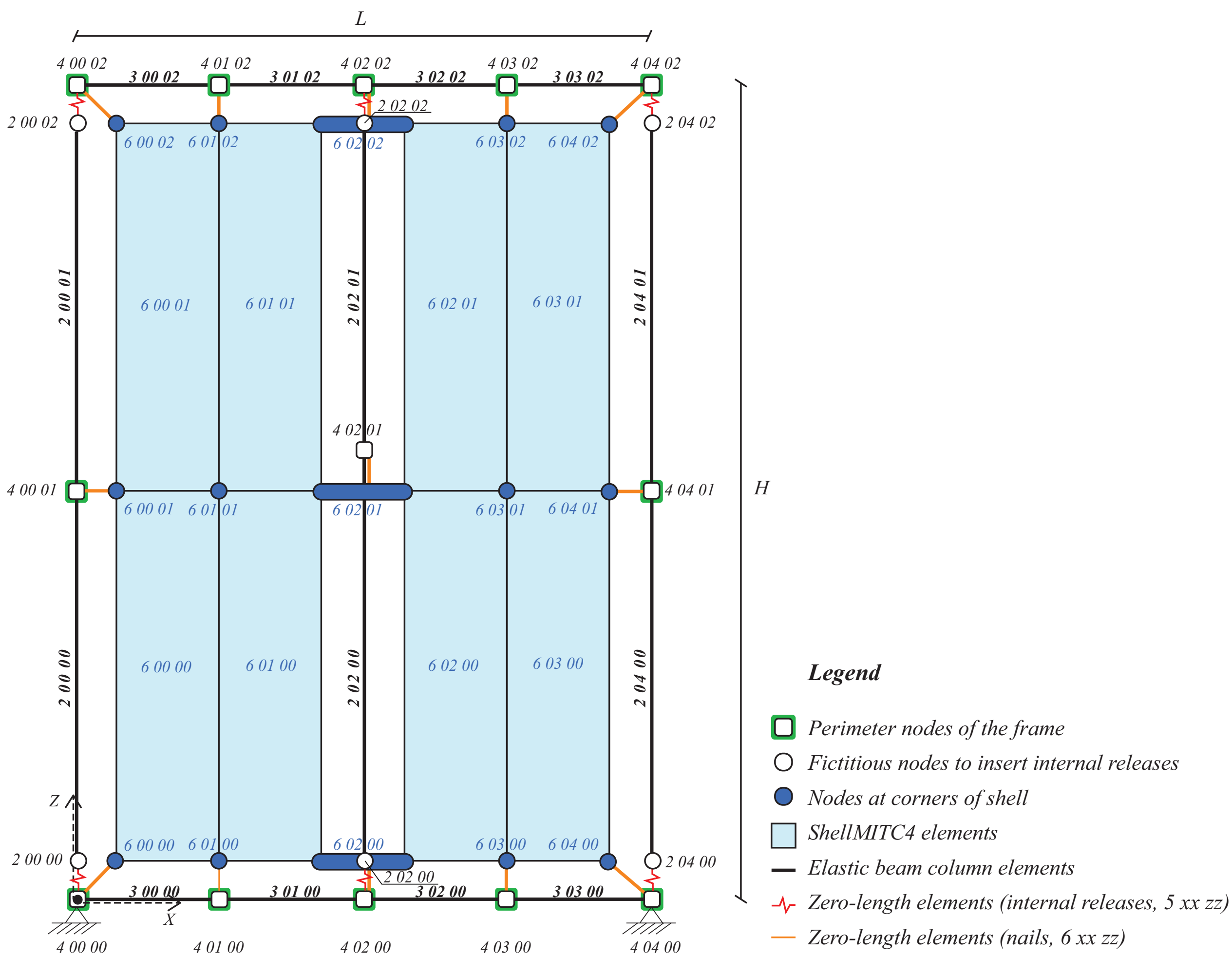

Figure 6.1. Layout of the FE model implemented in OpenSees.

The FE model is illustrated in Fig. 6.1, where base and height are aligned with the X-axis and the Z-axis, respectively. The frame elements have been modeled using *elastic beam column elements*. Zero-length elements are adopted to represent sheathing-to-framing connections. The number of connections placed along the horizontal and vertical framing elements is updated by setting the horizontal and vertical nails spacing, respectively. The sheathing panel is modeled by means of ShellMITC4 elements, whose mesh size is automatically adjusted based on the nails spacing (Fig. 6.2). The ShellMITC4 element is a four-node isoparametric shell element, which uses the *Mixed Interpolation of Tensorial Components* formulation introduced by Dvorkin and Bathe [103]. This element derives from the isoparametric shell element developed by Ahmad, Irons and Zienkiewicz [104, 105] known as Reissner/Mindlin shell element, characterized by independent C^0 interpolations for displacements and rotations (C^0 continuity), which implies the introduction of shear deformation in the formulations. Although this characteristic is desirable for the analysis of thick shells and makes possible the transition from 3D to shell elements, these shear deformations cause numerical difficulties known as *locking* phenomenon [105–109]. This drawback was first relieved by means of a reduced/selective numerical integration schemes that, unfortunately, compromises the reliability of the numerical results. The ShellMITC4 element, instead, is formulated for non-linear analysis and it is useful for the modeling of thin and moderately thick plates, i.e. where the condition of zero stresses through the thickness is still acceptable. Further details about the computation of the in-layer strain components and the transverse shear strains are provided in [110, § 3.1].

In order to represent the framing joints as hinges, two linear zero-length elements in vertical and horizontal directions as well as one linear zero-length element in the rotational direction have been implemented, as done in [101]. For the latter, a low stiffness for the rotational degree of freedom with respect to the Y-axis has been assigned. Particularly, the sheathing-to-framing connections have been modeled as *non-linear coupled zero-length elements* in order to consider a circular yielding surface. This prevents the overestimation of nail stiffness and force under non-linear loading. For further details the interested reader can refer to [19, 111]. Fully-fixed boundary constraints are assumed at the bottom corner nodes.

In order to identify nodes and elements an integer *tag* is employed. The tag of nodes is defined by five or six digits. It starts with a number that identifies the layer they belong to. Then two digits are used to identify the x-coordinate, and other two digits define the z-coordinate. Seven layers are defined (Fig. 6.1). Layer **1** includes nodes belonging to the main grid of the model. Layer number **2** includes *i)* the fictitious nodes used to insert the internal releases between the end of vertical studs and the horizontal joists and *ii)* the tag of elastic beam column elements used to model vertical studs. Layer number **3** includes tag of *elastic beam column* elements used to model horizontal joists. Layer number **4** includes the perimeter nodes belonging to the frame. The *zero-length* elements, representing the internal releases, are so defined with tag number **5**. They connect fictitious nodes with tag 2 and perimeter nodes with tag 4. Layer **6** includes nodes belonging to the shell as well as the shell elements. Finally, layer **7** includes the *zero-length* elements adopted to represent the sheathing-to-framing connections. As an example, the tag number **2 00 00** identifies a fictitious node, placed at the origin of the axes. Since the timber light-frame shear wall is double braced in this work, the symmetric shell and zero-length elements - which model sheathing panel and nails - are included in layer **13** and **14**, respectively.

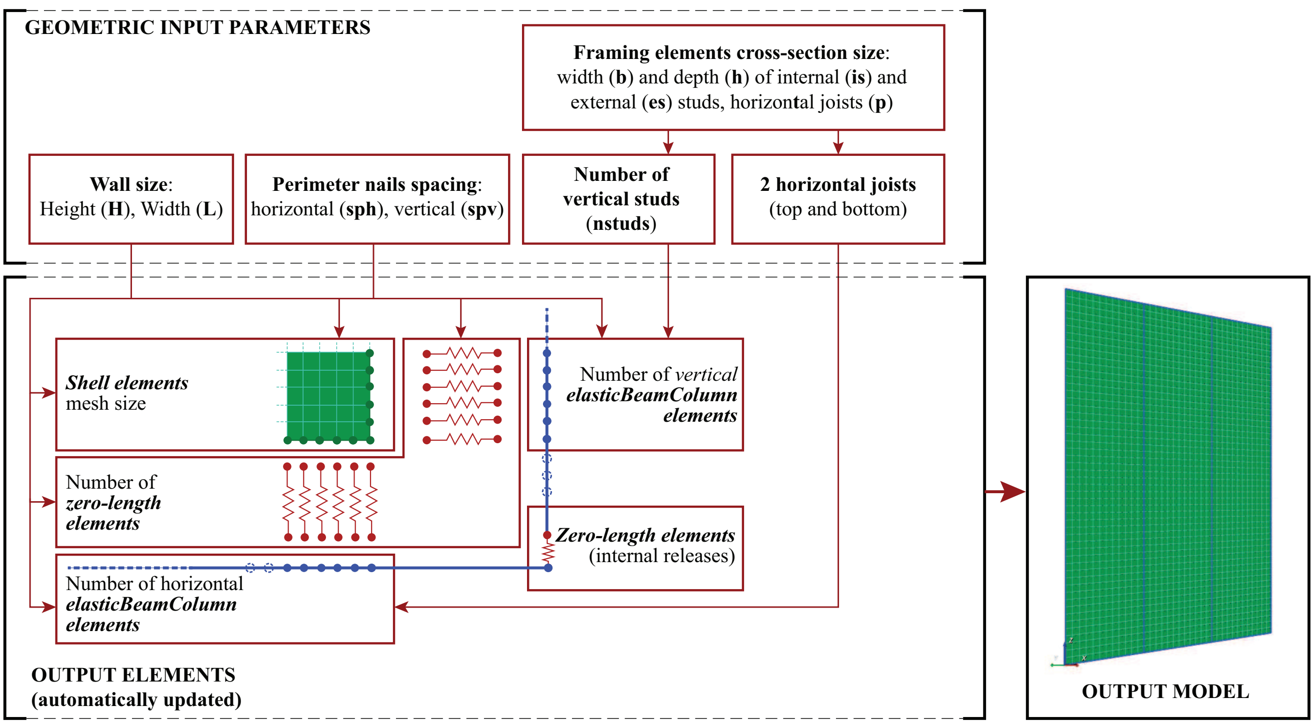

Figure 6.2. Process to build the parametric FE model. For further details about notations see Appendix A.

6.2 Parametric numerical model with openings

A parametric FE model of the shear wall able to take into account the presence of openings, has been also implemented. By setting the dimensions of the openings, the position of the vertical studs is automatically updated. The nodes and shell elements in correspondence of the opening are deleted with *remove* command. Moreover, the opening header is inserted with its own internal releases, in order to represent the real behavior of the joints connecting frame members behaving like hinges (Figs. 6.3 and 6.4).

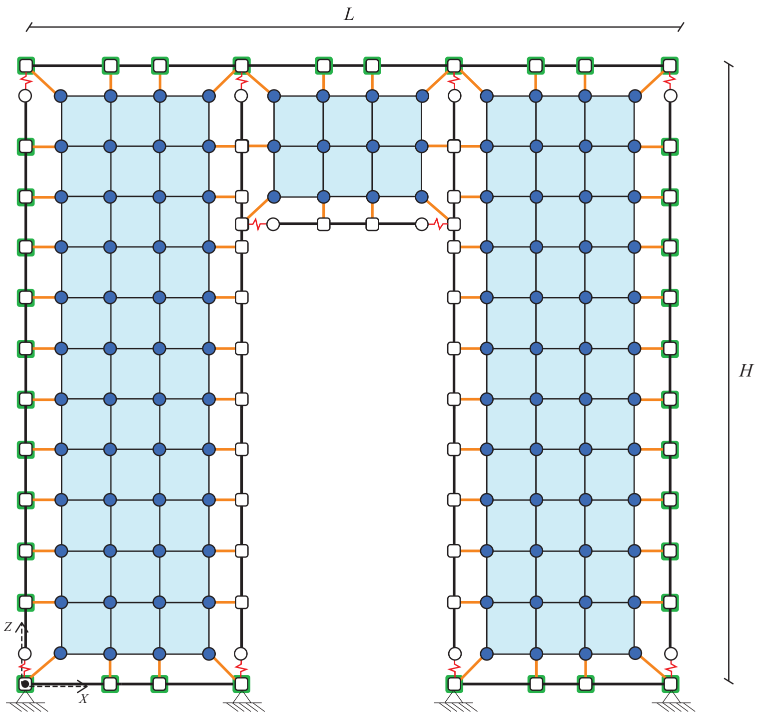

Figure 6.3. Layout of the FE model implemented in OpenSees considering the presence of an opening.

6.3 Parametric identification of fastener mechanical model

The SAWS mechanical model - originally proposed by Foschi [78] and developed in [87] - is here adopted to simulate the behavior of sheathing-to-framing connections. As declared in Sec. 4.4.2, this is the mechanical model mostly used to represent the behaviour of a single nail.

The identification of the corresponding model parameters has been performed with reference to the experimental results presented in [26] for a single nail $\phi 2.8$. The parametric identification is here formulated as an optimization problem.

The first step of the optimization problem consists in the definition of the parameters vector, which collects the model parameters to be identified:

$$\mathbf{x} = \{x_1, ..., x_j, ..., x_n\} \tag{6.1}$$

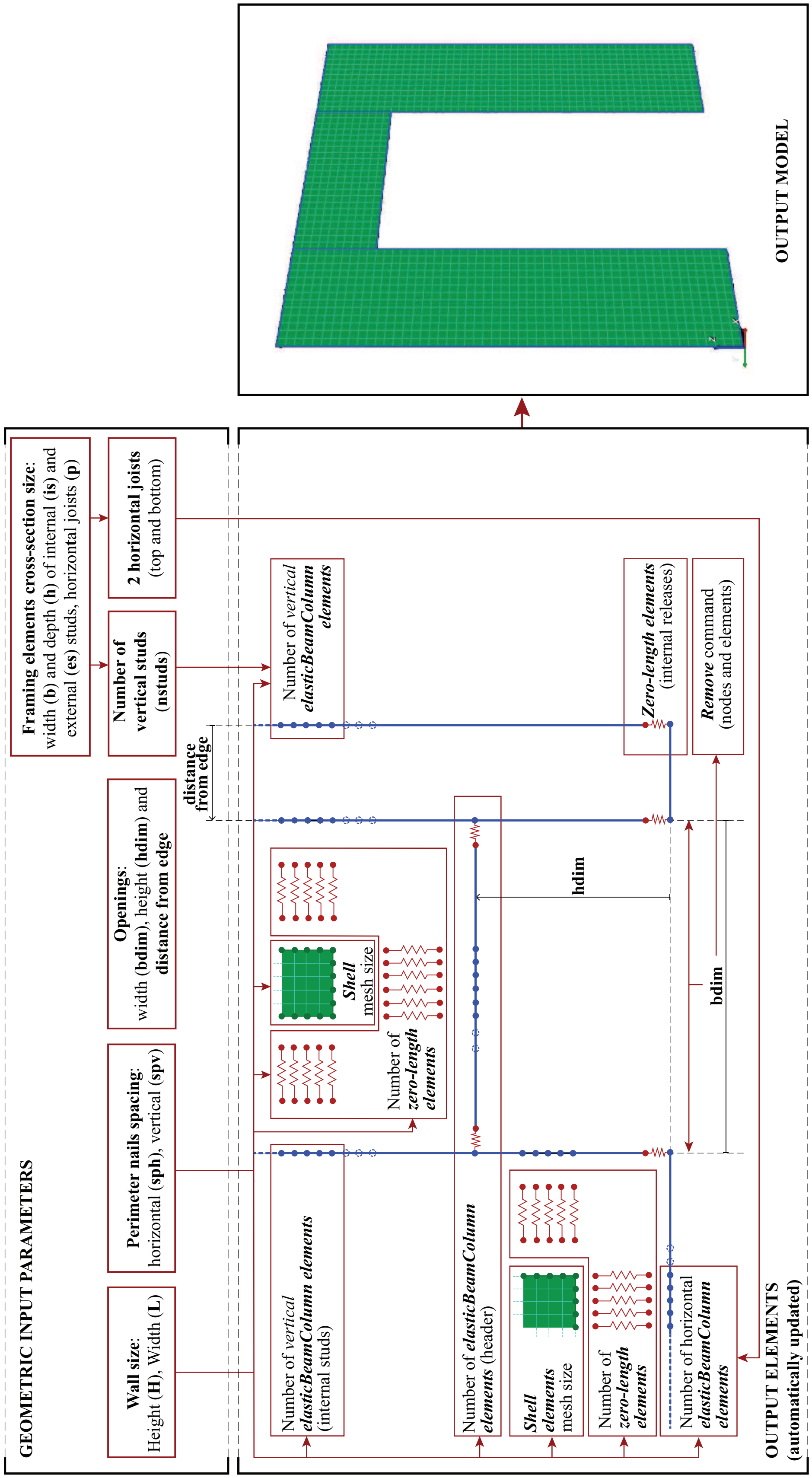

Figure 6.4. Process to build the parametric FE model with openings.

where, in the present application, $n = 10$ according to the SAWS mechanical model, described in Sec. 4.4.2. The parametric identification is thus expressed by the following optimization problem:

$$min_{\boldsymbol{x}}(f(\boldsymbol{x}))\ s.t.\ \mathbf{x}^l \leq \mathbf{x} \leq \mathbf{x}^u \tag{6.2}$$

where $\mathbf{x}^l = \left\{x_1^l, ..., x_j^l, ..., x_n^l\right\}$ and $\mathbf{x}^u = \left\{x_1^u, ..., x_j^u, ..., x_n^u\right\}$ are the lower and upper bound of the parameters vector, respectively.

The adopted objective function to minimize is defined as follows:

$$f(\boldsymbol{x}) = \frac{1}{S \cdot var(F^{exp})} \Sigma_{s=1}^{S} \left(F_s^m(\mathbf{x}) - F_s^{exp}\right)^2 \tag{6.3}$$

where F_s^m and F_s^{exp} are predicted and experimental force values, respectively. Moreover, s is the generic sample (S denotes the total number of samples) and $var(F_s^{exp})$ is the variance of the experimental force values.

The methods used for the parametric identification are:

- Differential Evolution Algorithms (DEA);
- Particle Swarm Optimization Algorithms (PSOA), based on the swarm intelligence theory, in which it is assumed that a Newtonian dynamic regulates the movement of the particles.

These optimization techniques belong to the class of so-called non-classical identification methodologies, a classification proposed by Koh et al. [112]. This class of numerical identification techniques implements socially, physically and/or biologically inspired paradigms [113]. Further numerical non-classical identification techniques are based on artificial neural networks, genetic algorithms, genetic programming. For a complete state-of-art about the identification by means of genetic algorithms, the interested reader can refer to [114]. These methodologies have attracted a lot of attentions because are gradient-free and start-point independent numerical techniques, and so they do not need an initial good estimation of the model parameters, even if a sensitivity analysis could be useful to determine their upper and lower bounds. Another interesting feature is their high robustness against the noise in experimental data. Further details can be found in [115, 116] (Fig. 6.5).

The comparison between experimental and identified force-displacement curves - obtained with DEA - is shown in Fig. 6.6.

6.4 Validation of the wall FE model

Starting from the experimental tests carried out by Gattesco and Boem [26] on different configurations of a timber light-frame shear wall, the

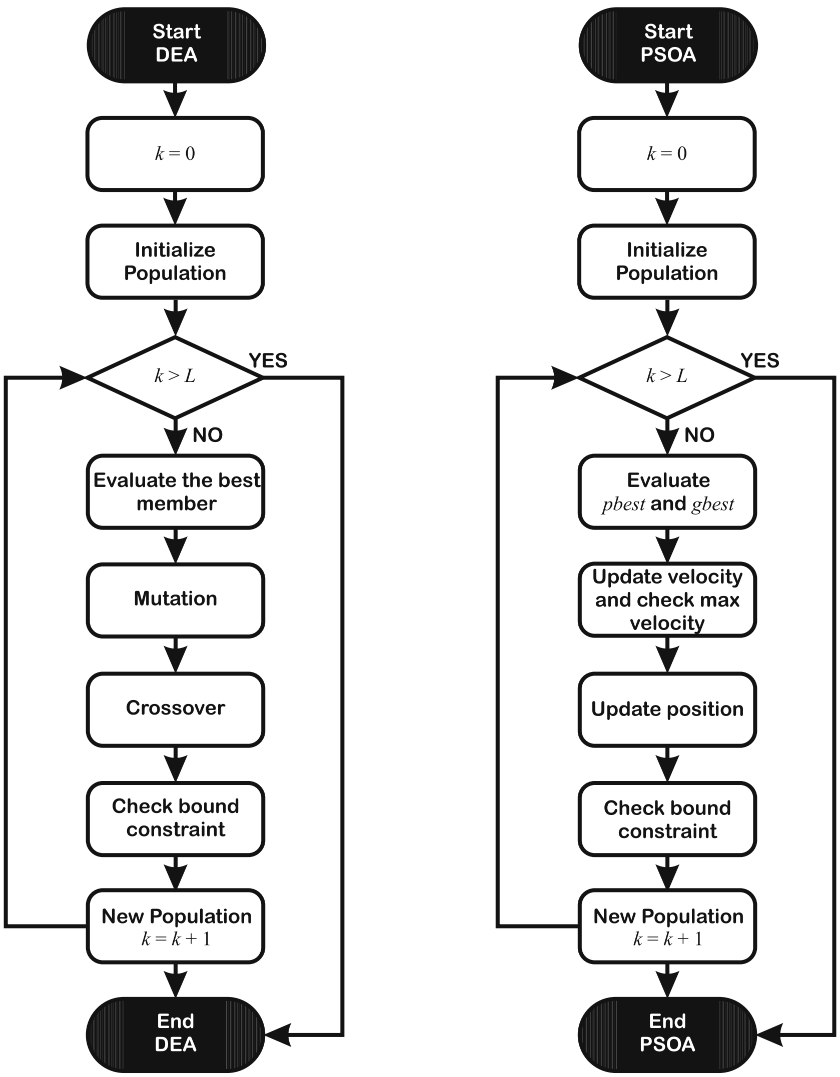

Figure 6.5. Computational steps for (left) Differential Evolution Algorithms and (right) Particle Swarm Optimization Algorithms (from [115]).

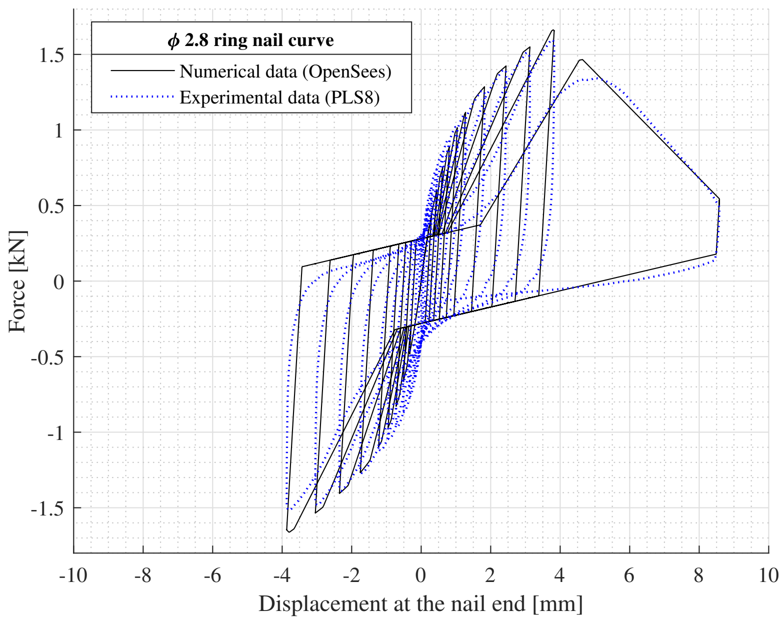

Figure 6.6. Identification of SAWS model parameters for the sheathing-to-framing connections: comparison between experimental values and identified force-displacement curve for a ring nail $\phi 2.8/70$.

sample called PLS8 in [26] has been selected for a numerical validation of the model developed in OpenSees. It is useful to remark that a timber shear wall is a series system [19], as described in Sec. 5.6.1.

Thus, from the experimental force-displacement curve obtained considering all the contributions (blue, Fig. 6.7) the one associated to the sheathing-to-framing connections (Fig. 6.8) has been derived by subtracting the displacements of the one related to the rigid rotation (controlled by the hold-downs, green in Fig. 6.7, $F - \delta_c$) and the displacements of the one associated to the rigid translation (controlled by the angle-brackets, orange in Fig. 6.7, $F - \delta_{sf}$) .

Racking capacity and hysteretic cycles obtained from the numerical simulation (by adopting the displacement increments used in [26]) are in good agreement with the outcomes of the experimental tests in [26] (Fig. 6.8).

Also the loading path is in good agreement with the results reported in [26] (Fig. 6.15).

To validate the accuracy of the model, accounting of the presence of openings, experimental data provided in [117] for specimen 2 have been considered.

The mechanical characteristics of the wood elements have been implemented in the FE parametric model for its validation. The mechanical characteristics used for the framing elements are those of the red spruce wood species. According to the European standards EN

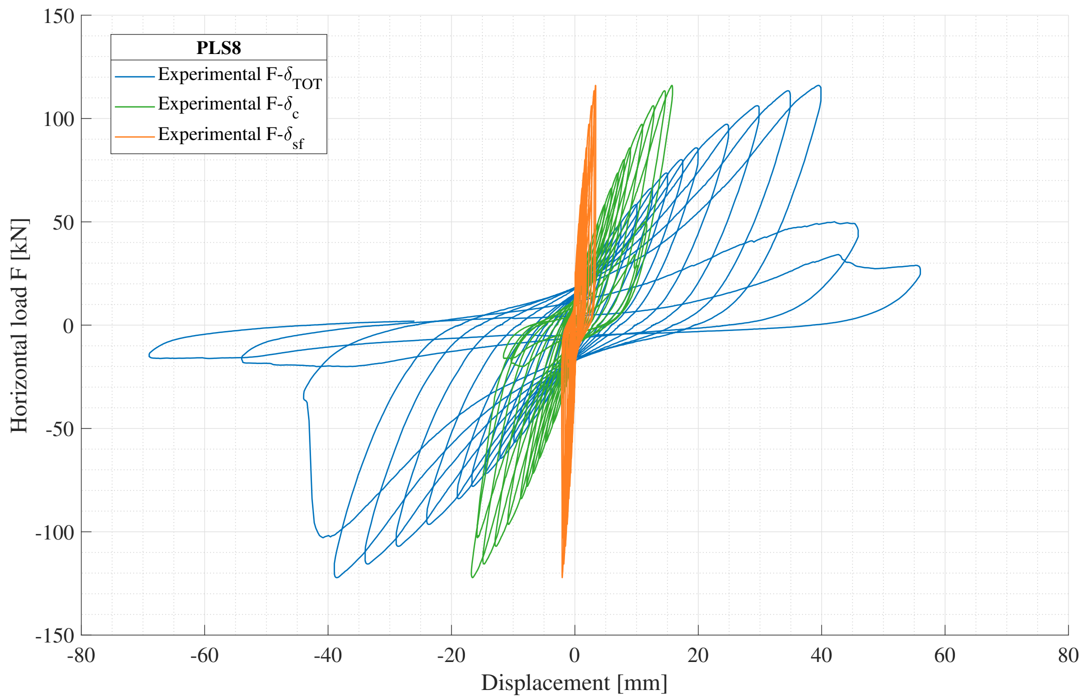

Figure 6.7. Experimental data of specimen PLS8 (from [26]).

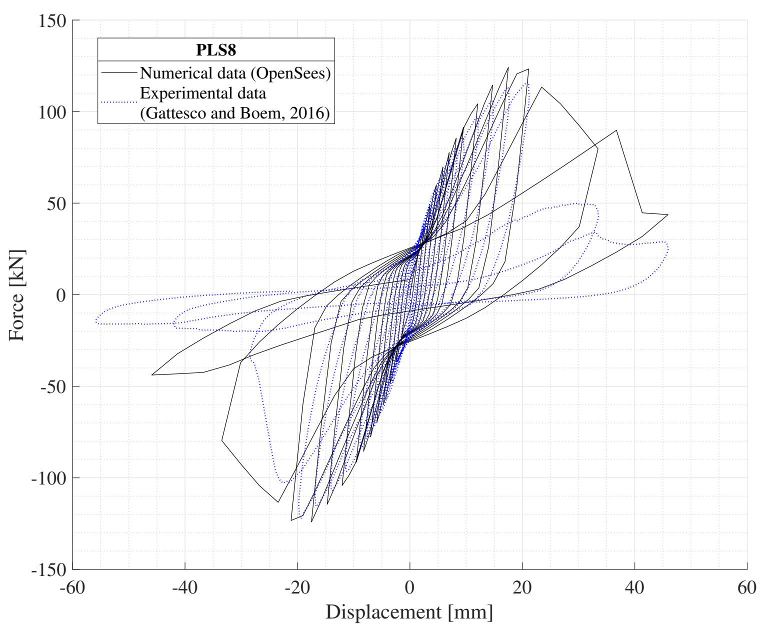

Figure 6.8. Comparison between experimental and predicted load-displacement curves for the reference wall configuration (specimen PLS8).

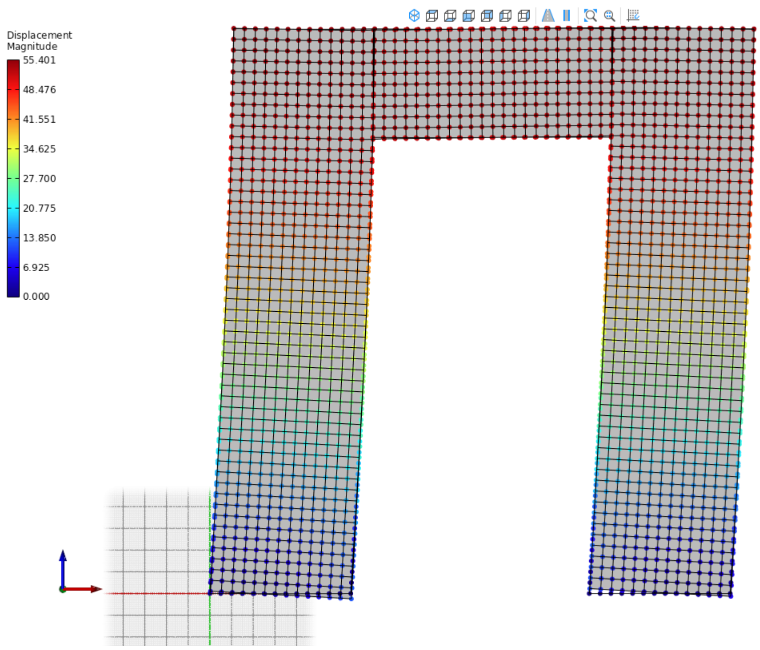

Figure 6.9. Deformed configuration of the shear wall considering the presence of opening (view of the FE model taken from STKO developed by [118]).

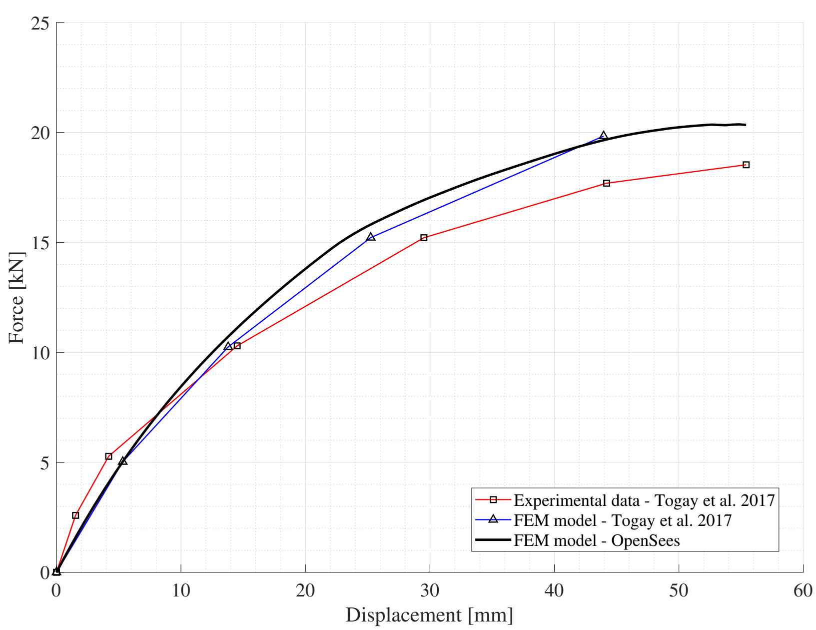

Figure 6.10. Comparison between experimental and predicted load-displacement curves for the reference wall configuration (specimen 2).

14080, 2013 [32] and EN 338, 2009 [31], they must have strength class not less than C16 (softwood, coniferous). In this work, strength class C24 has been considered. As shown in Fig. 6.10, the predicted force-displacement curve of a timber light-frame shear wall with an opening is in good agreement with the experimental tests performed in [117] (red).

The deformed configuration of the wall is shown in Fig. 6.9. The shell elements have size equal to 50 mm × 50 mm whereas nails spacing is 100 mm and 300 mm on the external edges and on the horizontal elements of the central section, respectively according to [117]. It is remarked that different finer mesh sizes have been also used, and no significant variations have been observed.

Actually, nails $\phi 3.1/80$ (mm) have been used to connect the OSB plates and timber framing elements. Without an experimental load-displacement curve, the performances related to a single fastener have been obtained by multiplying per 1.08 the ordinates of the $\phi 2.8$ nail force vs. displacement curve, following the procedure in [26]. Specifically, the amplification factor has been estimated as a mean value between the stiffness ratio and the resistance ratio of the two nail types, by exploiting the simplified analytical relationship proposed by EuroCode 5 [20] to predict the stiffness for timber-to-timber connections, considering nails without pre-drilling:

$$K_{ser} = \frac{\rho_m^{1.5} \cdot d^{0.8}}{30} \tag{6.4}$$

The ratio between the stiffness of the $\phi 3.1$ nail ($K_{ser,\phi 3.1}$) and $\phi 2.8$ nail ($K_{ser,\phi 2.8}$) has been evaluated as follows:

$$\frac{K_{ser,\phi 3.1}}{K_{ser,\phi 2.8}} = \left(\frac{\phi_{3.1}}{\phi_{2.8}}\right)^{0.8} \tag{6.5}$$

where ϕ is the nail diameter.

6.5 Sensitivity analyses on wall without openings

Starting from the experimental tests performed by Gattesco and Boem [26], sensitivity analyses were carried out by varying some input parameters in order to assess their influence on the wall behavior.

6.5.1 Method of analysis and loading conditions

A horizontal cyclic loading under displacement-controlled conditions is applied to evaluate the energy dissipation due to the nails, taking into account the relative displacement of the nodes between shells and frame. The overall response has been evaluated by varying: *i)* aspect ratio of the shear wall, *ii)* horizontal and vertical nails spacing, *iii)* number of vertical studs and *iv)* cross-section size of the framing elements. No vertical load is applied, so as to assess the behavior of the wall considering the configuration tested by Gattesco and Boem [26]. The reference wall configuration is the one denoted as PLS8 in [26].

By observing the overall behavior of the wall and the local behavior of the nails, the following definitions are adopted:

1. the Life Safety Limit State is recognized to occur in correspondence of the racking strength peak, when all fasteners along the perimeter framing elements are yielded (blue in Fig. 6.11);

2. the Collapse Limit State is recognized to occur when the most stressed fastener, usually at the bottom corner, reaches its failure displacement (red in Fig. 6.12).

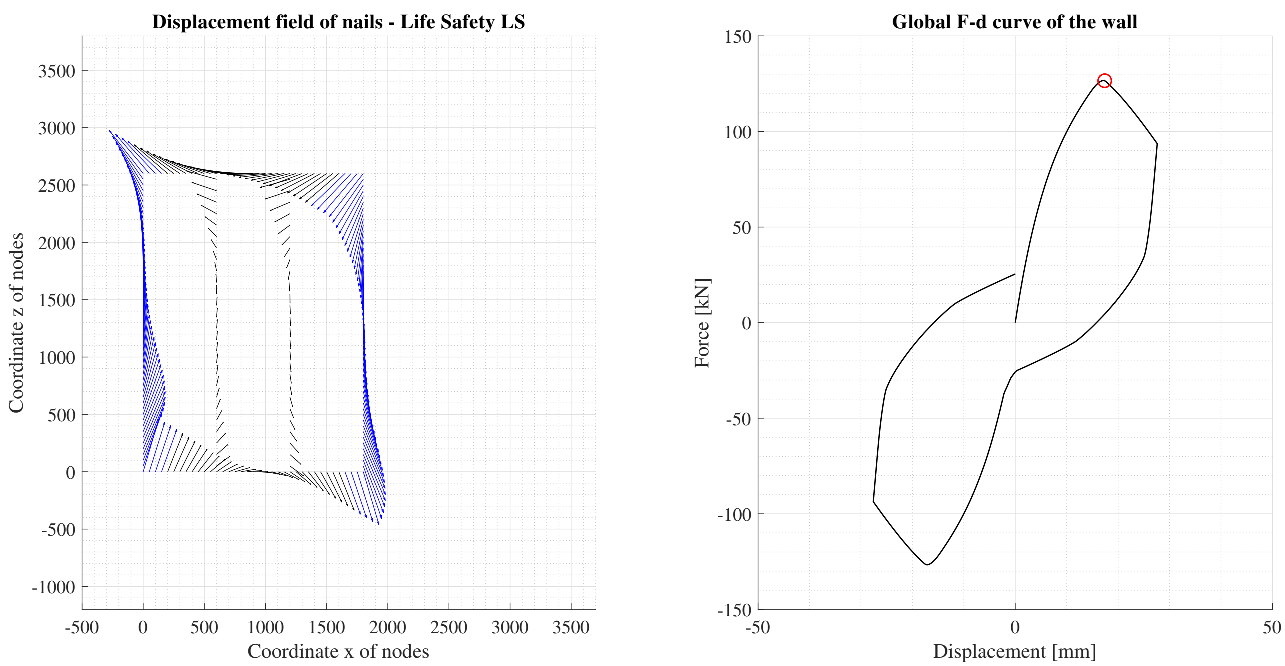

Figure 6.11. The behavior of the wall at Life Safety Limit State.

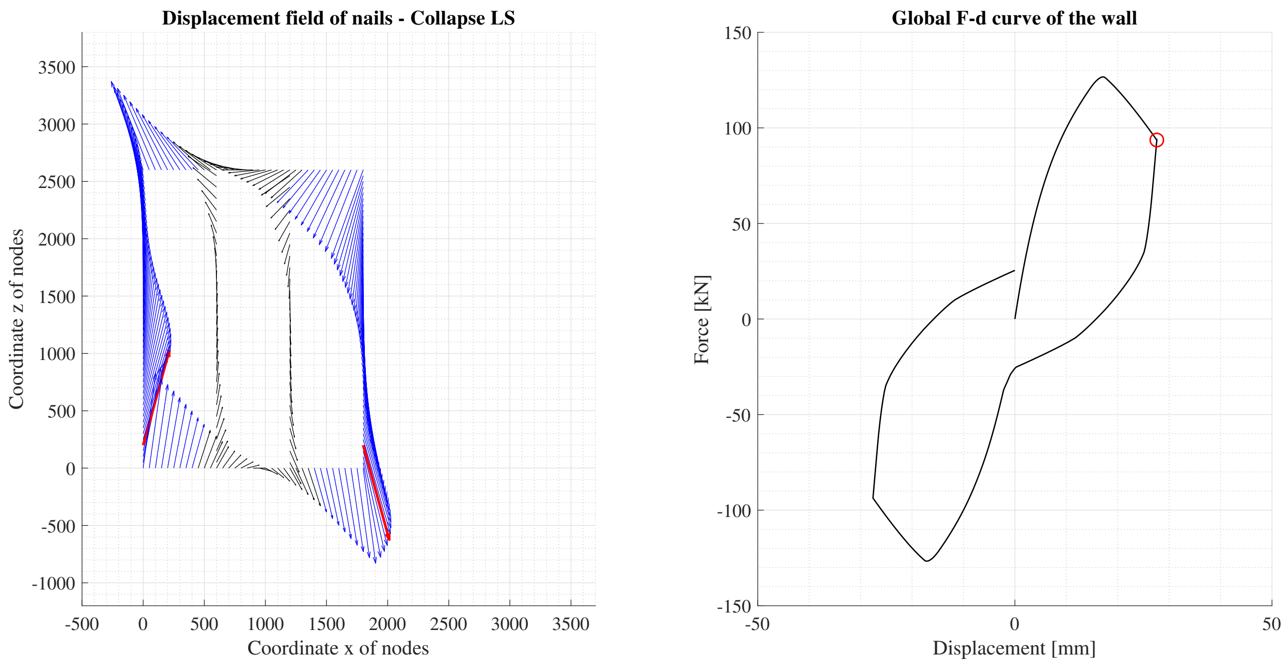

Figure 6.12. The behavior of the wall at Collapse Limit State.

In the latter case, the most stressed fastener is able to dissipate its maximum available energy, whereas all other fasteners dissipate only a fraction of it, because they undergo a displacement lower than their failure displacement. At the Collapse Limit State, the energy dissipation reaches its maximum value, since most of the nails have entered the plastic regime. As a consequence, a local failure displacement criterion was defined: the amount of dissipated energy is evaluated under the force-displacement curve of a certain configuration until the first fastener reached a resistance decrease equal to 65%, according to the experimental data in Gattesco and Boem [26].

6.5.2 Internal releases

It is worth nothing that the presence of internal releases between the ends of vertical studs and the horizontal joists affect significantly the response of the wall, as shown in Fig. 6.13.

The configuration assumed by the loading path of the nails is also different (Fig. 6.15). Without the internal releases, both shear and flexural deformations of the framing members affect the loading path of nails.

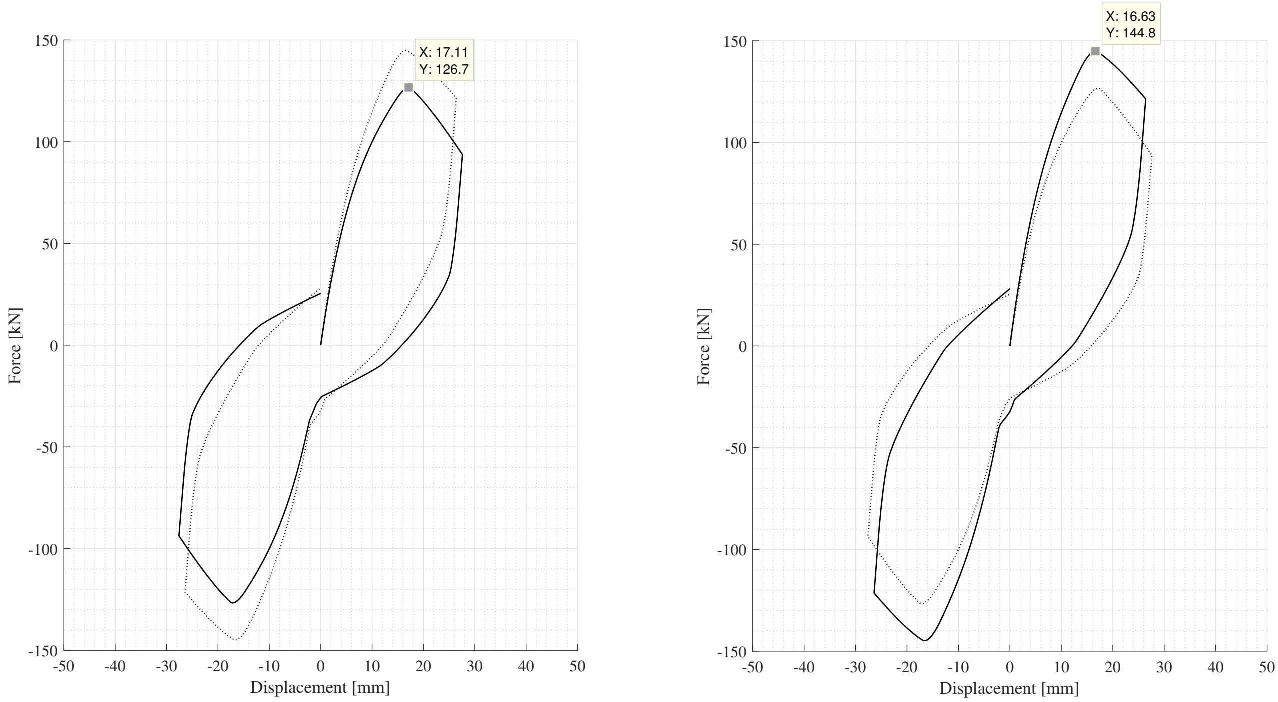

Figure 6.13. Overall behavior considering the shear wall: with internal releases (left), without internal releases (right).

6.5.3 Aspect ratio

As pointed out by Salenikovich [12], the response of partially anchored timber shear walls (as well as that of non-anchored walls) strongly depends on the aspect ratio (i.e., height-to-width ratio). The reduction of the aspect ratio (from slender to squat wall) leads to an increment of the racking capacity (as shown in Fig. 6.14) and the relative rigid rotation of the sheathing panel with respect to the frame mostly stresses the nails near the corners. As it can be inferred from the experimental tests presented in [90], a flexural behavior of the timber shear wall can be observed if the width is significantly less than the height (e.g., about 30%). Otherwise, the contribution of shear deformation to storey displacements increases, with a growth of stiffness and racking capacity. This is due to the fact that a larger studs number is required in this case, and thus the whole system is stiffer whereas only the perimeter nails contribute to the energy dissipation (the others remain in the elastic range).

Due to the available size of sheathing panels used in practice, a timber light-frame shear wall with low aspect ratios could be comprised of more than one panel to brace the wood frame. In order to quan-

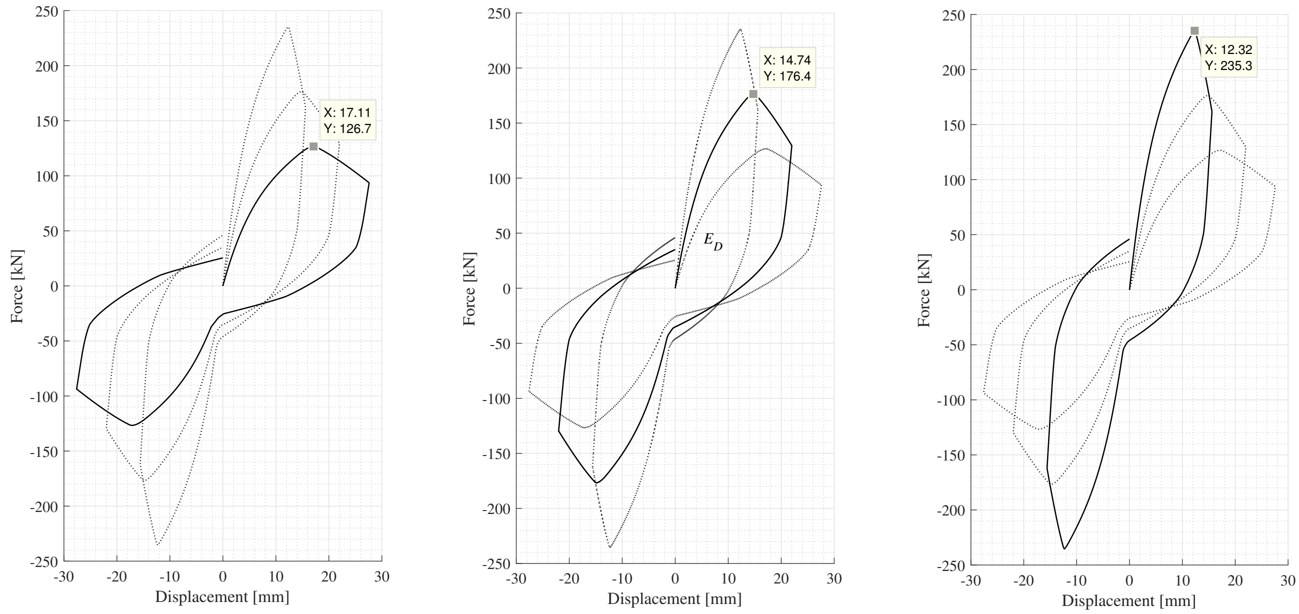

Figure 6.14. Influence of the aspect ratio (height-to-width ratio) on the overall response of the wall.

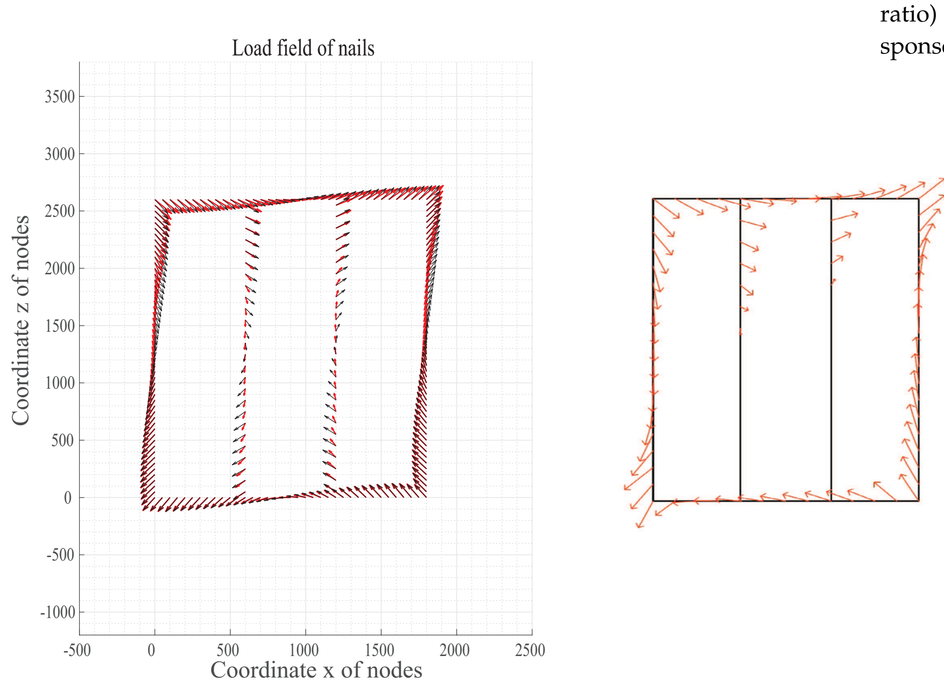

Figure 6.15. (left) Loading (kN) field of nails with (red) or without (black) internal releases; (right) Loading path for sample PLS8 in [26].

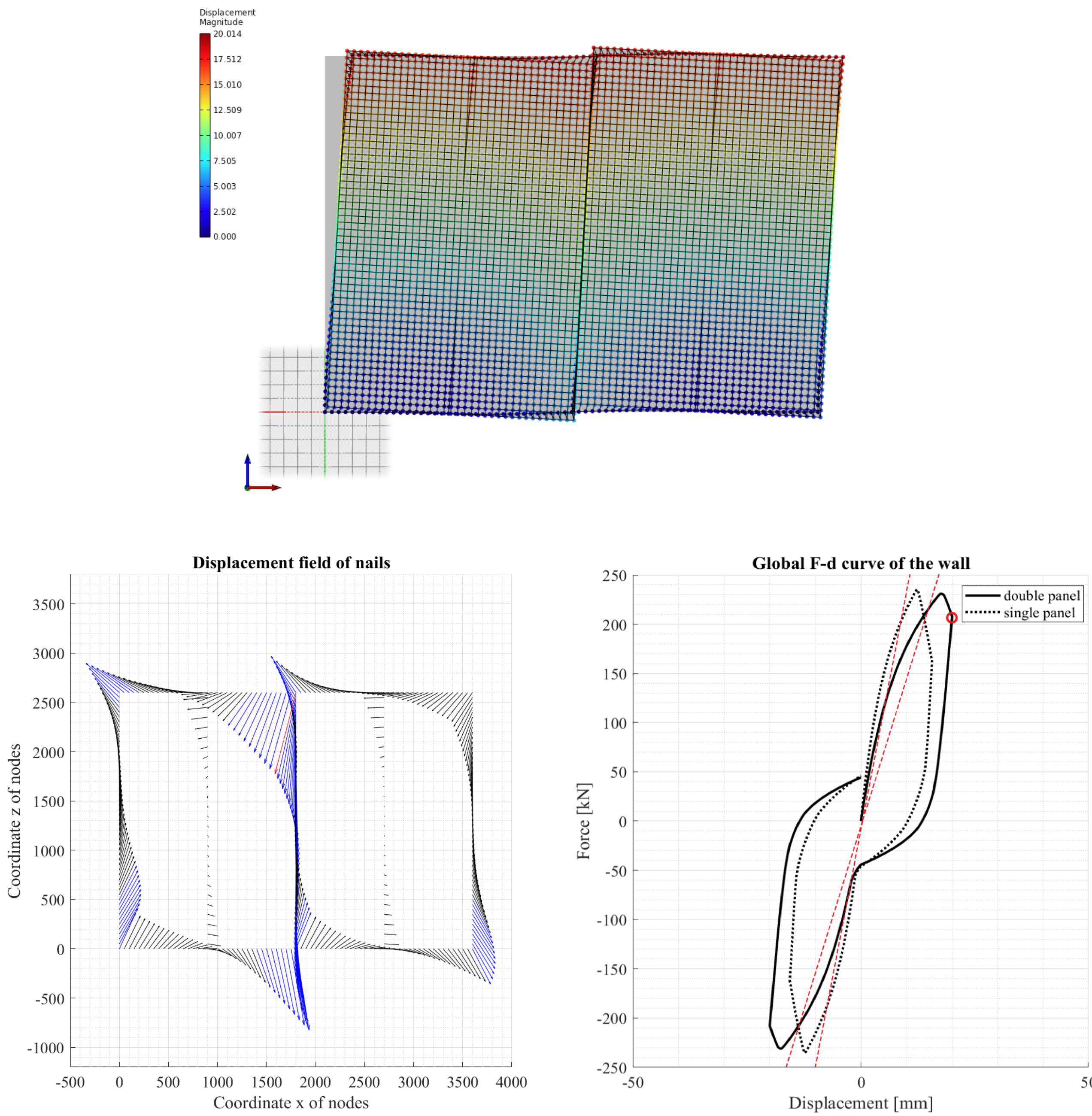

Figure 6.16. Aspect ratio equal to 0.7 considering 2 adjacent panels. To highlight the displacement field of nails the magnitude multiplier is equal to 10 (top) and to 100 (bottom, left).

tify the differences in terms of wall overall response, the parametric FE model has been developed to model this condition. As it is shown in Fig. 6.16, the racking load-carrying capacity and ductility of the wall are confirmed whereas a slightly different stiffness is observed (in red the analytical stiffness is provided for both cases[1]). This is due to the decrement of the panels inertia with respect to the in-plane actions. The [eq. 12, in 119] can be extended to a long wall with width l, sheathed with more long panels characterized by width b. The shape function $\lambda(\alpha)$ is then computed considering:

[1] For further details about the analytical procedure, see Sec. 7.

$$\begin{cases} 1\ \alpha = h/l & b = l \\ 2\ \alpha = h/b & b = \frac{l}{2} \end{cases} \tag{6.6}$$

where in 1 a single panel is considered, whereas in 2 two separate panels are employed.

6.5.4 Nails spacing

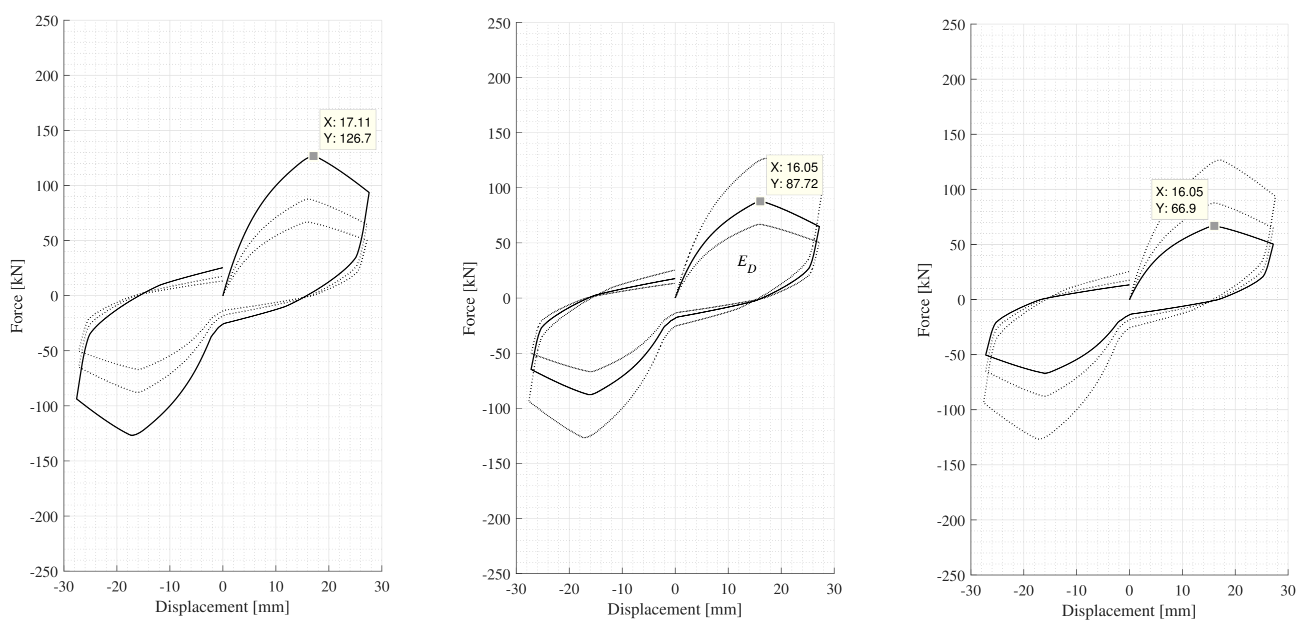

Figure 6.17. Influence of the nails spacing on the overall response of the wall.

Horizontal and vertical increment of nails spacing from 50 mm to 100 mm led to a decrease of the racking capacity of the wall up to 47% and a reduction of the stiffness close to 44% (Fig. 6.17). The racking capacity decrement depends on the reduced number of nails on the perimeter framing elements, which makes the overall system more flexible.

6.5.5 Number of vertical studs

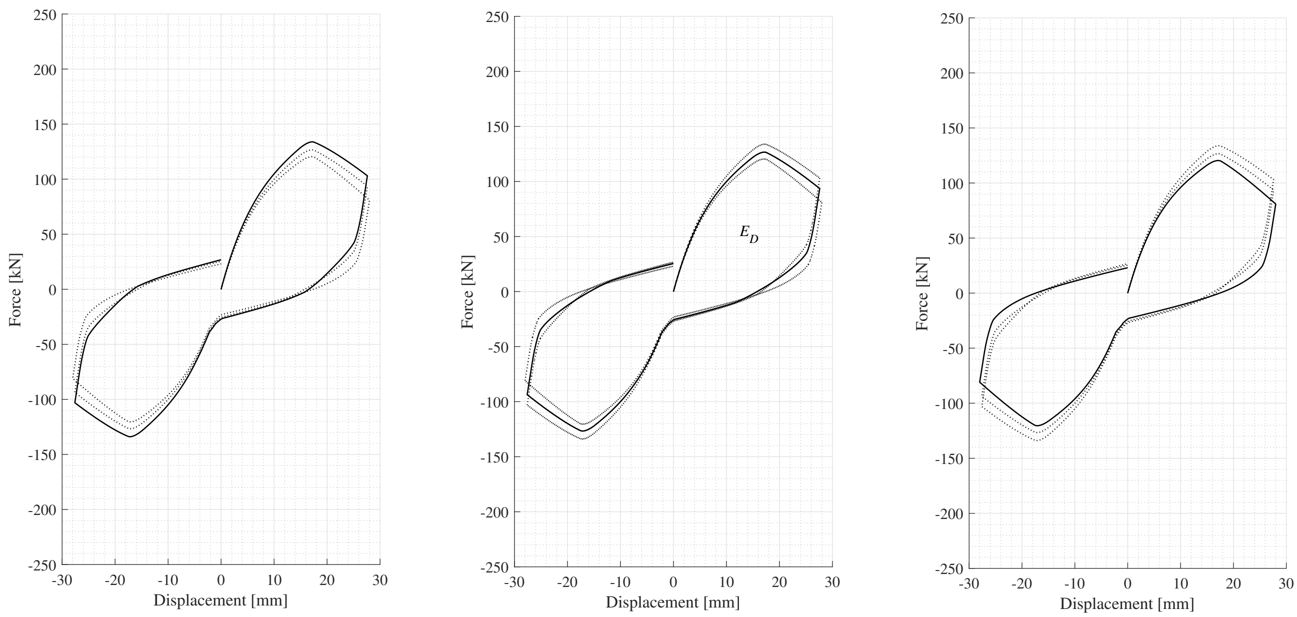

Figure 6.18. Influence of number of vertical studs on the overall response of the wall.

A stiffer wall with a higher racking capacity is obtained by increasing the number of vertical studs (the increment in terms of stiffness and racking capacity for the examined walls is about 11% as shown in Fig. 6.18). This is because the number of nails on the vertical studs is greater than the one considered in the previous configurations.

6.5.6 Cross-section size of framing elements

As it is shown in Fig. 6.19, the configurations of the wall with reduced size of the framing elements exhibit a reduced racking capacity. The larger the cross-section size of the framing elements, the larger the racking capacity and the dissipated energy. A further look at the results highlights that the increment in terms of stiffness and racking capacity for the examined walls is about of 82% and 38% by increasing the framing elements cross-section size.

This is attributable to the kinematic compatibility between the pure shear behavior of the framing elements and the behavior of the sheet, which rotates rigidly with respect to the frame and is also subjected to shear and flexural actions. Källsner and Girhammar [82] stated that: "*if fully flexibility of a framing member is assumed, no forces perpendicular to that member develop*". Hence, only a pure shear flow acts on fasteners in such a case. Actually, the configurations where nails are less stressed are those in which sheet or frame follows the imposed deformation of the other element. The relative in-plane stiffness is crucial to determine the stress level of the nails. If the stiffness of the sheet is larger than that of the framing elements or, conversely, the framing members are stiffer than the sheathing panel, then the nails do not exploit their maximum plastic deformation. If both the cross-section size of framing elements and the thickness of sheathing panel lead to a considerable relative displacements, then the maximum potential energy is dissipated by means of the plastic deformation of the nails.

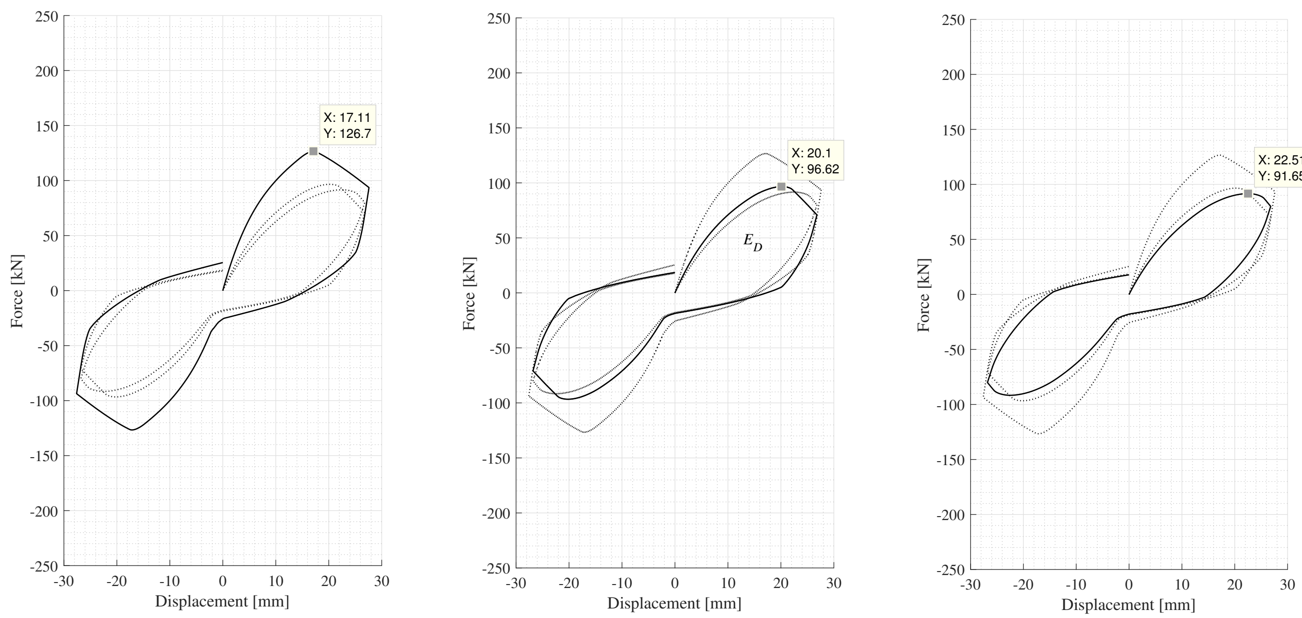

Figure 6.19. Influence of the cross-section size of the framing elements on the overall response of the wall.

6.5.7 Final comments on results

As it is shown in Fig. 6.20, the linear variation of the equivalent viscous damping as function of drift, observed by Filiatrault et al. [120], is fairly confirmed for different aspect ratios of a timber shear wall.

It can also be inferred that the energy dissipation strongly depends on the aspect ratio, thereby confirming the results in [12]. However, it is worth highlighting that the larger the wall size, the larger the number of vertical studs and the overall number of vertical nails. The resultant global system in this case is, therefore, much more stiff. This is due to the fact that a lower plasticity level is reached by increasing the number of vertical studs and, consequently, the overall number of nails. Conversely, the number of yielded nails grows by reducing the number of vertical studs, and thus a higher amount of dissipated energy is achieved. Particularly, a higher amount of nails, especially on the intermediate studs, makes the overall system more resistant, preventing buckling of the sheathing panel, without providing a contribution in terms of plastic deformation and energy dissipation. By reducing the nails spacing, a stiffer wall is observed. For the reference configuration (specimen PLS8 [26]), the equivalent viscous damping is about 23%. This means that the value of the total equivalent viscous damping required to estimate the reduction of the elastic demand spectrum is about of 28% (assuming an inherent viscous damping equal to 5%). Hence, the resulting η factor is about 0.55. A summary of the results related to the variation of racking capacity, equivalent viscous damping and damping factor, with respect to the geometric input parameters used in the parametric analyses, is shown in Fig. 6.21.

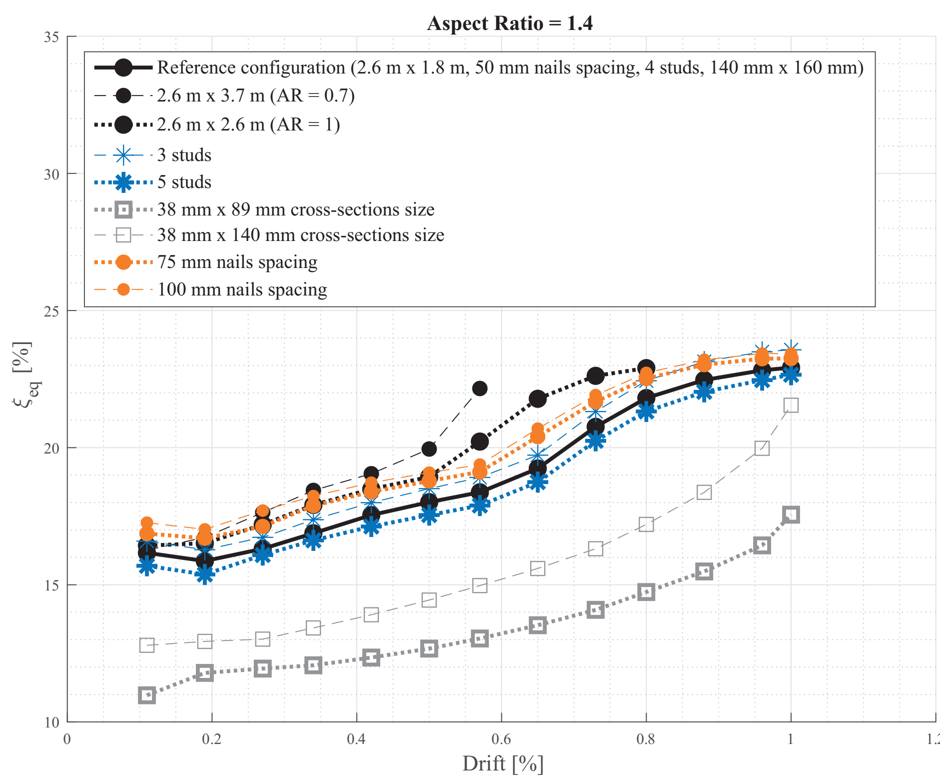

Figure 6.20. Equivalent viscous damping as function of the drift for different wall configurations. The solid black line indicates the reference configuration (named as PLS8 in [26]).

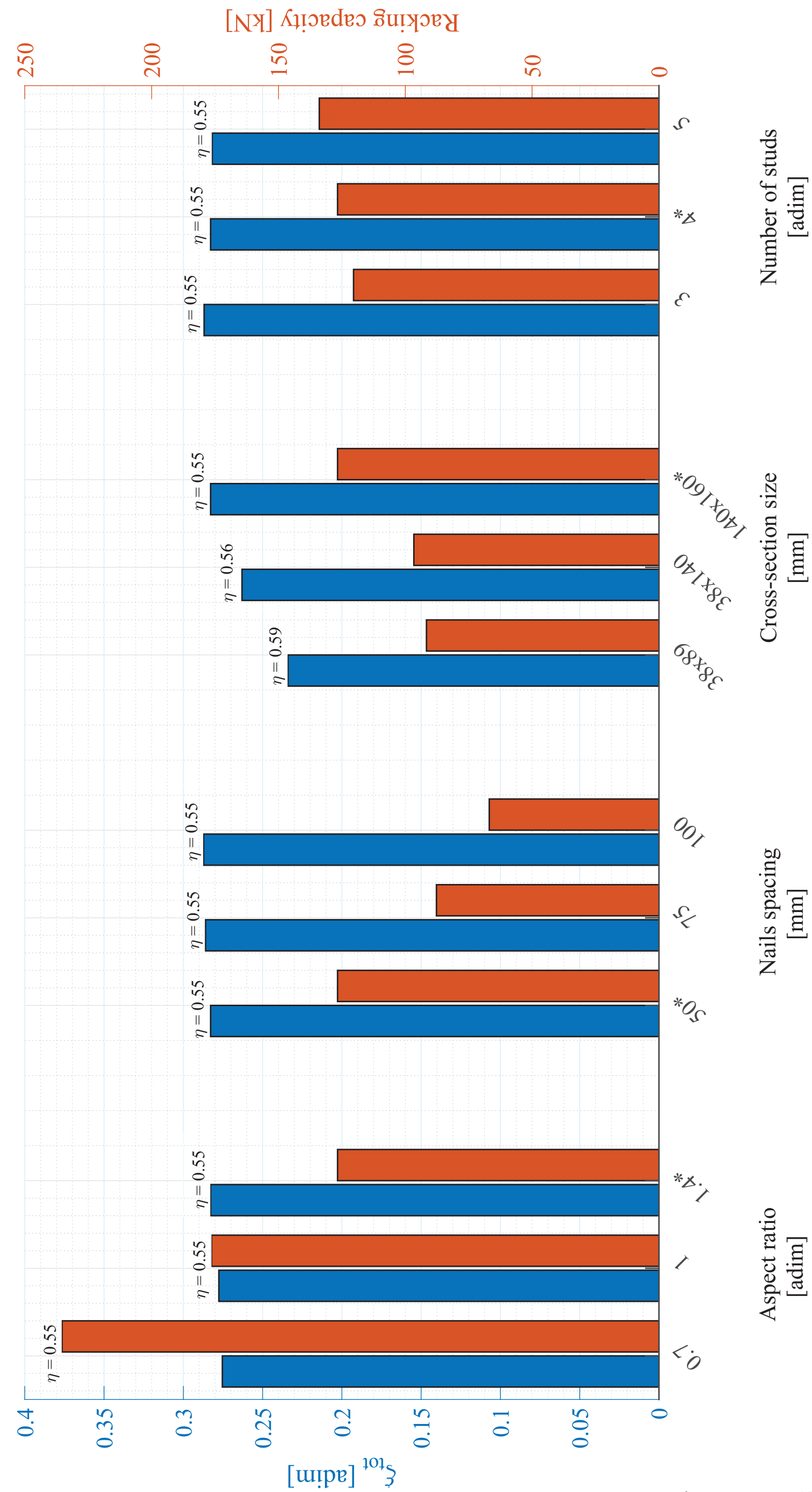

Figure 6.21. Equivalent viscous damping and racking capacity as function of some relevant parameters. The values of reference configuration are marked with symbol (*).

7 | Analytical procedure for seismic analysis and design

Abstract

Starting from the sensitivity analysis, an analytical procedure to predict the capacity curve of a timber light-frame shear wall is proposed. In order to compare the outcomes in a meaningful way, a definition of the equivalent viscous damping of a fastener is introduced, which also accounts for the softening that characterizes timber structures. All the input parameters that affect the overall behavior of the wall have been included to compute the output parameters of interest.

In particular:

- *The aspect ratio affects:*
  - *the energy dissipation distribution along the framing elements;*
  - *the racking capacity of the wall.*
- *The fasteners spacing affects:*
  - *the racking capacity of the wall;*
  - *the secant stiffness of the wall.*
- *The number of vertical studs affects:*
  - *the racking capacity of the wall;*
  - *the secant stiffness of the wall.*

7.1 Mechanical modeling

In order to capture the behavior of a timber light-frame shear wall corresponding to the defined Limit States (Sec. 6.1), the approach used in [20] has been followed. The maximum racking load-carrying capacity of the wall is computed starting from the maximum capacity of a single fastener [20, § 9.2.4.2 (4)]. In agreement with [19], the global secant stiffness (defined at the peak strength) is computed starting from the secant stiffness of a single fastener. Moreover, a close relation between the energy dissipated by each fastener and the global equivalent viscous damping has been observed. As a consequence, the wall ductility has been defined from the equivalent viscous damping, in such a way to compute the ultimate displacement. The sheathing-to-framing connection ductility results lower than the fastener ductility, as reported in [19]. Finally, once the fastener constitutive law is experimentally determined, the analytical procedure allows to obtain all the global quantities of interest, namely: *i)* the maximum lateral load-carrying capacity of the wall, *ii)* the yielding displacement, which corresponds to the peak strength, *iii)* the failure load-carrying capacity of the wall, *iv)* the ultimate displacement, which corresponds to the failure strength.

7.2 Single fastener for timber structures

7.2.1 Constitutive law

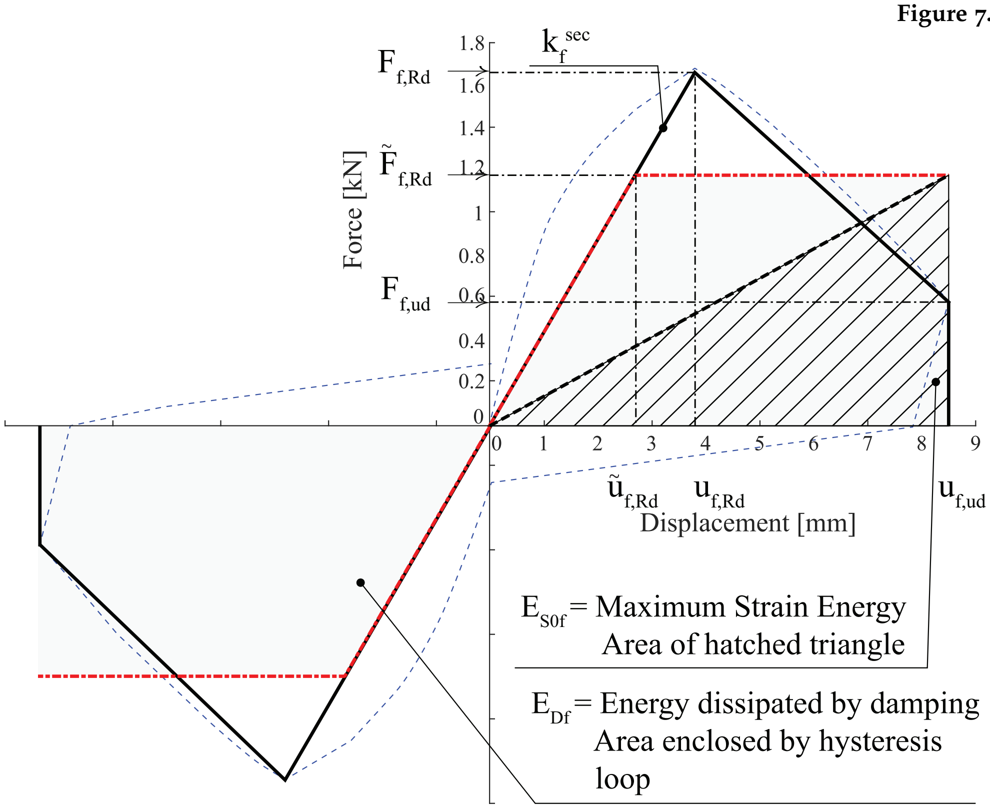

Figure 7.1. The constitutive law of a fastener Φ2.8/70. The blue dashed line denotes the experimental envelope [26]. The black solid line is the simplified experimental envelope. The red dash-dot line denotes the equivalent bilinearized system.

The constitutive law of a fastener is defined by three parameters (Fig. 7.1):

- k_f^{sec}= the secant stiffness, at the peak strength;
- $F_{f,Rd}$= the yield strength;
- $u_{f,ud}$= the ultimate displacement.

The yield displacement is:

$$u_{f,Rd} = \frac{F_{f,Rd}}{k_f^{sec}} \tag{7.1}$$

The constitutive law is of the softening type, so that, at the ultimate displacement $u_{f,ud}$, the corresponding force is:

$$F_{f,ud} = \alpha_f \cdot F_{f,Rd} \tag{7.2}$$

where α_f identifies the resistance decrement of the considered fastener (nail).

It should be noted that the available ductility of the fastener is defined as:

$$\mu_f = \frac{u_{f,ud}}{u_{f,Rd}} = \frac{k_f^{sec} \cdot u_{f,ud}}{F_{f,Rd}} \tag{7.3}$$

It is expedient to bilinearize the constitutive law up to failure, by imposing the same dissipated energy as in the original law. The dissipated energy under the original diagram is

$$E_{Df} = \frac{1}{2}\left[\frac{F_{f,Rd}^2}{k_f^{sec}} + (\alpha_f + 1)F_{f,Rd} \cdot (u_{f,ud} - u_{f,Rd})\right] \tag{7.4}$$

which can be simplified as follows:

$$E_{Df} = \frac{1}{2}\frac{F_{f,Rd}^2}{k_f^{sec}}\left[1 + (\alpha_f + 1) \cdot (\mu_f - 1)\right] = \frac{1}{2}\frac{F_{f,Rd}^2}{k_f^{sec}}\left[(\alpha_f + 1) \cdot \mu_f - \alpha_f\right] \tag{7.5}$$

The dissipated energy under the bilinearized diagram is:

$$\tilde{E}_{Df} = \tilde{F}_{f,Rd} \cdot u_{f,ud} - \frac{1}{2}\frac{\tilde{F}_{f,Rd}^2}{k_f^{sec}} \tag{7.6}$$

By equating the two previous equations, the fastener equivalent yield strength $\tilde{F}_{f,Rd}$ can be found as:

$$\tilde{F}_{f,Rd} = k_f^{sec} \cdot u_{f,ud} - \sqrt{\left(k_f^{sec}\right)^2 \cdot u_{f,ud}^2 - F_{f,Rd}^2\left[(\alpha_f + 1) \cdot \mu_f - \alpha_f\right]} \tag{7.7}$$

which can be written also as follows:

$$\tilde{F}_{f,Rd} = k_f^{sec} \cdot u_{f,ud} \left(1 - \sqrt{1 - \frac{\left[(\alpha_f + 1) \cdot \mu_f - \alpha_f \right]}{\mu_f^2}} \right) \tag{7.8}$$

7.2.2 Equivalent viscous damping and ductility

Starting from the bilinearization process described in the previous section, the bilinearized ductility is obtained as:

$$\tilde{\mu}_f = \frac{k_f^{sec} \cdot u_{f,ud}}{\tilde{F}_{f,Rd}} \tag{7.9}$$

and, finally, the fastener equivalent viscous damping can be computed as follows:

$$\xi_f = \frac{2\tilde{E}_{Df}}{2\pi \tilde{F}_{f,Rd} \cdot u_{f,ud}} = \frac{u_{f,ud} - \frac{1}{2}\frac{\tilde{F}_{f,Rd}}{k_f^{sec}}}{\pi u_{f,ud}} = \frac{1 - \frac{1}{2}\frac{\tilde{F}_{f,Rd}}{k_f^{sec} \cdot u_{f,ud}}}{\pi} \tag{7.10}$$

which can be simplified as follows:

$$\xi_f = \frac{1}{\pi}\left(1 - \frac{1}{2\tilde{\mu}_f}\right) \tag{7.11}$$

7.3 Timber Light-Frame shear wall

Timber light-frame shear wall is an assembly of modular panels with aspect ratio from 0.7 to 2 [13]. The common standard size used in practice are: 2.4 m× 3.6 m, 2.4 m× 2.4 m, 2.4 m × 1.2 m. As far as the clear distance between studs b_{net} and the thickness t of the sheathing panel are concerned, according to EuroCode 5 [20], the requirement $b_{net}/t \leq 100$ has to be satisfied in such a way to prevent buckling of the sheathing panel.

7.3.1 Definition of the equivalent viscous damping

Once the fastener equivalent viscous damping is defined, the total equivalent viscous damping of a wall with nail connections can be computed. The equivalent viscous damping is function of the global energy dissipated within a single hysteresis loop E_D and the global maximum strain energy, also known as stored energy of system E_{s0} (Sec. 5.3). Specifically:

$$\xi_{eq} = \frac{E_D}{4\pi E_{s0}} \tag{7.12}$$

In case of the Collapse Limit State, as defined in Sec. 6.1, the most stressed fastener is able to dissipate its maximum available energy. On the other hand, all other fasteners dissipate only a fraction of it because they undergo a displacement lower than their failure displacement. The energy dissipation reaches its maximum value, since most of the fasteners have displaced well into the plastic range. Figure 7.2 depicts the energy dissipation field produced by the fasteners along the framing elements (vertical studs and horizontal joists), for different aspect ratios of the wall.

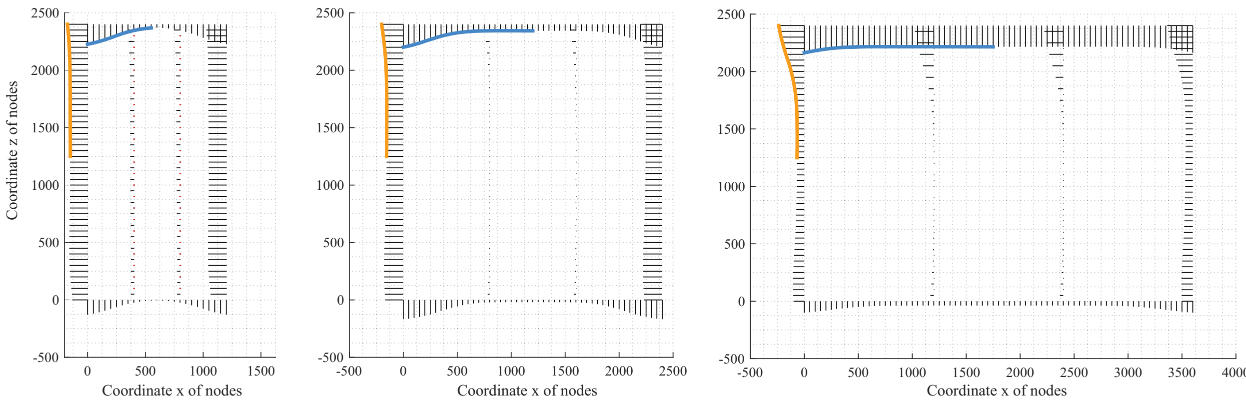

Figure 7.2. Energy dissipation distribution along the perimeter framing elements for different aspect ratios of the wall: (left) slender wall; (middle) square wall; (right) squat wall.

The energy E_D actually dissipated by all fasteners can be expressed as the sum of the energies dissipated by the fasteners along studs and joists, with the exception of the intermediate studs, where the dissipation is negligible:

$$E_D = \kappa f_v \cdot E_{Df} + \gamma f_h \cdot E_{Df} = E_{Df}(\kappa f_v + \gamma f_h) \tag{7.13}$$

Along each element, either perimeter studs or joists, the actually dissipated energy is given as the ratio, respectively κ and γ, of the available dissipating energy (Fig. 7.3). Notice that the latter is the maximum energy that can be dissipated if all fasteners failed at the same time. It is expressed as the maximum energy E_{Df} that can be dissipated by a single fastener times the total number of fasteners along perimeter studs and joists, f_v and f_h, respectively.

As far as the elastic energy E_{s0} in eq. (7.12) is concerned, this is computed as the sum of the elastic energy in the fasteners on the perimeter studs and on the horizontal joists, as follows:

$$E_{s0} = f_v \cdot E_{s0f} + f_h \cdot E_{s0f} = E_{s0f}(f_v + f_h) \tag{7.14}$$

where E_{s0f} is the elastic energy of a single fastener as shown in Fig. 7.1.

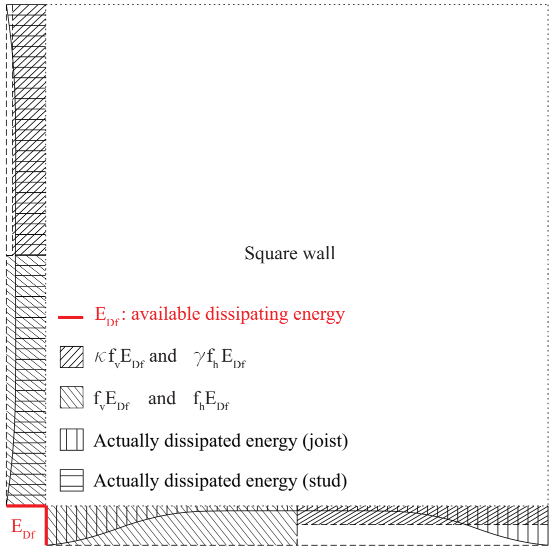

Figure 7.3. Energy dissipation fields along the vertical studs and the horizontal joists: calibration of κ and γ.

The equivalent viscous damping can be computed as follows, by replacing eq. (7.13) and eq. (7.14) into eq. (7.12):

$$\xi_{eq} = \frac{E_D}{4\pi E_{s0}} = \frac{E_{Df}}{4\pi E_{s0f}} \cdot \frac{\kappa f_v + \gamma f_h}{f_v + f_h} \tag{7.15}$$

Finally, recognizing that the equivalent viscous damping of the fastener that dissipates the maximum energy is:

$$\frac{E_{Df}}{4\pi E_{s0f}} = \xi_f \tag{7.16}$$

the global equivalent viscous damping of a timber light-frame shear wall can be expressed as follows:

$$\xi_{eq} = \xi_f \cdot \frac{\kappa f_v + \gamma f_h}{f_v + f_h} \tag{7.17}$$

The values of the coefficients κ and γ have been identified by looking at the energy dissipation of walls with different aspect ratios, i.e. equal to 0.7, 1, 2, with 3 studs (except for the aspect ratio 0.7, see Sec. 7.3), 4 and 5 studs. These coefficients turn out to be defined as follows (Fig. 7.4):

$$\kappa = min(AR; 1) \tag{7.18}$$

$$\gamma = min(\frac{1}{AR}; 0.8) \tag{7.19}$$

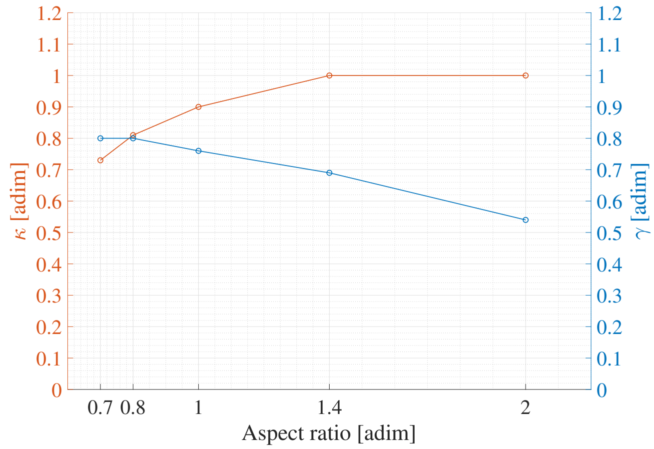

Figure 7.4. Calibration of κ and γ according to different aspect ratios.

The total equivalent viscous damping is then computed by adding the inherent viscous damping ξ_{in} (assumed equal to 5%):

$$\xi_{tot} = \xi_{in} + \xi_{eq} \tag{7.20}$$

and according to the EuroCode 8 [21], the damping correction factor is computed as follows:

$$\eta = \sqrt{\frac{10}{5 + \xi_{tot}}} \tag{7.21}$$

7.3.2 Definition of the racking load-carrying capacity

Starting from the proposals of the EuroCode 5 [20] (see Sec. 5.7.1), and [19] (see Sec. 5.6.1), the equation to compute the racking capacity of the wall $F_{v,Rd}$ becomes (Fig. 7.5):

$$R_{SH} = F_{v,Rd} = n_{bs} \cdot F_{f,Rd} \cdot \frac{\sum b_i \cdot c_i}{s} \tag{7.22}$$

where $c_i = \begin{cases} 1 & \alpha < 2 \\ \frac{\alpha}{2} & 2 < \alpha < 4 \\ 0 & \alpha > 4 \end{cases}$, with $\alpha = \frac{h}{b}$ aspect ratio (AR) of the wall panel and b_i is the panel width.

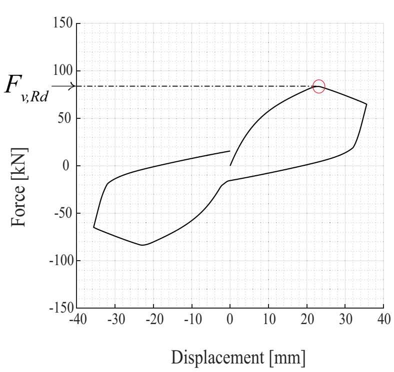

Figure 7.5. Step 1: computation of the wall racking load-carrying capacity.

To take into account more than 3 vertical studs for each panel as an alternative to the summation in eq. (7.22), the presence of one more fastener for each added stud can be considered in the previous equation as follows:

$$R_{SH} = F_{v,Rd} = n_{bs} \cdot F_{f,Rd} \cdot c \cdot \left[\frac{b}{s} + (n_s - 3)\right] \tag{7.23}$$

where n_s is the number of vertical studs.

7.3.3 Definition of the ultimate strength

Starting from the experimental force-displacement curve of a ring fastener $\phi 2.8/70$ (Fig. 6.6), the stress distribution on fasteners along the perimeter framing elements has to be considered in collapse conditions (Fig. 7.6). The strength distribution can be approximated reasonably to the yield force of the bilinearized diagram of the fastener, $\tilde{F}_{f,Rd}$.

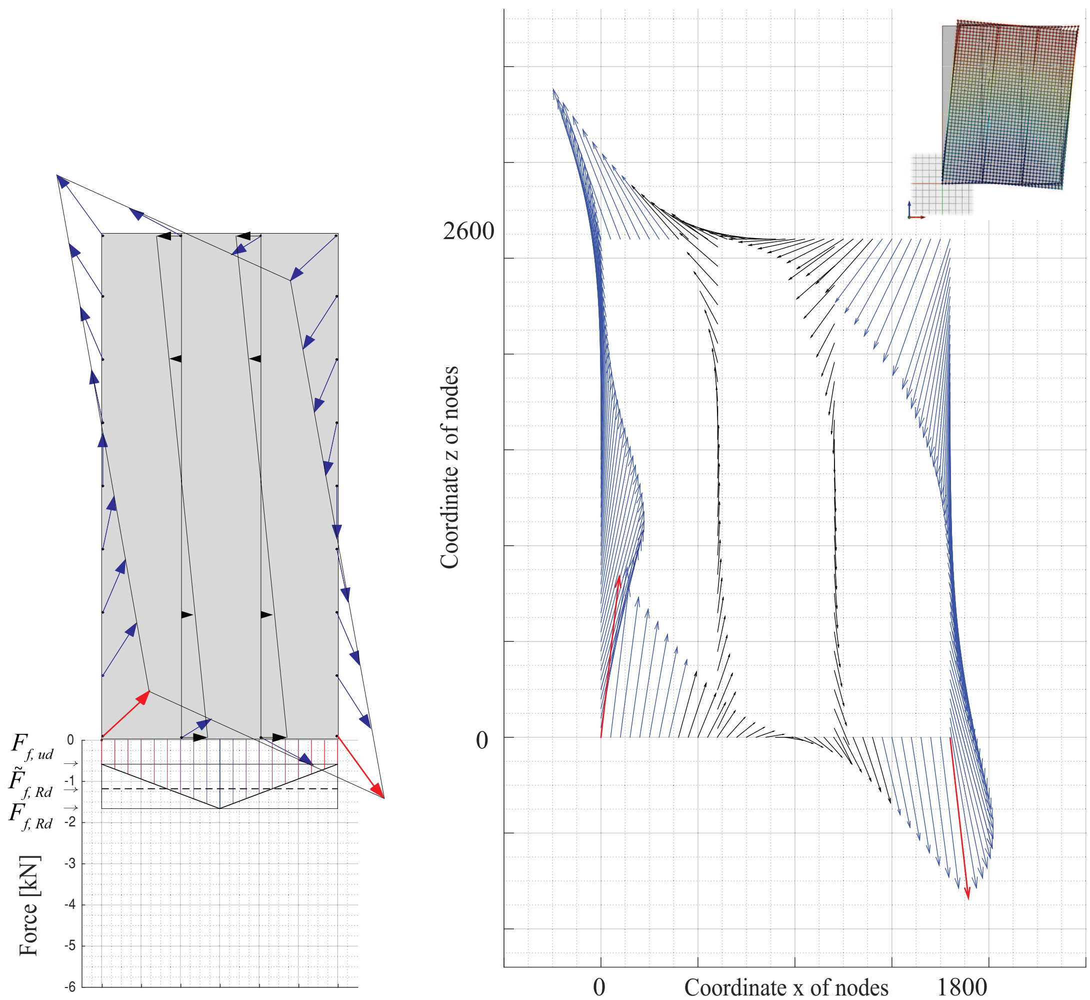

Figure 7.6. The stress distribution on fasteners in collapse conditions. On the left (bottom) the force levels of one fastener (with subscript "f") derived from the experimental tests in [26]; on the right the displacement field of fasteners (the magnitude multiplier is equal to 100 whereas, for the deformed configuration of the wall shown on the top, it is equal to 10).

Thus, the ultimate global force of the wall $F_{v,ud}$ is determined as done in [20] for the maximum load-carrying capacity (Fig. 7.7):

$$F_{v,ud} = n_{bs} \cdot \tilde{F}_{f,Rd} \cdot \frac{\Sigma b_i \cdot c_i}{s} \tag{7.24}$$

that becomes:

$$F_{v,ud} = n_{bs} \cdot \tilde{F}_{f,Rd} \cdot c \cdot \left[\frac{b}{s} + (n_s - 3) \right] \tag{7.25}$$

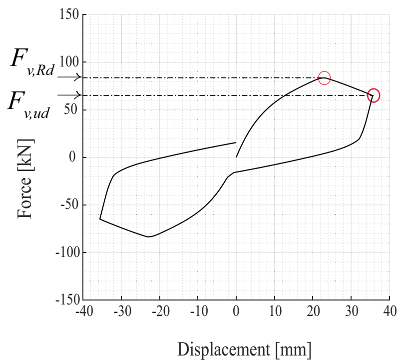

Figure 7.7. Step 2: computation of the wall ultimate strength.

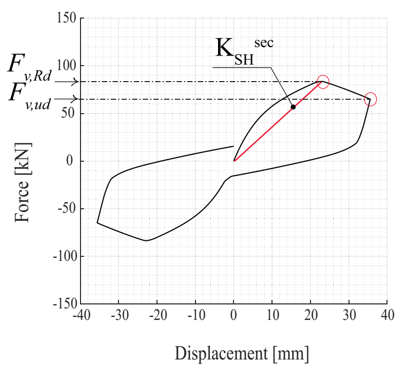

Figure 7.8. Step 3: computation of the wall secant stiffness.

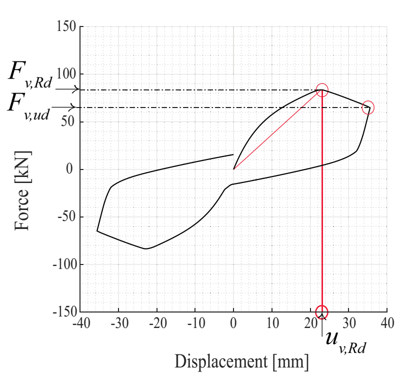

Figure 7.9. Step 4: computation of the yield displacement.

to take into account more than 3 vertical studs, as done for the racking capacity.

7.3.4 Definition of the overall secant stiffness

The global secant stiffness, starting from the analytical model proposed by Casagrande et al. [19], is computed as follows (Fig. 7.8):

$$K_{SH}^{sec} = \frac{n_{bs} \cdot k_f^{sec}}{\left(\frac{s}{l}\right) \cdot \lambda(\alpha_i)} \tag{7.26}$$

where $\lambda = 0.81 + 1.85\alpha_i$ is a shape function depending on the aspect ratio of the wall panel and l is the wall width.

In order to capture the global secant stiffness of the wall corresponding to the peak strength, the stress distribution on fasteners along the perimeter framing elements has to be considered, as done within the previous section for the ultimate strength. In this condition, all the effective nails are yielded, but for different local displacements. When the last nail yields, most of them are already beyond the elastic limit (softening part of the constitutive law). This, in turn, is the main cause of the global softening behaviour of the wall. As it has been done for the determination of the ultimate strength, the nails stiffness distribution for the global strength peak can be reasonably assumed as the average between the stiffness reached by the most stressed nail (not failed, yet) and the stiffness of the last yielded one k_f^{sec}. The latter corresponds to the secant stiffness at peak strength of a single fastener, as defined in Sec. 7.2.1.

The previous definition of fastener stiffness to be used, equal to 80% of k_f^{sec}, provides good results for a wall when the timber frame can be assumed as rigid, namely when flexural deformation of studs and joists is negligible. This assumption is valid for the reference configuration of the wall considered in this work.

7.3.5 Definition of the analytical backbone F-d curve

The yield displacement is, then, automatically determined (Fig. 7.9) as:

$$\Delta_{SH} = u_{v,Rd} = \frac{F_{v,Rd}}{K_{SH}^{sec}} \tag{7.27}$$

Thus, the yield force of the bilinearized global curve is (Fig. 7.10):

$$\tilde{F}_{v,Rd} = \frac{F_{v,Rd} + F_{v,ud}}{2} \tag{7.28}$$

and the associated displacement is defined as follows, assuming the same secant stiffness (Fig. 7.10):

$$\tilde{u}_{v,Rd} = \frac{\tilde{F}_{v,Rd}}{K_{SH}^{sec}} \tag{7.29}$$

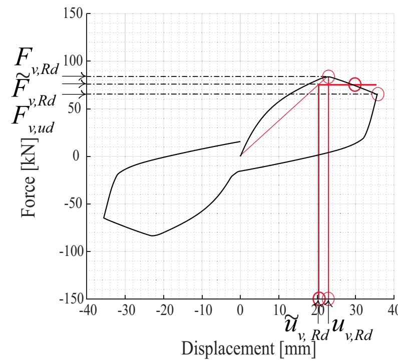

Figure 7.10. Step 5: computation of the yield force of the bilinearized global curve.

7.3.6 Definition of the global ductility and computation of the global ultimate displacement

By considering the same procedure applied to define the fastener equivalent viscous damping, the unknown global ultimate displacement $u_{v,ud}$ can be estimated. Starting from the definition of the global equivalent viscous damping (eq. 7.12), it results:

$$\xi_{eq} = \frac{2\tilde{E}_D}{2\pi\tilde{F}_{v,Rd} \cdot u_{v,ud}} = \frac{u_{v,ud} - \frac{1}{2}\frac{\tilde{F}_{v,Rd}}{K_{SH}^{sec}}}{\pi u_{v,ud}} = \frac{1 - \frac{1}{2}\frac{\tilde{F}_{v,Rd}}{K_{SH}^{sec} \cdot u_{v,ud}}}{\pi} \tag{7.30}$$

which can be simplified as follows:

$$\xi_{eq} = \frac{1}{\pi}\left(1 - \frac{1}{2\tilde{\mu}_{SH}}\right) \tag{7.31}$$

Once the equivalent viscous damping is computed as in eq. 7.17, by inverting eq. 7.31, the global bilinearized ductility can be obtained as:

$$\tilde{\mu}_{SH} = \frac{1}{2(1 - \pi\xi_{eq})} \tag{7.32}$$

and the ultimate global displacement is obtained as follows (Fig. 7.11):

$$u_{v,ud} = \tilde{u}_{v,Rd} \cdot \tilde{\mu}_{SH} \tag{7.33}$$

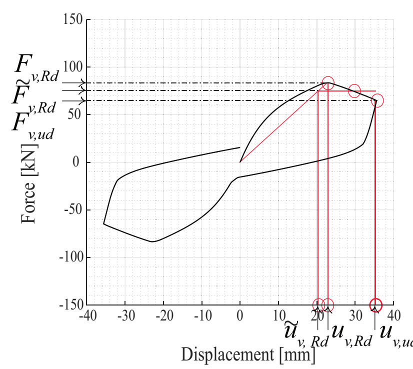

Figure 7.11. Step 6: computation of the wall ultimate displacement.

7.3.7 A simplified equation to correlate equivalent viscous damping and inter-storey displacement demand

As shown in Fig. 7.12, the linear variation of the equivalent viscous damping as function of drift, observed by [120], is confirmed for different aspect ratios of a timber shear wall.

Starting from the linear variation observed in Fig. 6.20, a simplified equation to predict the equivalent viscous damping with respect to a drift value is here proposed:

$$\xi_{eq} = m \cdot drift + q \tag{7.34}$$

where $m = 9$, *drift* is the drift value in percent and q is the value of the intercept with the y-axis (Fig. 7.13). This value is about 14 for upper trend-lines, that refer to variations of fasteners spacing and number of

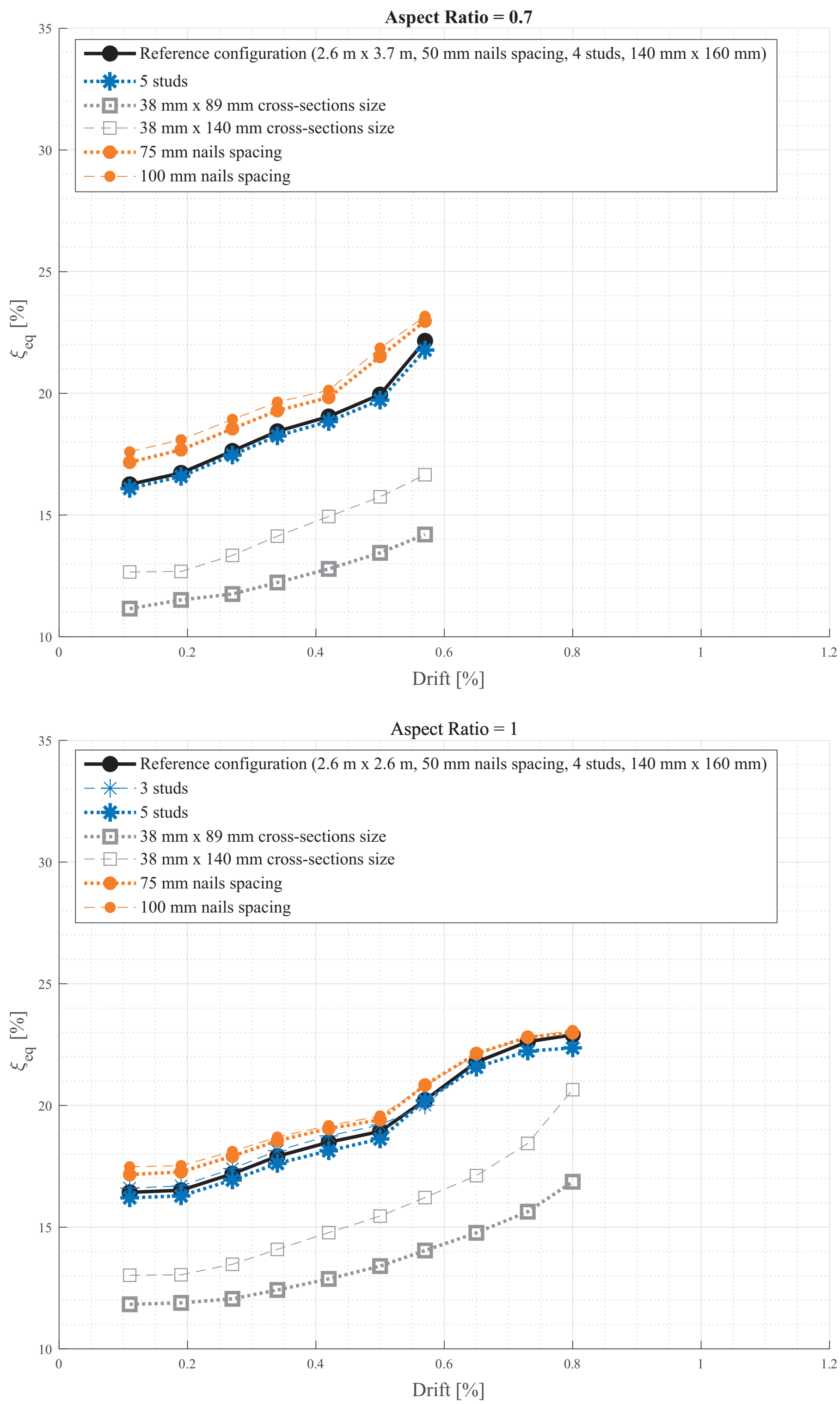

Figure 7.12. Equivalent viscous damping vs. drift for aspect ratio equal to 0.7 (top) and 1 (bottom), by varying the considered input parameters.

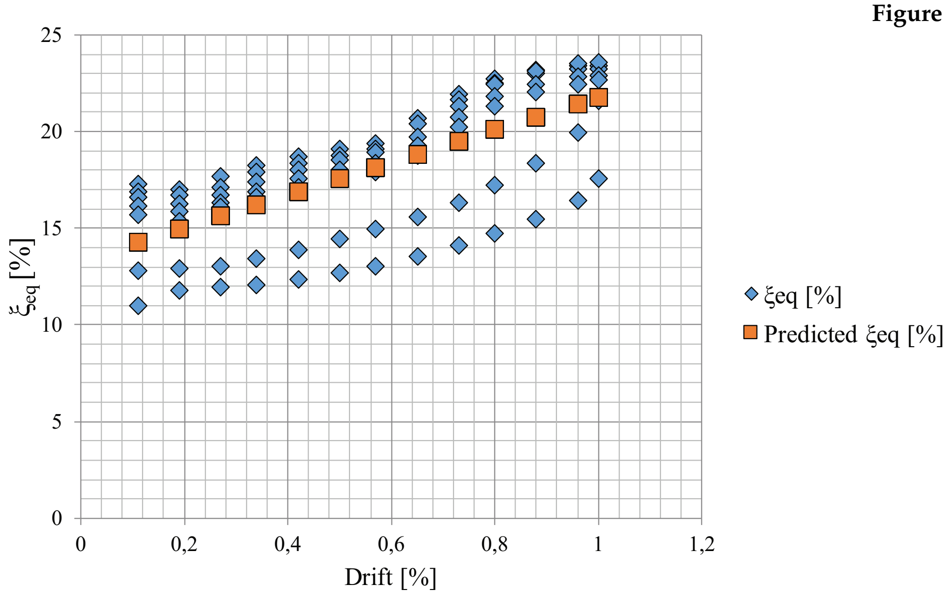

Figure 7.13. Regression line considering the variation of input parameters (aspect ratio equal to 1.4).

vertical studs. On the other hand, it is about 10 for the variation of cross-sections size.

It is worth to highlight that the drift limit has to be defined for different aspect ratios of a timber shear wall, according to the displacement failure criterion defined in sec. 6.1.

On the basis of the behavior of the timber shear wall, the function that defines the drift limit for each aspect ratio can be defined as:

$$drift_{lim} = \frac{AR}{2} + 0.3 \tag{7.35}$$

7.4 Validation of the analytical procedure

In order to validate the analytical procedure, a variation of common design variables has been considered, namely: *i)* aspect ratio, *ii)* fasteners spacing and *iii)* number of vertical studs. Both variations from the reference configuration [Specimen PLS8 in 26] and variations based on the wall sizes commonly used in practice (1.2 m × 2.4 m, 2.4 m × 2.4 m, 3.6 m × 2.4 m) have been considered. A good agreement between numerical and experimental load-displacement curves can be observed in Figs. 7.14 and 7.15, for both single-braced (SB) and double-braced (DB) timber light-frame shear walls. The proposed procedure predicts quite correctly the results for different configurations of a timber light-frame shear wall, often with a conservative estimate of the ultimate displacement (10-15% less than the maximum value predicted by the refined numerical model).

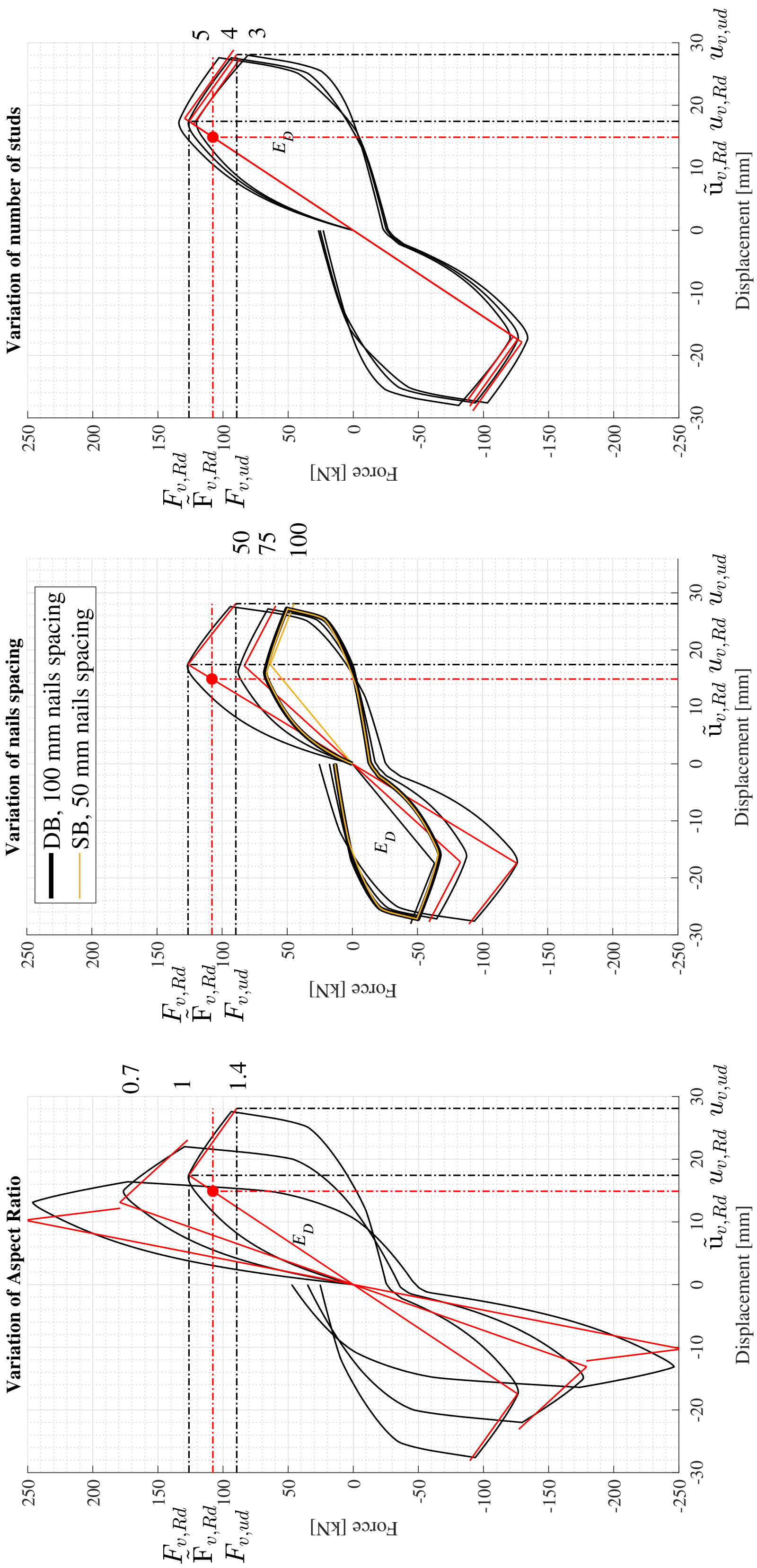

Figure 7.14. Validation of the analytical procedure: variation on the reference configuration [Specimen PLS8 in 26].

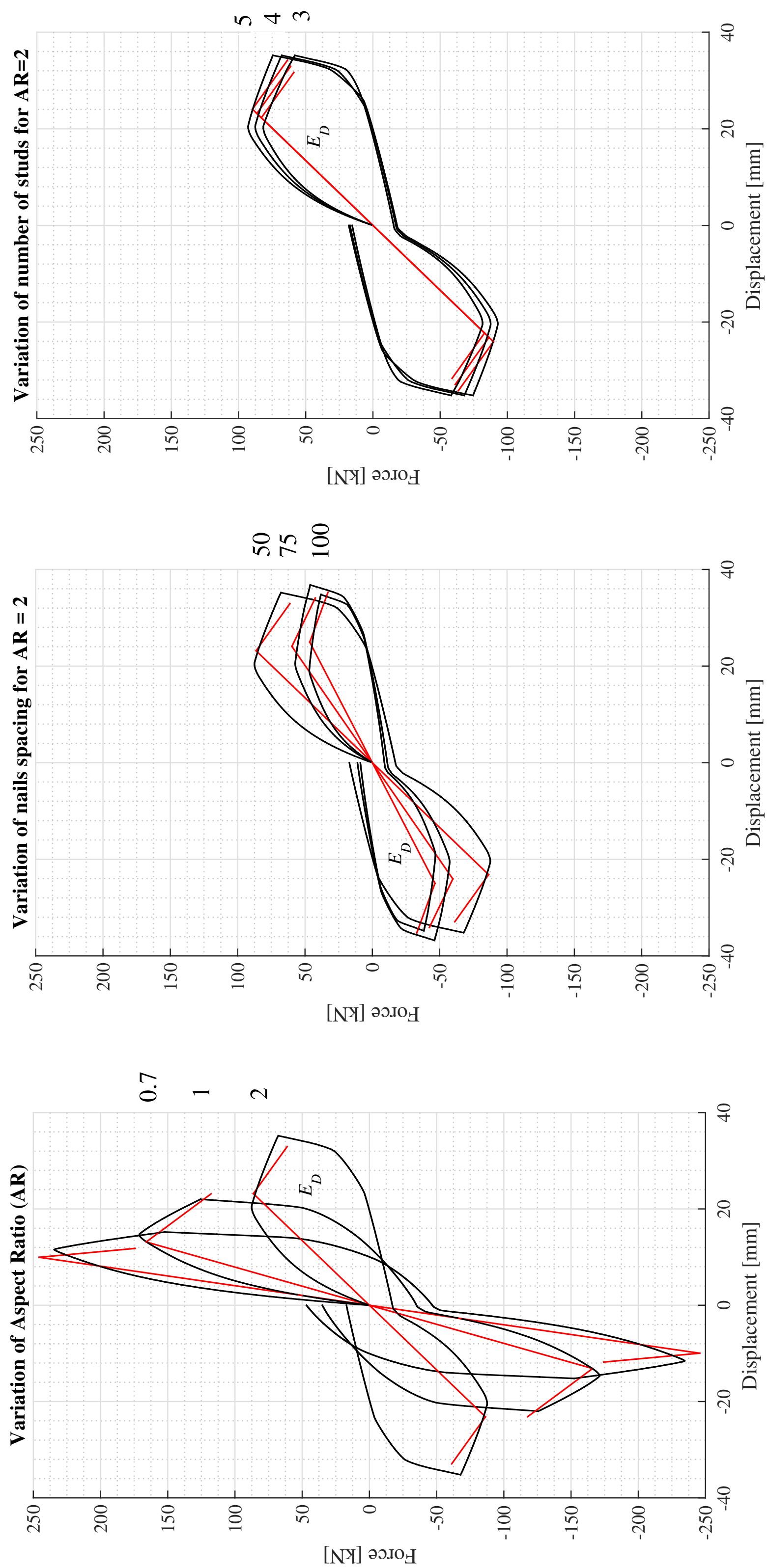

Figure 7.15. Validation of the analytical procedure: sensitivity analysis considering common values for each design variable.

7.5 Prediction of backbone curve considering the hold-downs contribution

As it is described in Sec. 5.6.1, the overall response of a timber light-frame shear wall is governed by the response of the weakest connection, i.e. it depends on the mechanism that first activates during the wall deformation. For the wall configuration considered in this work [Specimen PLS8 in 26] the weakest connection is the sheathing-to-framing connection. This usually holds true for walls where hold-downs are directly connected to the timber studs of the frame. Thus, once secant stiffness and bilinearized ductility of sheathing-to-framing connections are defined (Secs. 7.3.4 and 7.3.6), the secant stiffness of the wall K_v^{sec}considering the hold-downs contribution is obtained as follows:

$$\frac{1}{K_v^{sec}} = \frac{1}{K_{SH}^{sec}} + \frac{1}{K_H^{sec}} \tag{7.36}$$

$$K_v^{sec} = \left(\frac{1}{K_{SH}^{sec}} + \frac{1}{K_H^{sec}} \right)^{-1}. \tag{7.37}$$

where the hold-downs secant stiffness is:

$$K_H^{sec} = n_h \cdot k_h^{sec} \cdot \left(\frac{b}{h} \right)^2 \tag{7.38}$$

with n_h the number of hold-downs for each corner of the wall.

In order to obtain the secant stiffness at the peak strength of the hold-downs contribution K_H^{sec}, the experimental data related to *WHT 620 - prismatic with thick washer* from [26] have been considered. The plastic displacement of the equivalent bilinearized system ($\tilde{\blacksquare}$) to be considered is the plastic displacement of the weakest contribution (marked with the subscript i):

$$\tilde{u}_{v,pl} = \tilde{u}_{i,pl}. \tag{7.39}$$

The plastic displacement is, in turn, computed as follows:

$$\tilde{u}_{i,pl} = u_{i,ud} - \tilde{u}_{i,Rd} = \frac{\tilde{F}_{i,Rd}}{K_i^{sec}} \cdot (\tilde{\mu}_i - 1) \tag{7.40}$$

where $\tilde{F}_{i,Rd}$, K_i^{sec} and $\tilde{\mu}_i$ are the bilinearized strength, the secant stiffness and the bilinearized ductility of the wall weakest connection respectively, whereas the wall bilinearized ductility is defined as follows:

$$\tilde{\mu}_{v,SH+H} = \frac{u_{v,ud}}{\tilde{u}_{v,Rd}} = \frac{\tilde{u}_{v,Rd} + \tilde{u}_{v,pl}}{\tilde{u}_{v,Rd}} = 1 + \frac{\tilde{u}_{v,pl}}{\tilde{u}_{v,Rd}} = 1 + \frac{\tilde{u}_{i,pl}}{\tilde{u}_{v,Rd}} \tag{7.41}$$

where

$$\tilde{u}_{v,Rd} = \frac{\tilde{F}_{v,Rd}}{K_v^{sec}}. \tag{7.42}$$

By replacing eqs. 7.40 and 7.42 in eq. 7.41, having $\tilde{F}_{v,Rd} = \tilde{F}_{i,Rd} = \tilde{F}_{SH,Rd}$, the following simplified equation to compute the bilinearized ductility is obtained [19]:

$$\tilde{\mu}_{v,SH+H} = 1 + \frac{K_v^{sec}}{K_{SH}^{sec}} \cdot (\tilde{\mu}_{SH} - 1) \tag{7.43}$$

As it is shown in Fig. 7.16 (bottom), the experimental data related to the specimen PLS8 (considering both the sheathing-to-framing connections and hold-downs contributions) and the predicted backbone curve are in good agreement.

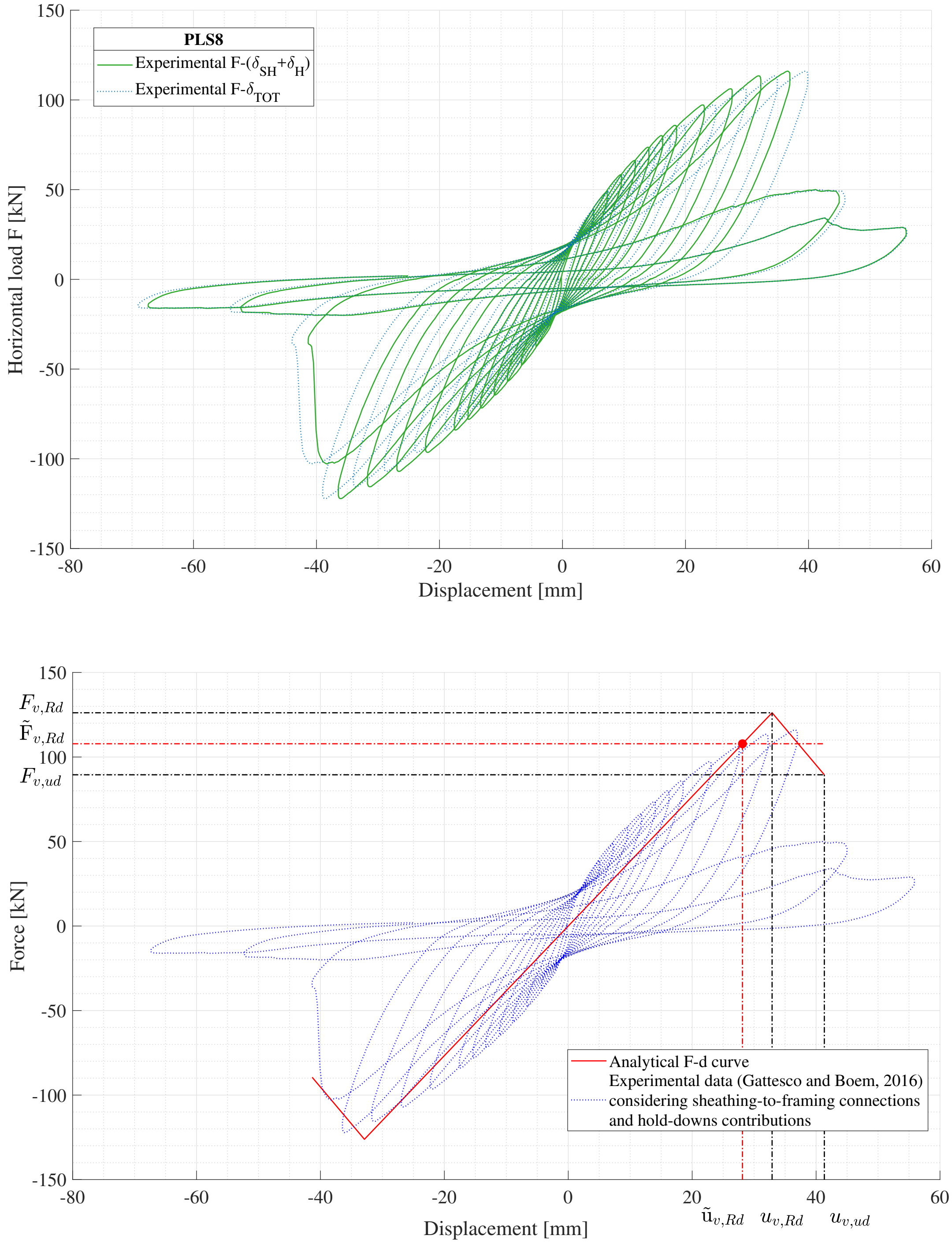

Figure 7.16. Experimental data of specimen PLS8 from [26] (top) and validation of the procedure considering both sheathing-to-framing connections and hold-downs contributions (bottom).

8 | Optimal configurations of Timber Light-Frame shear walls

Abstract

The developed parametric FE model has been employed to identify the optimal configurations of timber light-frame shear walls. Typical values for wall size, framing elements cross-section size and nails spacing have been considered, in compliance with EuroCode 5 and taking into account the number of vertical studs commonly used in practice. Finally, non-dominated solutions have been collected, i.e. the best solutions in terms of racking capacity and costs.

8.1 Optimum design criteria

The sensitivity analysis carried out by means of the parametric numerical model developed in OpenSees has allowed to assess how each design variable affects the overall behavior of a timber light-frame shear wall. As it was expected, the higher the size and number of elements that comprise the wall, the higher the racking capacity and the costs. This means that racking capacity and costs have to be balanced to fulfill both structural performances and economic needs, in order to find optimal configurations of the wall.

The design variables accounted to find the optimal configurations of a timber light-frame shear wall, used in practice, are:

- number of vertical studs;
- horizontal and vertical nails spacing, to establish the total number of nails;
- framing elements cross-section size (their depth is kept constant, in order to ensure that the frame thickness is homogeneous).

These design variables are referred to a certain aspect ratio of the wall, to be used according to the structural project.

A multi-objective optimization problem has to be solved, because the design process aims at optimizing simultaneously racking capacity and cost, which are conflicting design criteria. The Pareto optimality criterion [121] is the most common concept in defining the optimal solution for such class of optimization problems.

A point, $x^*{\in}X$, is Pareto optimal iff there does not exist another point, $x{\in}X$, such that $F(x){\leq}F(x^*)$, and $F_i(x) < F_i(x^*)$ for at least one function.

Here x^* is the optimal solution in Pareto' sense whereas X is the feasible design space, also known as decision space.

A point is Pareto optimal if there is no other point that improves at least one objective function without detriment to another one. The Pareto optimality criterion is associated to the concept of non-domination.

A vector of objective functions $F(x^*){\in}Z$ is non-dominated iff there does not exist another vector $F(x){\in}Z$ such that $F(x){\leq}F(x^*)$ with at least one $F_i(x) < F_i(x^*)$. Otherwise, $F(x^*)$ is dominated.

Here Z is the feasible criterion space defined as $\{F(x)|x \in X\}$ and the set $F(x^*)$ is named Pareto front.

8.2 Results

Figures 8.1 and 8.2 show the variation of the racking capacity as function of design variables and costs, the latter evaluated as the ratio between current cost and maximum cost attainable within the considered design space. For each point of the Pareto front, a miniature of the optimal wall configuration is provided to show the corresponding number of employed vertical studs and the nails spacing, whereas the bar chart identifies (in non-dimensional form), the corresponding cross-section size of the framing elements (each dimension is represented as the ratio between current and maximum size). Finally, under each configuration, the value of the equivalent viscous damping is reported. It can be observed that it is fairly constant for the considered aspect ratio of the wall.

Since the nails have significant effect on the racking capacity and very small influence on the wall cost, different levels of the maximum capacity are achieved by varying nails spacing. The best nails spacing is, as expected, the lowest one (50 mm). A stiffer wall is obtained by increasing the number of horizontal and vertical nails (thus reducing the nails spacing) and the number of vertical studs, along with the increase of cross-section size of framing elements. As it has been discussed in Sec. 6.5.6, the kinematic compatibility conditions between the shear behaviour of the framing elements and the one of the sheathing panel (which also rigidly rotates with respect to the frame) is crucial because the higher the relative displacements, the higher the energy dissipation of nails due to their plastic deformation. This implies that both the frame and the sheet must have an in-plane stiffness such that they are able to follow only their own deformative behaviour. As it is confirmed by the practice, the base of intermediate studs is kept lower than the one of the other framing elements. It is a design variable that do not substantially affect the increase of racking capacity. The solution that considers the non-dimensional cost equal to 1 has been omitted for the slender wall because the gain in terms of racking capacity is negligible from a practical standpoint. As it is shown in Figs. 8.1 and 8.2, the equivalent viscous damping slightly decreases when the number of intermediate studs increases for configurations with the same cross-section size of the framing elements. As it is explained in Sec. 6.5.5, the higher the number of vertical studs, the higher the overall number of nails. In particular, nails placed on the intermediate studs do not contribute significantly to the energy dissipation but make the overall system stiffer and stronger.

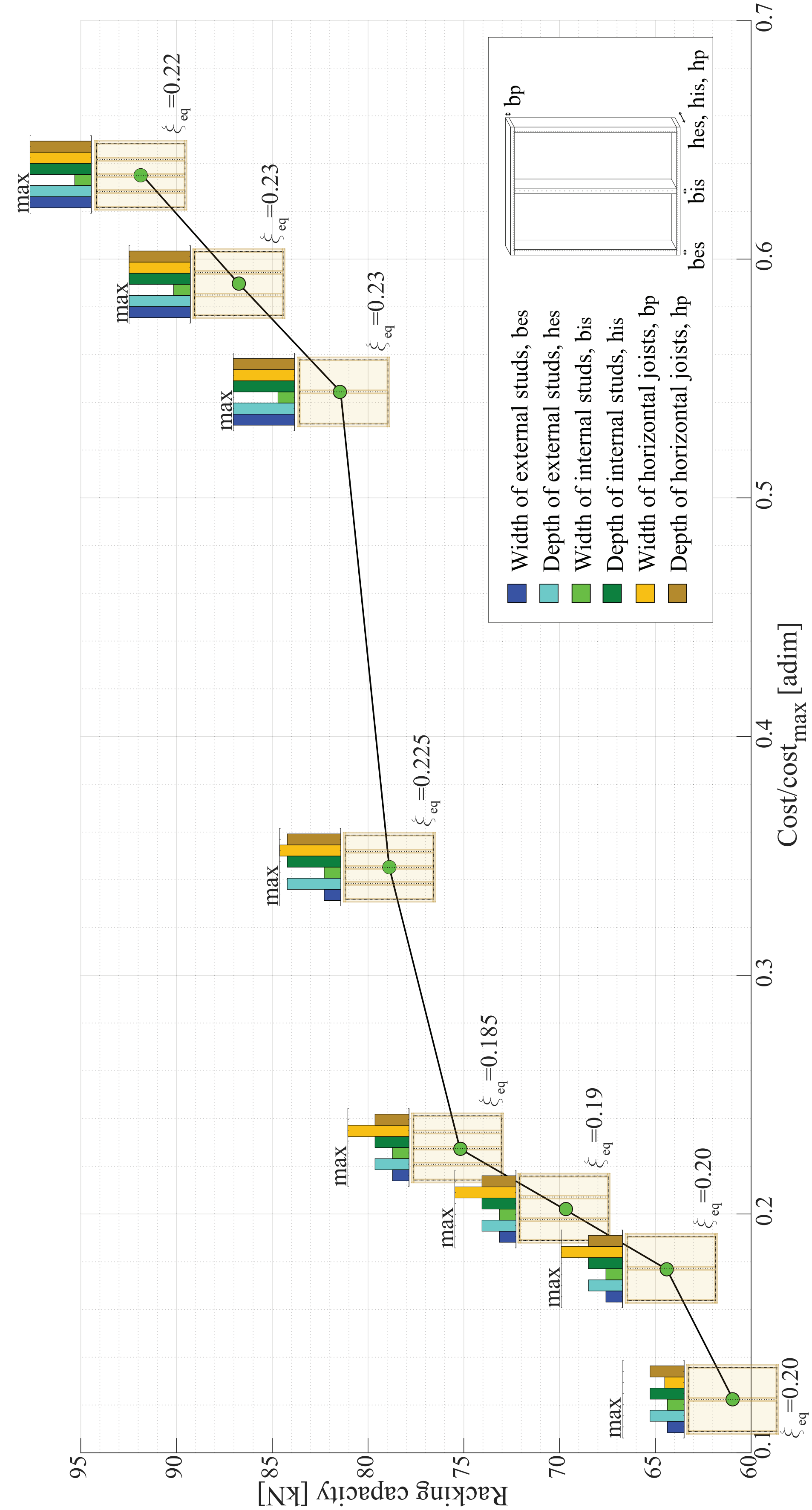

Figure 8.1. Slender wall configuration (1.2 m × 2.4 m).

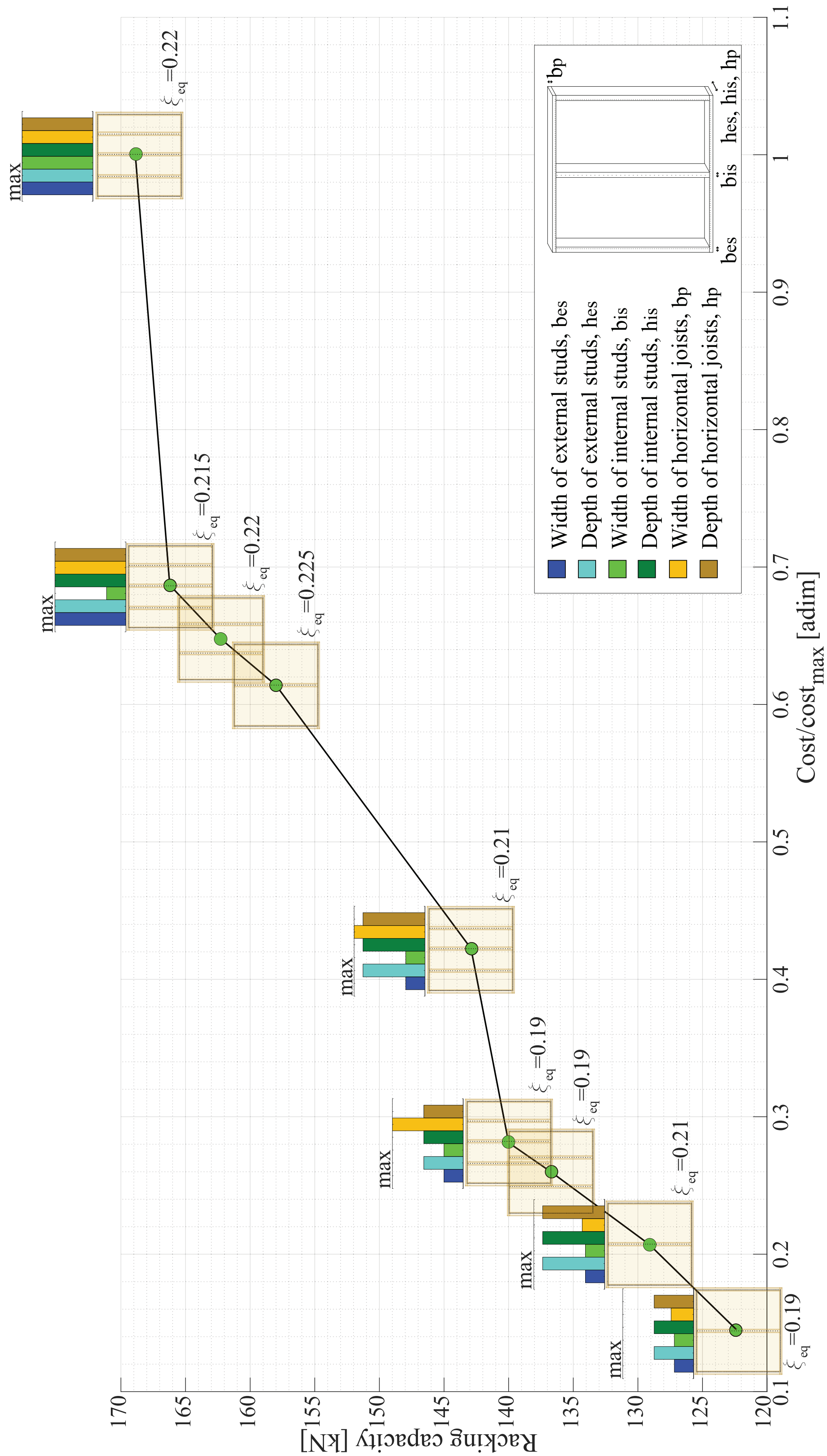

Figure 8.2. Square wall configuration (2.4 m× 2.4 m).

9 | Conclusions and future developments

The present thesis has been focused on the structural analysis and seismic design of timber light-frame shear walls. In order to study the energy dissipation phenomenon related to the sheathing-to-framing connections behaviour an original parametric FE model using the open-source software OpenSees has been developed. To the best author's knowledge this is the first parametric model of a timber shear wall developed in OpenSees.

According to the current code framework, the overall behavior of a timber light-frame shear wall can be assessed by means of the EuroCode 5 [20]. Its racking load-carrying capacity is computed starting from the lateral design capacity of a single fastener, taking into account the aspect ratio of the wall and the nails spacing.

By observing the numerical results carried out by means of the implemented parametric numerical model, the simplified method proposed by the EuroCode 5 is sound. For this reason, the original developments of this work are in line with this approach, even if some new aspects that have been neglected so far are now taken into account for a better evaluation of the effective behavior in Ultimate Limit State conditions.

First of all, sensitivity studies for some common design variables of a timber light-frame shear wall have been carried out, taking into account the typical characteristics of the elements used in practice. As it is well described in [19, 37], the main contributions to the horizontal displacement of a timber light-frame shear wall is associated to the sheathing-to-framing connections (which are adopted to link the sheathing panel to the frame) as well as to the hold-down steel brackets (which are employed to connect the wall to the foundation or to the upper/lower storey, thereby controlling the uplift of the wall due to its rigid rotation). Although the energy dissipation ensured by the sheathing-to-framing connections and the variation of the racking capacity were already analyzed by different studies, little attention has been paid so far to the analysis of the mechanical behaviour of a single wall considering just the nails contribution. Moreover, there are few parametric analyses for different wall configurations [13, 14]. A timber light-frame shear wall is a series system, thus the wall strength is defined as the minimum value from the strength of each component comprising the wall itself, namely: *i)* sheathing-to-framing, *ii)* hold-downs, *iii)* angle-brackets connections and *iv)* sheathing panel. The collapse, for the configuration named PLS8 in [26], is obtained by reaching the fastener shear resistance. This usually holds true for walls where hold-downs are directly connected to the timber studs of the frame. Once the first fastener - often placed at the bottom corner of the wall - fails, adjacent fasteners along the studs length fail as well, ultimately affecting a portion of joists length. The experimental tests on a single fastener in [26] have been used to calibrate the mechanical model chosen to represent the non-linear behavior of the sheathing-to-framing connections as well as to validate the global response of the wall considering just their contribution. By observing the overall behavior of the wall, the following definitions have been given: 1) the Life Safety Limit State occurs when the racking strength peak is achieved, which occurs when all fasteners along the perimeter framing elements are yielded; 2) the Collapse Limit State occurs when the most stressed fastener, usually at the bottom corner, reaches its failure displacement. In the latter case, the most stressed fastener is able to dissipate its maximum available energy, whereas all other fasteners dissipate only a fraction of it, because they undergo a displacement lower than their failure displacement. As a consequence, the following criterion was adopted: the amount of dissipated energy is evaluated from the force-displacement curve of a certain configuration of shear wall once the first fastener attains a resistance decrement equal to 65%, according to the experimental data in [26].

As it is discussed in chapter 6, some design variables sensibly affect the overall behaviour of a timber light-frame shear wall, namely: *i)* aspect ratio, *ii)* nails spacing, *iii)* cross-section size of the wall. The number of intermediate vertical studs make the overall system stiffer but they not substantially affect the racking load-carrying capacity of the wall.

An analytical procedure has been also developed to predict the capacity curve of a timber light-frame shear wall. First, the main quantities related to the constitutive law of a single fastener have been defined, along with the equivalent viscous damping ensured by the most stressed one, often placed at the bottom corner of the wall. In line with the EuroCode 5 approach and with the developments in [19, 37], the main global quantities of interest correspondent to the defined Limit States, are derived from the design ones of a single fastener. It is worth to highlight the relevant aspect of the analytical procedure, which is the computation of the equivalent viscous damping offered by a timber light-frame shear wall. The equivalent viscous damping is obtained as function of the common geometric input parameters of the wall, in order to directly derive its ductility, thereby allowing the identification of its global ultimate displacement.

The final part of the present thesis has addressed the optimum design of timber light-frame shear walls. Specifically, a multi-objective optimization problem has been defined because the conceived design process aims at optimizing simultaneously racking capacity and cost, which are design criteria in contrast each other. A summary of the optimal wall configurations has been provided, in order to design a timber light-frame shear wall exploiting the force-based and DDBD methods.

Final results have demonstrated that the proposed model can be effectively used to carry out non-linear analyses and to calibrate the damping factor η in use within the Capacity Spectrum Method. The following issues are worthy of future investigations:

- further and refined calibrations of both the SAWS and the BWBN mechanical models, designated to simulate the sheathing-to-framing connections, in order to improve the parametric numerical modeling of the wall;
- new experimental tests on timber specimens in order to characterize different type and diameter of fasteners to be implemented in both numerical model and analytical procedure;
- calibration of the non-linear zero-length elements to be used in the FE model representing the hold-down connections, with reference to experimental tests performed in literature or, if possible, by new experimental tests;
- improvement of the analytical procedure in order to capture the behavior of the wall, in terms of racking capacity, taking into account the reduced cross-section size of the framing elements;
- enhancement and automation of the numerical modeling in OpenSees, in order to easily model a 3D building.

Particularly, the improvement of the parametric FE model developed in this thesis will be used for new developments of the analytical procedure and will be distributed on OpenSees website as a tool to design this type of structural system. Moreover, the FE model could be useful for analyses of bamboo shear walls, by varying the mechanical parameters related to framing elements and sheathing panels.

A | Appendix

A.1 The OpenSees code

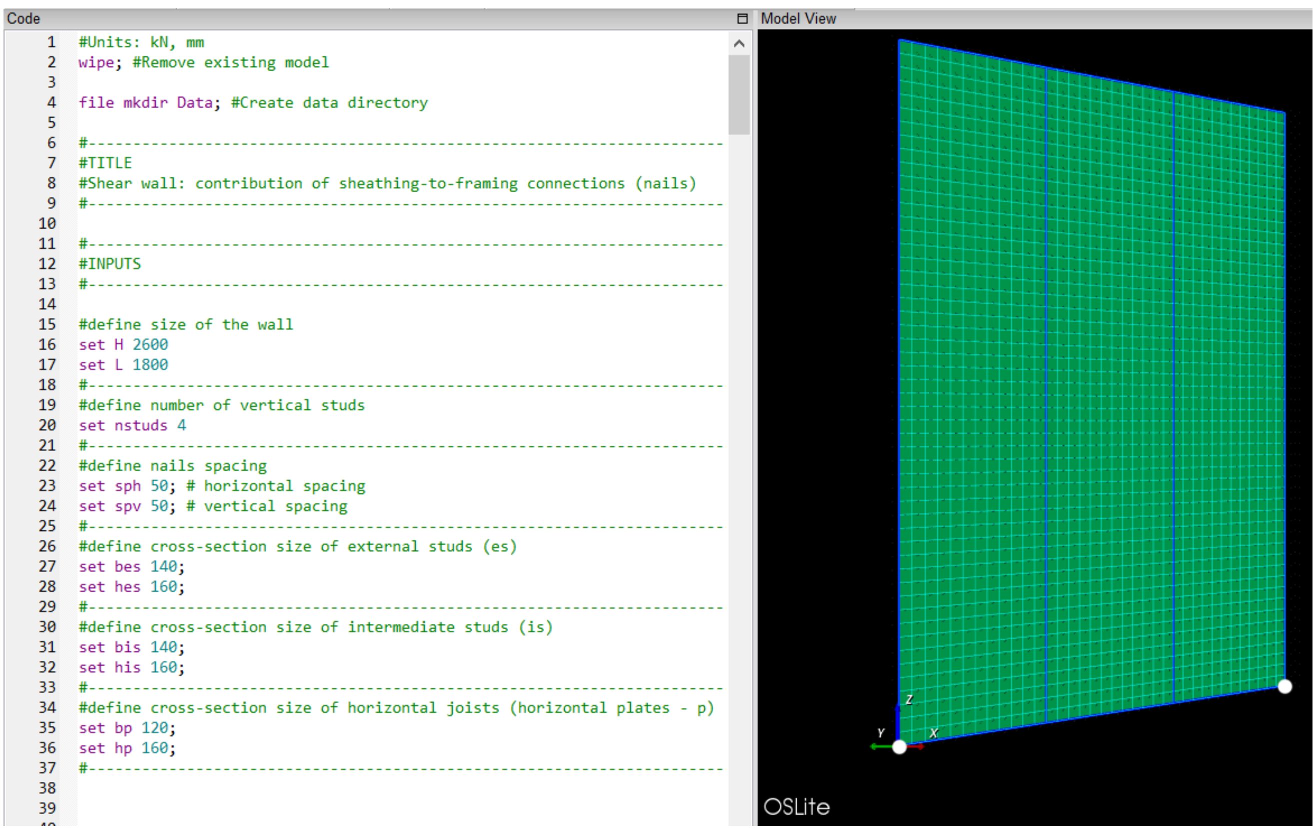

Figure A.1. The FE model developed in OpenSees.

To better understand the development of the numerical model of the shear wall, some tcl code lines are reported below. With the *wipe* command, any previous OpenSees-objects definition is deleted in order to start a new type of analysis, whereas a new folder named Data is created with *file mkdir Data*.

```
#Units:     kN, mm

wipe;       #Remove existing model

file mkdir Data; #Create data directory
#------------------------------------------------------------------------
#TITLE
#Shear wall:  contribution of sheathing-to-framing connections (nails)
#------------------------------------------------------------------------
#define size of the wall, mm

set         H 2600

set         L 1800

#define number of vertical studs, adim

set         nstuds 4

#define nails spacing, mm

set         sph 50; # horizontal spacing

set         spv 50; # vertical spacing

#define cross-section size of external studs (es), mm

set         bes 140;

set         hes 160;

#define cross-section size of intermediate studs (is), mm

set         bis 140;

set         his 160;

#define cross-section size of horizontal joists (horizontal plates - p), mm

set         bp 120;

set         hp 160;
```

Once the design variables are defined, the main model recalls some other .tcl files that contain the information related to nodes and elements used to defined the wall configuration, by means of the command *source*. In particular, an identification number is assigned to the layers into the file **Layers.tcl**. Layers allow to create nodes and elements belonging to the wall.

In order to identify nodes and elements, an integer *tag* is employed. The tag of nodes is defined by five or six digits. It starts with a number that identifies the layer they belong to. Then two digits are used to identify the x-coordinate, and other two digits define the z-coordinate. Seven layers are defined (Fig. 6.1). Layer **1** (layergrid) includes nodes belonging to the main grid of the model. Layer number **2** (layerframe) includes *i)* the fictitious nodes used to insert the internal releases between the end of vertical studs and the horizontal joists and *ii)* the tag of *elastic beam column* elements used to model vertical studs. Layer number **3** (layerjoists) includes tag of *elastic beam column* elements used to model horizontal joists. Layer number **4** (layernode) includes the perimeter nodes belonging to the frame. The *zero-length* elements, representing the internal releases, are defined with tag number **5** (layerzerol). They connect fictitious nodes with tag 2 and perimeter nodes with tag 4. Layer **6** (layershell) includes nodes belonging to the shell as well as the shell elements. Finally, layer **7** (layernails) includes the *zero-length* elements adopted to represent the sheathing-to-framing connections. As an example, the tag number **2 00 00** identifies a fictitious node, placed at the origin of the axes. Since the timber light-frame shear wall is double braced in this work, the symmetric shell and zero-length elements - which model sheathing panel and nails - are included in layer **13** (layershell_1) and **14** (layernails_1), respectively (Fig. 6.2).

In order to allow the connection between sheathing panel and framing element, each *elastic beam column* element is built between two consecutive nodes and also the shell elements mesh size varies with the nails spacing, to place *zero-length* elements.

```
#---------------------------------------------------------------------------
#LAYERS
#---------------------------------------------------------------------------
source Layers.tcl
#---------------------------------------------------------------------------
#PROPERTIES OF ELEMENTS
#---------------------------------------------------------------------------
source Properties_ele.tcl
#---------------------------------------------------------------------------
#MODEL
#---------------------------------------------------------------------------
model BasicBuilder -ndm 3 -ndf 6
#---------------------------------------------------------------------------
#MATERIALS
#---------------------------------------------------------------------------
source Materials.tcl
#---------------------------------------------------------------------------
#SOURCE OF MODEL
#---------------------------------------------------------------------------
#Source Code FRAME
source Frame.tcl
#Source Code SHELL
source Sheathing_panels.tcl
```

As an example, the .tcl source **Frame.tcl**, contains the generation of nodes and elements related to the framing elements. The nodes are created by means of loops, increasing them in global X-axis and Z-axis according to design input variables; the string *puts $element* is used to check the right generation on the screen: a variable is set in the model to allow plot on the screen (`$plotputs`); the command *append varName* is used to append each value to the value stored in the variable named by *varName* and provides an efficient way to build up long variables incrementally; *format "%02d" $varName* allows to create an integer with 2 digits; the command *unset -nocomplain varName* is used to suppress an error related to the repetition of data about the created element.

```
#Units:  kN, mm
#TITLE
#Shear wall:  frame
#---------------------------------------------------------------------------
#MODEL
#---------------------------------------------------------------------------
#Create nodes for studs

for {set x 0} {$x<$hn+1} {incr x $horizncamp} {for {set z 1} {$z<$vn} {incr
z} {
node [append d $layernode [format "%02d" $x] [format "%02d" $z]]
[expr {$x*$sph}] 0 [expr {$z*$spv}]
unset -nocomplain d

if {$plotputs == 1} {
puts "node [append d $layernode [format "%02d" $x] [format "%02d" $z]]
[expr {$x*$sph}] 0 [expr {$z*$spv}]"
unset -nocomplain d}
}}

#Create nodes for joists
for {set x 0} {$x<$hn+1} {incr x} {for {set z 0} {$z<$vn+1} {incr z $vn} {
node [append d $layernode [format "%02d" $x] [format "%02d" $z]]
[expr {$x*$sph}] 0 [expr {$z*$spv}]
unset -nocomplain d

if {$plotputs == 1} {
puts "node [append d $layernode [format "%02d" $x] [format "%02d" $z]]
[expr {$x*$sph}] 0 [expr {$z*$spv}]"
unset -nocomplain d}
}}
```

In order to connect the vertical studs to the horizontal joists by means of *zero-length* elements and to avoid the superposition of two zero-length elements on the same node, the generation increment for studs nodes starts from 1, whereas for joists nodes it starts from 0. The variables named *sph* and *spv* represent the horizontal and vertical nails spacing (in mm) respectively, *hn* and *vn* are number of horizontal and vertical nails, respectively, whereas the variable *horizncamp* represents the number of horizontal nails within each span between two consecutive vertical studs. Then, in order to introduce the internal releases that represent the behaviour of framing joints, base and top nodes belonging to vertical studs are linked to the fictitious nodes.

```
#---------------------------------------------------------------------------
#Modeling of studs
#---------------------------------------------------------------------------
#create studs linking fictitious nodes (for frame hinges) and frame (for
external studs - “es”)
for {set x 0} {$x<$hn+1} {incr x $hn} {for {set z 0} {$z<$vn} {incr z} {
if {$z == 0} {
#element elasticBeamColumn $eleTag $iNode $jNode $A $E $G $J $Iy $Iz
$transfTag
element elasticBeamColumn [append d $layerframe [format "%02d" $x] [format
"%02d" $z]] [append e $layerframe [format "%02d" $x] [format "%02d" $z]]
[append f $layernode [format "%02d" $x] [format "%02d" [expr $z+1]]]
$Aes $E $G $Jes $I2es $I3es 2
unset -nocomplain d e f

} elseif {$z == [expr {$vn-1}]} {
element elasticBeamColumn [append d $layerframe [format "%02d" $x] [format
"%02d" $z]] [append e $layernode [format "%02d" $x] [format "%02d" $z]]
[append f $layerframe [format "%02d" $x] [format "%02d" [expr $z+1]]]
$Aes $E $G $Jes $I2es $I3es 2
unset -nocomplain d e f

} else {
element elasticBeamColumn [append d $layerframe [format "%02d" $x] [format
"%02d" $z]] [append e $layernode [format "%02d" $x] [format "%02d" $z]]
[append f $layernode [format "%02d" $x] [format "%02d" [expr $z+1]]]
$Aes $E $G $Jes $I2es $I3es 2
unset -nocomplain d e f
}
}}
```

The way by which the element coordinates correlate to the global model coordinates is defined using the OpenSees *Geometric Transformation* command. In particular, it defines how the solver transforms beam element stiffness and resisting force from the basic system to the global-coordinate system. The command *geomTransf transfType? arg1? ...* assigns the geometric transformation type *transfType?* with its arguments *arg1? ...* to the geometric transformation rules. The *Linear Transformation* performs a linear geometric transformation of beam stiffness and resisting force from the basic system to the global-coordinate system.

The framing joints placed at the top are implemented as follows (the same is done at the bottom as well as for both intermediate and perimeter studs) [101]:

```
#-------------------------------------------------------------------------------
#Modeling of internal releases
#-------------------------------------------------------------------------------
set z $vn
for {set x 0} {$x<$hn+1} {incr x $hn} {
node [append d $layerframe [format "%02d" $x] [format "%02d" $z]] [expr
{$x*$sph}] 0 [expr {$z*$spv}]
unset -nocomplain d
#element zeroLength $eleTag $iNode $jNode -mat $matTag1 $matTag2...  -dir
$dir1 $dir2...
element zeroLength [append d $layerzerol [format "%02d" $x] [format "%02d"
$z]] [append e $layernode [format "%02d" $x] [format "%02d" $z]] [append f
$layerframe [format "%02d" $x] [format "%02d" $z]] -mat 2 2 3 -dir 1 3 5
unset -nocomplain d e f

if {$plotputs == 1} {
puts "node [append d $layerframe [format "%02d" $x] [format "%02d" $z]]
[expr {$x*$sph}] 0 [expr {$z*$spv}]"
unset -nocomplain d
puts "element zeroLength [append d $layerzerol [format "%02d" $x] [format
"%02d" $z]] [append e $layernode [format "%02d" $x] [format "%02d" $z]]
[append f $layerframe [format "%02d" $x] [format "%02d" $z]] -mat 2 2 3 -dir
1 3 5"
unset -nocomplain d e f}
}
```

As reported in [122], the load-slip relation of a nails joint in the lateral direction is not important because the rotational strength of this kind of connection is weak, thus it is modeled with a perfect hinge.

As an example, *timeSeries* and *load Pattern* are defined as follows to set the analyses in displacement-controlled loading conditions:

```
#-------------------------------------------------------------------------------
#Set the controlled node and apply the load pattern
#-------------------------------------------------------------------------------
#to set the node to which the load pattern is applied (node tag)
set controlled_node [append d $layernode [format "%02d" 0] [format "%02d"
$vn]]
unset -nocomplain d

timeSeries Linear 1
pattern Plain 1 1 {
load $controlled_node 1 0 0 0 0 0
}
#recorder:  the first column contains the load multiplier whereas the second
one contains the displacement of the chosen node
recorder Node -file Data/DNodes_x1.out -time -node $controlled_node -dof 1
disp
```

Before the loads are applied, a TimeSeries object should be defined which represents the relationship between the time in the domain t and the load factor applied to the loads λ in the load pattern, with which the TimeSeries object is associated, i.e. $\lambda = F(t)$. In general, the command *timeSeries seriesType? arg1? ...* creates a time series with time series objects *seriesType?* with a number of arguments. Among the time series objects that can be constructed, there are: *Constant*, *Linear*, *Rectangular*, etc.

In this case, the load is linearly increased from zero to the assigned value. This can be expressed in the form: $\lambda = F(t) = C_{factor} \cdot t$. The command *timeSeries Linear $tag <-factor $cFactor>* creates a Linear time series with *$tag*, which is an integer tag identifying timeSeries. The *factor* switch defines the optional argument *$cFactor,* which is the linear factor, C_{factor} (for default equal to 1.0).

After the creation of the time series, the loads can be added. In OpenSees, the *pattern* command is used to construct a LoadPattern and to add it to the Domain. Each LoadPattern in OpenSees has an associated TimeSeries. In fact, the provided load value is a reference one, while the time series provides the load factor. The load factor times the reference value gives the current load applied to the node in one time step of the analysis. The pattern may contain *ElementLoads*, *NodalLoads* and *SinglePointConstraints*. Some of these SinglePoint constraints may be associated with GroundMotions. The command *pattern patternType? arg1? ...* creates a pattern of type *patternType?* with a number of arguments.

Finally, the displacement increment for the analysis is assigned as follows:

```
#--------------------------------------------------------------------------
#Cyclic analysis
#--------------------------------------------------------------------------
constraints Plain;
numberer RCM;
test EnergyIncr 1.0e-6 300 5
system UmfPack;
algorithm KrylovNewton;
integrator DisplacementControl $controlled_node 1 0
analysis Static;
analyze 1

set Da 100
foreach Dincr [lindex $disp] {
integrator DisplacementControl $controlled_node 1 $Dincr
analyze $Da}
```

The *system UmfPack* command is used to construct a sparse system of equations which uses the UmfPack solver. The command *numberer RCM* is used to construct an RCM degree-of-freedom numbering object to provide the mapping between the degrees-of-freedom at the nodes and the equation numbers. The *numberer RCM* uses the Symmetric Reverse Cuthill-McKee permutation algorithm to order the matrix equations, in order to reduce the bandwidth of global stiffness matrix and, thus, the computational time. *KrylovNewton* algorithm, developed by [123], accelerated the convergence of the Modified Newton iteration bringing the rate of convergence close to that of Newton-Raphson at a lower computation effort. The interested reader can refers to [124] for further details. The analysis starts from zero (`integrator DisplacementControl $controlled_node 1 0`) and by means of the *foreach* loop, goes ahead following the assigned steps ($Da) to reach the chosen displacement levels contained into the variable *$disp*. With *lindex $disp*, it is ensured that the displacement levels are chosen in the right order.

B | Appendix

B.1 Connection load-carrying capacity calculations according to EuroCode 5

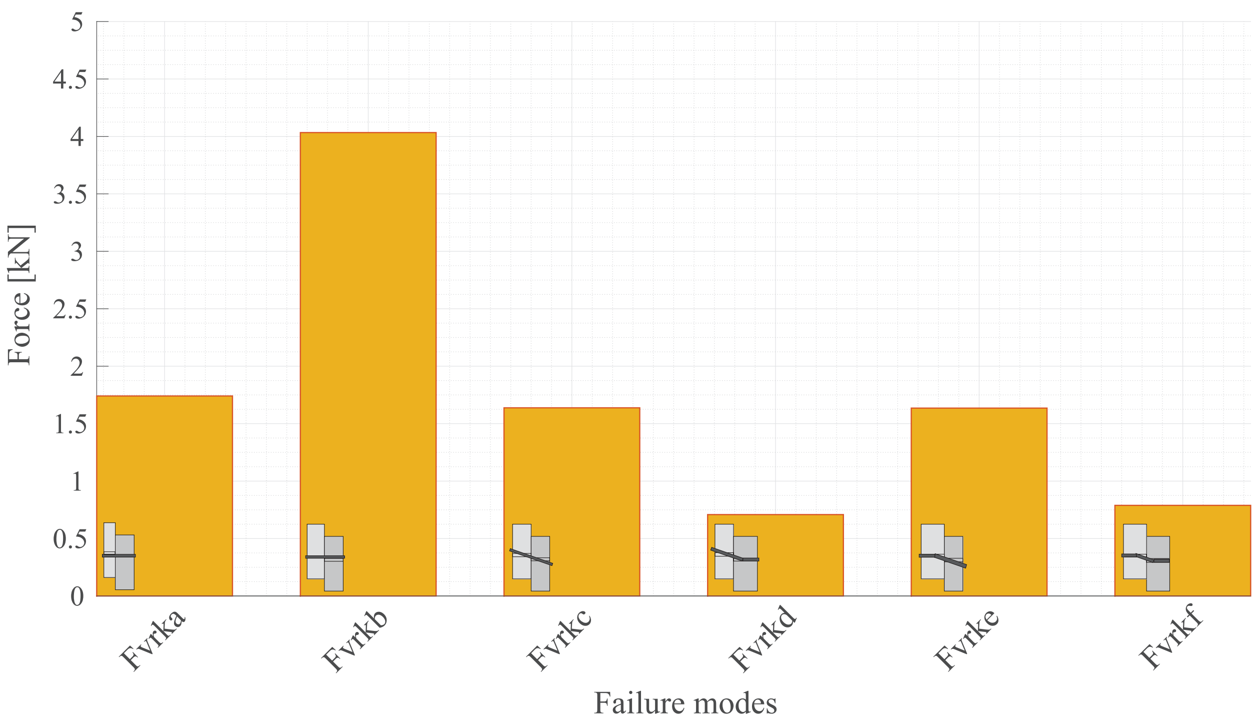

Figure B.1. The load-carrying capacity of a single nail, considering the failure modes defined in Johansen's theory [58].

The load-carrying capacity of a single nail is computed in this appendix [125], considering geometric and mechanical features used for the reference configuration denoted as PLS8 in [26]. The focus is on sheathing-to-framing connections contribution only. This is because the overall response of a timber light-frame shear wall mainly depends on the weakest connection as shown in [26]. Moreover, the resistance decrement is due to their progressive plasticization until the rupture of several nails at the bottom corner of the wall. It is here shown that, by computing the load-carrying capacity of a single nail through the Johansen's theory, the minimum value provided by the equations in [20] is associated to the failure modes denoted as (d) and (f) corresponding to the yielding of the fasteners.

Initially, the mechanical features of nails and density of timber-based members are defined.

```
%----------------------------------------------------------------------------
%% Calculation of strength of nail connections - not pre-drilled
%  according to [20]
%----------------------------------------------------------------------------
%% Nail fastener properties
% Tensile strength of the wire , kN/mmq

fu          = 0.6;

% Nail diameter, mm

d           = 2.8;

%% Particleboard side member
% Thickness of member, mm

t1          = 15;

% Mean density of particleboard, kg/mc

rhom_part   = 710;

%% Wood side member
% Depth of penetration, mm

t2          = 55;

% Mean density of wood according to [31] for C24, kg/mc

rhom        = 435;
```

Then, the embedment strength of timber-based members is computed, along with the relative ratio among them.

```
% Yield Moment (cf.  Eq.  8.14 in [20]), kN mm

Myrk        = 0.3*fu*(d)^2.6 = 2.62;

% Embedment strength for particleboard and OSB (cf.  Eq.  8.22 in [20]),
kN/mmq

fh1k        = (65*d^(-0.7)*t1^(0.1))/1000 = 0.0414;

% Embedment strength of Wood (cf.  Eq.  8.15 in [20]), kN/mmq

fh2k        =(0.082*rhom*d^(-0.3))/1000 = 0.0262;

%% Calculation of failure modes

beta        = fh2k/fh1k = 0.63;

% Rope effect contribution (cf.  par.  8.2.2 (2) in [20])

Faxrk       = 0;
```

Finally, the failure modes are assessed.

```
%% Failure modes
% Single shear plane failure modes (cf.  Eq.  8.6 in [20]), kN

Fvrka       =fh1k*t1*d = 1.74; % Mode (a)

Fvrkb       =fh2k*t2*d = 4.03; % Mode (b)

% Mode (c)

Fvrkc       =((fh1k*t1*d)/(1+beta))*(sqrt(beta+((2*((beta)^2))*(1+(t2/t1)+...

            ((t2/t1)^2)))+(((beta)^3)*((t2/t1)^2))))-(beta*(1+(t2/t1)))+...

            +Faxrk/4=   1.64;

% Mode (d)

Fvrkd       = 1.05*((fh1k*t1*d)/(2+beta))*((sqrt((2*beta*(1+beta))+...

            +((4*beta*(2+beta)*Myrk)/(fh1k*d*((t1)^2)))))-beta)+Faxrk/4  =
            =           0.71;

% Mode (e)

Fvrke       = 1.05*(fh1k*t2*d)/(1+2*beta)*((sqrt(2*((beta)^2)*(1+beta))+...

            +((4*beta*(1+2*beta)*Myrk)/(fh1k*d*((t2)^2))))-beta)+Faxrk/4  =
            =           1.63;

% Mode (f)

Fvrkf       = 1.15*(sqrt((2*beta)/(1+beta)))*(sqrt(2*Myrk*fh1k*d))+Faxrk/4=

            =           0.79;

Fvrk_all=[Fvrka;Fvrkb;Fvrkc;Fvrkd;Fvrke;Fvrkf];

% Connection capacity

Fvrk        = min(Fvrk_all) = 0.71;
```

C | Appendix

C.1 Experimental tests: materials and methods

Some preliminary results related to experimental tests already performed on bamboo specimens are here presented. The final goal of this experimental campaign is to investigate the behaviour of a single nail by varying the material used in the assembly as well as diameter and length of the nail. Other tests will be performed on shear wall specimens to take into account the effects on nails stress distribution related to base connections. The resulting experimental database will be useful to define the constitutive law of a single nail in order to *i)* carry out the identification of the mechanical model parameters used within the parametric FE model developed in OpenSees and *ii)* to improve the reliability of the analytical procedure in predicting the global backbone curve of a timber light-frame shear wall.

C.2 Bamboo

C.2.1 Test specimens

Two types of ply-bamboo boards are available, namely: *i)* thick strip ply-bamboo board laminated by bamboo strips of section 7.2×22 mm and *ii)* thin strip ply-bamboo board laminated by bamboo strips of about 2 mm (Fig. C.1). The orientation of the strips in thick strip ply-bamboo is typically the same of the longitudinal direction. The configuration of the strips in thin strip ply-bamboo is more complicated, the ratio of longitudinal grains and transverse grains is typically 4:1 for the applications in Glued Laminated Bamboo (GluBam) beams or columns. In this research, thick strip ply-bamboo boards are considered for framing elements whereas thin strip ply-bamboo are used for sheathing panel. The density of ply-bamboo, according to Li et al. [126] is around 850 kg/m^3.

The number of specimen tested is 32: 3 monotonic tests and 5 cyclic tests for both parallel and perpendicular loading direction have been performed, considering a stud/beam cross-section size about 50 mm

$\times$ 100 mm made by thick strip ply-bamboo and a sheathing panel with thickness about 8 mm (Tab. C.1).

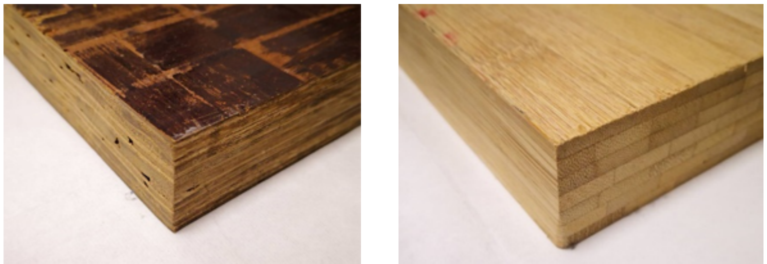

Figure C.1. Thin strip ply-bamboo board (left) and thick strip ply-bamboo board (right).

Fastener type	Sheathing panel	Loading direction	Number of specimens
50 mm *HS** nail	8 mm ply-bamboo (thin strips)	Parallel	3 Monotonic + 5 Cyclic
		Perpendicular	3 Monotonic + 5 Cyclic
60 mm common nail		Parallel	3 Monotonic + 5 Cyclic
		Perpendicular	3 Monotonic + 5 Cyclic
Total number of specimens			32

**HS* : high strength

Table C.1. Matrix of sheathing-to-framing connections tests.

C.2.2 Test setup

As it is shown in Fig. C.2, steel jigs have been designed to apply monotonic and cyclic load on panel-frame nail connections in order to assess their lateral resistance. Two different types of panel-frame connections are tested under monotonic and cyclic loading, namely: parallel to bamboo fiber direction of GluBam frame and perpendicular to bamboo fiber direction.

Monotonic tests have been performed under deformation control with a loading rate of 2.5 mm/min, in accordance with the ASTM D1761 standard [127]. The Consortium of Universities for Research in Earthquake Engineering (CUREE)-Caltech loading protocol [128] was adopted for the cyclic tests with a loading rate of 15 mm/min.

The reference deformation Δ for cyclic tests was determined from the monotonic tests. Once having monotonically captured the displacement Δ_m, defined where the resistance force drops to $0.8F_{max}$, the value $0.6\Delta_m$ is considered as the reference cyclic deformation Δ. If the load did not drop to $0.8F_{max}$, then the failure displacement should be used as the monotonic deformation Δ_m. The program of cyclic loading consists of four parts: the first part was 6 cycles at 0.05Δ peak displacement; the next was 7 cycles at 0.075Δ and 0.1Δ; then, 4 cycles at $0.2\ \Delta$ and 0.3Δ; the number of cycles in the final part was 3 of amplitudes $0.4\ \Delta$, $0.7\ \Delta$, $1.0\ \Delta$, 2.0Δ, respectively.

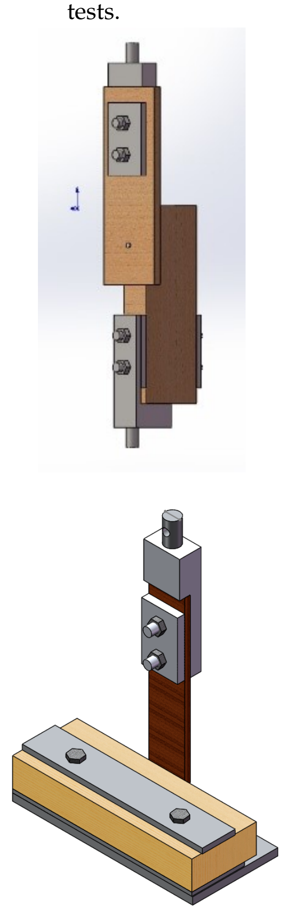

Figure C.2. Test setup for nails lateral strength tests.

C.2.3 Results

In monotonic tests of 50 mm high strength (HS) nail connections, the main damage pattern consists of the nail pulled through ply-bamboo sheet whereas, in few cases and in perpendicular direction, the yielding failure of nail was observed. In cyclic tests (Fig. C.3, Tab. C.2), the main failure mode consists of the nail pulled through sheathing panel and brittle failure of nail in parallel direction, whereas only brittle failure was observed in perpendicular direction (Fig. C.4). For 60 mm common nail connections, in both loading directions, the most frequent failure mode consists of the nail pulled through sheathing panel in monotonic tests and fatigue failure of nail in cyclic tests. In few cases, in parallel direction, yielding and withdrawal of nail have been observed (Fig. C.5). The summary of failure modes of nail connections between ply-bamboo sheathing panel and GluBam frame is provided in Tab. C.3.

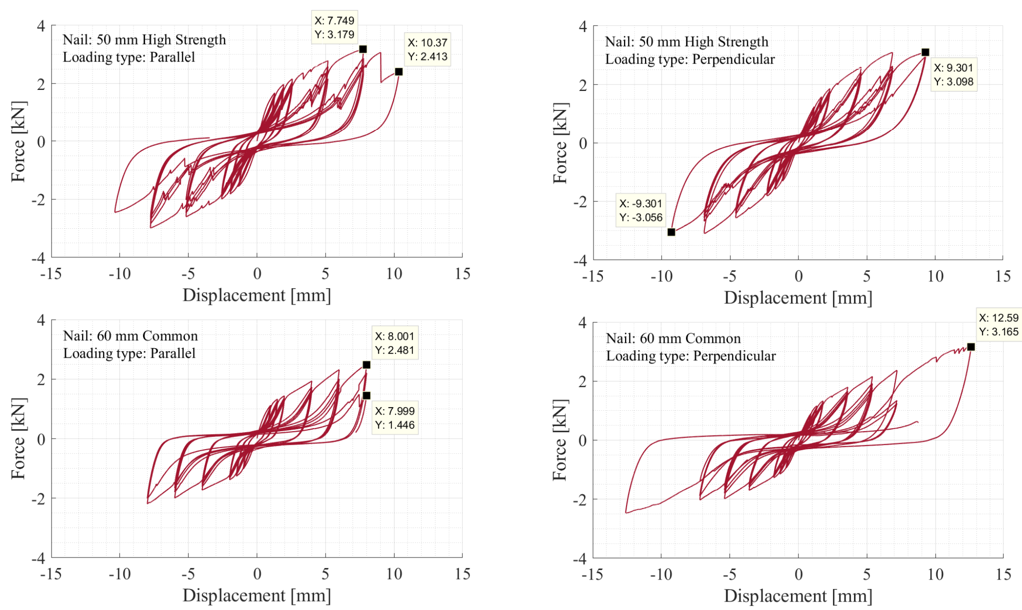

Figure C.3. Cyclic tests results.

Fastener type	**Loading type**	k_f^{sec}	$F_{f,Rd}$**[kN]**	$u_{f,Rd}$**[mm]**	$F_{f,ud}$**[kN]**	$u_{f,ud}$**[mm]**
50 mm HS nail	Parallel	0.41	3.18	7.75	2.4	10.4
	Perpendicular	0.33	3.10	9.30	-	-
60 mm common nail	Parallel	0.31	2.48	8.00	1.44	7.99
	Perpendicular	0.25	3.16	12.59	-	-

Table C.2. Results of cyclic tests.

Pull through Brittle failure Yielding

Figure C.4. Failure modes of 50 mm high strength nails.

Pull through Fatigue failure Yielding and withdrawal

Figure C.5. Failure modes of 60 mm common nails.

Nail type	Loading direction	Loading type	Failure mode
50 mm HS nail	Parallel to bamboo grain	Monotonic	Pull through
		Cyclic	Pull through / Fatigue failure
	Perpendicular to bamboo grain	Monotonic	Pull through / Yielding
		Cyclic	Fatigue failure
60 mm common nail	Parallel to bamboo grain	Monotonic	Pull through / Yielding
		Cyclic	Fatigue failure
	Perpendicular to bamboo grain	Monotonic	Pull through
		Cyclic	Fatigue failure

Table C.3. Failure modes of sheathing-to-framing connections.

D | Appendix

D.1 Example of global behavior prediction of a Timber Light-Frame shear wall

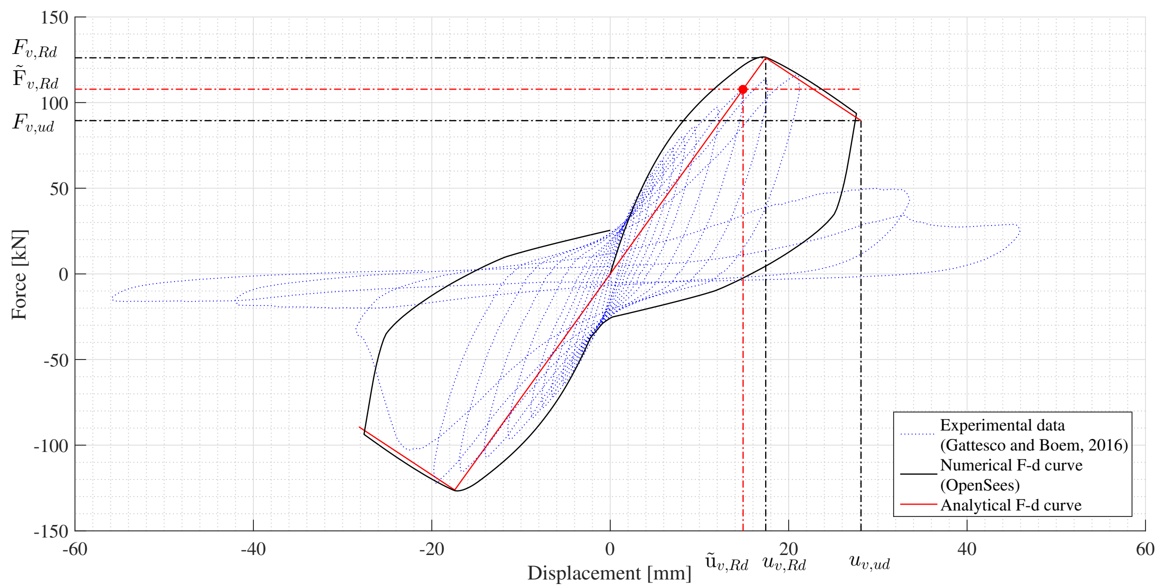

Figure D.1. Prediction of the capacity curve of a timber light-frame shear wall: comparison among experimental, numerical and analytical results.

The timber light-frame shear wall is comprised of solid section of timber (red spruce), strength class C24, according to [31]. It is double-braced with 15-mm-thick particleboard panel, type P5 as in [26], and it is fixed by nails at 50 mm spacing. The height is equal to 2.6 m and the width is equal to 1.8 m.

The parameters related to the type of fastener used in the configurations are defined, according to experimental data in [26]:

```
%--------------------------------------------------------------------------
%% FASTENER
%--------------------------------------------------------------------------
%INPUT PARAMETERS
%Yield strength, kN

Ff_Rd       = 1.66;

%Yield displacement, mm

uf_Rd       = 3.8;

%Ultimate force, kN

Ff_ud       = Ff_Rd*0.35 = 0.58;

%Ultimate displacement, mm

uf_ud       = 8.5;

%Diameter of fastener, mm

d           = 2.8;
```

Service parameters are then computed:

```
%--------------------------------------------------------------------------
%% FASTENER
%--------------------------------------------------------------------------
%DERIVED PARAMETERS
%Secant stiffness, kN/mm

kf_sec      = Ff_Rd/uf_Rd = 0.44;

%Ductility of fastener, adim

mu_f        = uf_ud/uf_Rd = 2.24;

%Yield strength of the bilinearized curve, kN

Ff_Rdb      =((kf_sec*uf_ud)*(1-(sqrt(1-(((1.35*mu_f)-0.35)/((mu_f)^2))))))
            = 1.18;

%Bilinearized ductility of fastener, adim

mu_fb       =((kf_sec/Ff_Rdb)*uf_ud) = 3.15;

%Equivalent viscous damping of fastener, adim

xi_eq_f     =((1/pi)*(1-(1/(2*mu_fb)))) = 0.267;
```

Geometric input parameters of the timber shear wall are given.

```
%------------------------------------------------------------------------
%% Timber Light-Frame shear wall
%------------------------------------------------------------------------
%Define dimensions
%Height, mm

H            = 2600;

%Width, mm

L            = 1800;

%Number of braced sides, adim

nbs          = 2;

%define size of spacing among nails
%horizontal spacing, mm

sph          = 50;

%vertical spacing, mm

spv          = 50;

%define number of studs

nstuds       = 4;

%define number of joists

njoists      = 2;

%define cross-section size of framing elements
%width of external studs, mm

bes          = 140;

%height (depth) of external studs, mm

hes          = 160;

%width of internal studs, mm

bis          = 140;

%height (depth) of internal studs, mm

his          = 160;

%height of joists, mm

bp           = 120;

%width (depth) of joists, mm

hp           = 160;
```

Once the overall features of the system are given the proposed analytical procedure is applied.

```
%-----------------------------------------------------------------------------
%% PROCEDURE
%-----------------------------------------------------------------------------
%Aspect ratio, adim

AR          = H/L = 1.44;

%Define the parameter "c" - [37], adim
if AR<2
c=1;
else if 2<AR<4
          c=AR/2;
    else c=0;
    end
end

%Total number of perimeter vertical fasteners, adim

fv_p        = ((H/spv)*2*nbs) = 208;

%Total number of perimeter horizontal fasteners, adim

fh_p        =(((L/sph)+1)*njoists*nbs) = 148;

%Number of horizontal fasteners on the top timber wall to compute Fv,Rd
according to [20], adim

fh_t        = ((L/sph)+1)+(nstuds-3) = 38;

%Parameter κ for the shape of energy dissipation along the perimeter
vertical studs, adim

kappa       = min(AR, 1) = 1;

%Parameter γ for the shape of energy dissipation along the horizontal
joists, adim

gamma       = min(1/AR, 0.8) = 0.69;

%Shape coefficient defined by [37], function of the aspect ratio, adim

lambda      = 0.810+(1.85*AR) = 3.48;
```

Now it is possible to compute the parameters required to derive the F-d backbone curve, considering the sheathing-to-framing connections contribution.

```
%-----------------------------------------------------------------------------
%% FINAL COMPUTATION
%-----------------------------------------------------------------------------
%Total equivalent viscous damping, adim

xi_eq       = xi_eq_f*(((kappa*fv_p)+(gamma*fh_p))/(fv_p+fh_p)) = 0.23;

%Bilinearized ductility of
%sheathing-to-framing connections contribution, adim

mu_SHb      =(1/(2*(1-(pi*xi_eq)))) = 1.89;

%Racking capacity, kN

Fv_Rd       = nbs*Ff_Rd*c*fh_t = 126.16;

%Nails secant stiffness distribution at global strength peak, kN/mm

kf_sec_g    = 0.35;

%Global secant stiffness at strength peak as in [37], kN/mm

K_SH        =((nbs*kf_sec_g)/(sph*(lambda/L))) = 7.24;

%Yield displacement, mm

uv_Rd       = Fv_Rd/K_SH = 17.43;

%Ultimate strength of the wall, kN

Fv_ud       = nbs*Ff_Rdb*c*fh_t = 89.5;

%Strength of the bilinearized curve, kN

Fv_Rdb      = (Fv_Rd+Fv_ud)*0.5 = 107.8;

%Yield displacement of the bilinearized curve, mm

uv_Rdb      = Fv_Rdb/K_SH = 14.9;

%Ultimate displacement of the wall, mm

uv_ud       = uv_Rdb * mu_SHb = 28;
```

Bibliography

[1] http://www.wbdg.org/, 2018.

[2] Energy Policy Act. Energy policy act of 2005. In *US Congress*, 2005.

[3] C. J. Kibert. *Sustainable construction: green building design and delivery*. John Wiley & Sons, 2016.

[4] UE. Energy performance directive 2010/31/ce. *Official Journal of the European Union*, 18, 2010.

[5] S. Schimschar, A. Hermelink, T. Boermans, L. Pagliano, P. Zangheri, K. Voss, and E. Musall. Towards nearly zero-energy buildings - definition of common principles under the epbd. *Ecofys, Politecnico di Milano, University of Wuppertal (Unpublished) for European Commission*, 2013.

[6] C.D. Frenette, D. Derome, R. Beauregard, and A. Salenikovich. Identification of multiple criteria for the evaluation of light-frame wood wall assemblies. *Journal of Building Performance Simulation*, 1(4):221–236, 2008.

[7] J.S. Wang, C. Demartino, Y. Xiao, and Y.Y. Li. Thermal insulation performance of bamboo- and wood-based shear walls in light-frame buildings. *Energy and Buildings*, pages –, 2018. ISSN 0378-7788. DOI: https://doi.org/10.1016/j.enbuild.2018.03.017. URL `https://www.sciencedirect.com/science/article/pii/S0378778817305960`.

[8] Canadian Wood Council. *Energy and the environment in residential construction*. Canadian Wood Council, 1996.

[9] G. Minke. *Building with bamboo: Design and Technology of a Sustainable Architecture*. Birkhäuser, 2016. ISBN 9783035608663. URL `https://books.google.it/books?id=0wiqAQAACAAJ`.

[10] M. Mahdavi, P.L. Clouston, and S.R. Arwade. Development of laminated bamboo lumber: review of processing, performance, and economical considerations. *Journal of Materials in Civil Engineering*, 23(7):1036–1042, 2010.

[11] F. McKenna and G.L. Fenves. The opensees command language manual. version 1.2. berkeley, usa: Pacific earthquake engineering research center, University of California, 2007.

[12] A.J. Salenikovich. *The racking performance of light-frame shear walls*. PhD thesis, Virginia Tech, 2000.

[13] A.J. Salenikovich and J.D. Dolan. The racking performance of shear walls with various aspect ratios. part i. monotonic tests of fully anchored walls. *Forest products journal*, 53(10):65, 2003.

[14] R. Dhonju, B. D'Amico, A. Kermani, J. Porteous, and B. Zhang. Parametric evaluation of racking performance of platform timber framed walls. In *Structures*, volume 12, pages 75–87. Elsevier, 2017.

[15] André J. and M. Fragiacomo. General notes on ductility in timber structures. *Engineering structures*, 33(11):2987–2997, 2011.

[16] R.L. Tuomi and W.J. McCutcheon. Racking strength of light-frame nailed walls. *Journal of the Structural Division*, 104(7):1131–1140, 1978.

[17] A.K. Gupta and G.P. Kuo. Behavior of wood-framed shear walls. *Journal of Structural Engineering*, 111(8):1722–1733, 1985.

[18] A.K. Gupta and G.P. Kuo. Wood-framed shear walls with uplifting. *Journal of Structural Engineering*, 113(2):241–259, 1987.

[19] D. Casagrande, S. Rossi, R. Tomasi, and G. Mischi. A predictive analytical model for the elasto-plastic behaviour of a light timber-frame shear-wall. *Construction and Building Materials*, 102: 1113–1126, 2016.

[20] EN. 1-1: 2004 eurocode 5: Design of timber structures-general-common rules and rules for buildings, 1995.

[21] Eurocode 8: Design of structures for earthquake resistance-part 1: General rules, seismic actions and rules for buildings. *Brussels: European Committee for Standardization*, 2005.

[22] K. Pintarič and M. Premrov. Mathematical modelling of timber-framed walls using fictive diagonal elements. *Applied Mathematical Modelling*, 37(16-17):8051–8059, 2013.

[23] K. Kobayashi and M. Yasumura. Evaluation of plywood sheathed shear walls with screwed joints tested according to iso 21581. In *Proceedings of CIB-W18 meeting*, 2011.

[24] E. ASTM. 2126-09. standard test methods for cyclic (reversed) load test for shear resistance of vertical elements of the lateral load resisting systems for buildings. *ASTM Int*, 2009.

[25] J. Hummel. *Displacement-based seismic design for multi-storey cross laminated timber buildings*, volume 8. kassel university press GmbH, 2017.

[26] N. Gattesco and I. Boem. Stress distribution among sheathing-to-frame nails of timber shear walls related to different base connections: Experimental tests and numerical modelling. *Construction and Building Materials*, 122:149–162, 2016.

[27] J. Vivenzio. *Istoria e teoria de'tremuoti in generale ed in particolare di quelli della Calabria, e di Messina del 1783*. Stamperia regale, 1783.

[28] N. Ruggieri. Il sistema antisismico borbonico, muratura con intelaiatura lignea, genesi e sviluppo in calabria alla fine del '700. *Bollettino degli Ingegneri*, 10:3–14, 2013.

[29] R. Tomasi. Costruire in sicurezza in zona sismica. il contributo del legno, ricerca e normativa. *promolegno*, 2012.

[30] Italian Building Code. Dm 14.01. 2008: Norme tecniche per le costruzioni. *Italian Ministry of Infrastructures and Transportation, Rome, Italy*, 2008.

[31] EN 338. Structural timber strength classes, 2016.

[32] EN 14081. Timber structures - strength graded structural timber with rectangular cross section, 2009.

[33] EN 14080. Timber structures - glued laminated timber and glued solid timber, 2009.

[34] J. Porteous and A. Kermani. *Structural timber design to Eurocode 5*. John Wiley & Sons, 2013.

[35] J.P. Wacker. Use of wood in buildings and bridges. 2010.

[36] M. Metha, W. Scarbororough, and D. Armpriest. *Building Construction–Principles, Materials and Systems, building code and sustainability update*. Prentice-Hall, Englewood Cliffs, NJ., 2009.

[37] D. Casagrande, S. Rossi, T. Sartori, and R. Tomasi. Proposal of an analytical procedure and a simplified numerical model for elastic response of single-storey timber shear-walls. *Construction and Building Materials*, 102:1101–1112, 2016.

[38] S. Varela, J. Correal, L. Yamin, and F. Ramirez. Cyclic performance of glued laminated guadua bamboo-sheathed shear walls. *Journal of structural engineering*, 139(11):2028–2037, 2012.

[39] J. Kolb. *Systems in timber engineering: loadbearing structures and component layers*. Walter de Gruyter, 2008.

[40] B/525/5. Structural use of timber. code of practice for permissible stress design, materials and workmanship, 1984.

[41] Thomasnet.com. *www.thomasnet.com/articles/hardware/screw-nail-sizes*. 2017.

[42] R. Tomasi and T. Sartori. Mechanical behaviour of connections between wood framed shear walls and foundations under monotonic and cyclic load. *Construction and Building Materials*, 44:682–690, 2013.

[43] G.C. Foliente. Hysteresis modeling of wood joints and structural systems. *Journal of Structural Engineering*, 121(6):1013–1022, 1995.

[44] J. Ehlbeck. *Nailed joints in wood structures*, volume 166. Virginia Polytechnic Institute and State University, Wood Research and Wood Construction Laboratory, 1979.

[45] W. Stewart. The seismic design of plywood sheathed shear walls. 1987.

[46] J.D. Dolan. *The dynamic response of timber shear walls*. PhD thesis, University of British Columbia, 1989.

[47] Y.K. Wen. Equivalent linearization for hysteretic systems under random excitation. *Journal of Applied Mechanics*, 47(1):150–154, 1980.

[48] T.T. Baber and Y. Wen. Random vibration hysteretic, degrading systems. *Journal of the Engineering Mechanics Division*, 107(6): 1069–1087, 1981.

[49] T.T. Baber and M.N. Noori. Modeling general hysteresis behavior and random vibration application. *Journal of Vibration, Acoustics, Stress, and Reliability in Design*, 108(4):411–420, 1986.

[50] A. Ceccotti and A. Vignoli. Engineered timber structures: An evaluation of their seismic behaviour. In *Proceedings, 1990 International Timber Engineering Conference, Tokyo, Japan*, pages 946–953, 1990.

[51] B.T. Kivell, P.J. Moss, and A.J. Carr. Hysteretic modelling of moment-resisting nailed timber joints. *Earthquake Engineering*, 14(4), 1981.

[52] C. Lee. A composite-beam finite element for seismic analysis of wood-framed buildings. 1987.

[53] A. Polensek and H.I. Laursen. *Seismic Behavior of Bending Components and Intercomponent Connections of Light Frame Wood Buildings*. Oregon State University, 1984.

[54] C. Chou. Modeling of nonlinear stiffness and nonviscous damping in nailed joints between wood and plywood. 1987.

[55] L. Sakamoto and Y. Ohashi. Seismic response and required lateral strength of wooden houses and its applications. In *Proc., Int. Conf. of Timber Engineering*, volume 2, pages 243–247, 1988.

[56] F. Kamiya. Nonlinear earthquake response analysis of sheathed wood walls by a computer-actuator on-line system. In *Proc., Int. Timber Engineering Conf*, pages 838–837, 1988.

[57] K. Miyazawa. Study on nonlinear static and dynamic structural analysis of wooden wall-frame buildings subjected to horizontal force. In *Proc., 13th Symp. on Computer Technol. of Information, Systems and Applications*, 1990.

[58] K.W. Johansen. Theory of timber connections. *Int Assoc Bridge and Struct Eng*, 9:249–262, 1949.

[59] R.L. Hankinson. Investigation of crushing strength of spruce at varying angles of grain. *Air service information circular*, 3(259): 130, 1921.

[60] M.P. Lauriola. Dispense per gli studenti del corso 'costruzioni in legno' di ingegneria edile e civile (unifi). 2014.

[61] R.O. Foschi. Load-slip characteristics of nails. *Wood Sci*, 7(1): 69–76, 1974.

[62] M. Patton-Mallory and W.J. McCutcheon. Predicting racking performance of walls sheathed on both sides. *Forest products journal*, 37(9):27–32, 1987.

[63] INGV. *http://zonesismiche.mi.ingv.it/*.

[64] M.J.N. Priestley and D.N. Grant. Viscous damping in seismic design and analysis. *Journal of earthquake engineering*, 9(spec02): 229–255, 2005.

[65] A. Shibata and M.A. Sozen. Substitute-structure method for seismic design in r/c. *Journal of the structural division*, 102(ASCE# 11824), 1976.

[66] C.A. Blandon and M.J.N. Priestley. Equivalent viscous damping equations for direct displacement based design. *Journal of earthquake Engineering*, 9(sup2):257–278, 2005.

[67] L.S. Jacobsen. Steady forced vibrations as influenced by damping. *Transactions*, 52(15):169–181, 1930.

[68] G.W. Housner. Limit design of structures to resist earthquakes. In *Proc. of 1st WCEE*, pages 5–1, 1956.

[69] E. Rosenblueth and I. Herrera. On a kind of hysteretic damping. *Journal of the Engineering Mechanics Division*, 90(4):37–48, 1964.

[70] W.D. Iwan. Estimating inelastic response spectra from elastic spectra. *Earthquake Engineering & Structural Dynamics*, 8(4):375–388, 1980.

[71] EN DIN. 12512 (2002) timber structures test methods - cyclic testing of joints made with mechanical fasteners. german version en 12512: 2001.

[72] A. ATC. 40, seismic evaluation and retrofit of concrete buildings. *Applied Technology Council, report ATC-40. Redwood City*, 1996.

[73] Federal Emergency Management Agency. Improvement of nonlinear static seismic analysis procedures. *FEMA 440, prepared by Applied Technology Council (ATC-55 Project)*, 2005.

[74] S.A. Freeman. Prediction of response of concrete buildings to severe earthquake motion. *Special Publication*, 55:589–606, 1978.

[75] S.A. Freeman. The capacity spectrum method. In *Proceedings of the 11th European conference on earthquake engineering, Paris*, 1998.

[76] P. Fajfar. Capacity spectrum method based on inelastic demand spectra. *Earthquake Engineering & Structural Dynamics*, 28(9):979–993, 1999.

[77] W. Muñoz, M. Mohammad, A. Salenikovich, and P. Quenneville. Need for a harmonized approach for calculations of ductility of timber assemblies. In *Proceedings of the Meeting*, volume 41, 2008.

[78] R.O. Foschi. Load-slip characteristics for connections with common nails. *Wood Sci*, 9:118–123, 1977.

[79] G.C. Foliente. Issues in seismic performance testing and evaluation of timber structural systems. 1996.

[80] T. Paulay and M.J.N. Priestley. Seismic design of reinforced concrete and masonry buildings. 1992.

[81] J. Peterson. Bibliography on lumber and wood panel diaphragms. *Journal of Structural Engineering*, 109(12):2838–2852, 1983.

[82] B. Källsner and U.A. Girhammar. Analysis of fully anchored light-frame timber shear walls-elastic model. *Materials and Structures*, 42(3):301–320, 2009.

[83] T. Sartori and R. Tomasi. Experimental investigation on sheathing-to-framing connections in wood shear walls. *Engineering Structures*, 56:2197–2205, 2013.

[84] J. Humbert, C. Boudaud, J. Baroth, S. Hameury, and L. Daudeville. Joints and wood shear walls modelling I: Constitutive law, experimental tests and fe model under quasi-static loading. *Engineering Structures*, 65:52–61, 2014.

[85] F. Germano, G. Metelli, and E. Giuriani. Experimental results on the role of sheathing-to-frame and base connections of a european timber framed shear wall. *Construction and Building Materials*, 80:315–328, 2015.

[86] I. Gavric, M. Fragiacomo, and A. Ceccotti. Cyclic behaviour of typical metal connectors for cross-laminated (clt) structures. *Materials and structures*, 48(6):1841–1857, 2015.

[87] B. Folz and A. Filiatrault. Cyclic analysis of wood shear walls. *Journal of Structural Engineering*, 127(4):433–441, 2001.

[88] B. Källsner. Panels as wind-bracing elements in timber-framed walls. *Wood Technology Report*, 56, 1984.

[89] S. Åkerlund. A simple calculation model for sheathed wood-framed shear walls. *Bygg Teknik*, 1:45–48, 1984.

[90] Ö. Anil, A. Togay, Ü.K. Işleyen, N. Döngel, and C. Söğütlü. Effect of timber type and nail spacing on the hysteretic behavior of timber-framed shear walls with openings. *International Journal of Civil Engineering*, 16(6):629–646, 2018.

[91] American Forest and Paper Association (AF&PA). Special design provisions for wind and seismic with commentary, 2005.

[92] H. Sugiyama. The evaluation of shear strength of plywood-sheathed walls with openings. *Mokuzai Kogyo (Wood Industry)*, 36(7):3–8, 1981.

[93] M. Yasumura and H. Sugiyama. Shear properties of plywood-sheathed wall panels with opening. *Transactions of the Architectural Institute of Japan*, 338:88–98, 1984.

[94] M. Li, F. Lam, B. Yeh, T. Skaggs, D. Rammer, and J. Wacker. Modeling force transfer around openings in wood-frame shear walls. *Journal of Structural Engineering*, 138(12):1419–1426, 2012.

[95] K. Vogrinec, M. Premrov, and E.K. Šilih. Simplified modelling of timber-framed walls under lateral loads. *Engineering Structures*, 111:275–284, 2016.

[96] E.K. Šilih and M. Premrov. Analysis of timber-framed wall elements with openings. *Construction and Building Materials*, 24(9): 1656–1663, 2010.

[97] E.K. Šilih and M. Premrov. Influence of openings on horizontal load-carrying capacity of timber-frame wall elements with fibre-plaster sheathing boards. *Advances in Engineering Software*, 43(1): 19–26, 2012.

[98] E.K. Šilih, M. Premrov, and S. Šilih. Numerical analysis of timber-framed wall elements coated with single fibre-plaster boards. *Engineering Structures*, 41:118–125, 2012.

[99] Canadian Standard Association (CSA). Engineering design in wood, 2005.

[100] G. Doudak, I. Smith, G. McClure, M. Mohammad, and P. Lepper. Tests and finite element models of wood light-frame shear walls with openings. *Progress in Structural Engineering and Materials*, 8 (4):165–174, 2006.

[101] M. Yasumura. Racking resistance of panel-sheathed shear walls with openings. In *World Conference on Timber Engineering, WCTE, Riva del Garda, Trentino, Italy*, 2010.

[102] G. Rinaldin, G.H. Poh'Sie, C. Amadio, and M. Fragiacomo. Modelling the seismic behaviour of light-frame timber structures. *Ingegneria Sismica, International Journal of Earthquake Engineering*, 4: 82–98, 2013.

[103] E.N. Dvorkin and K. Bathe. A continuum mechanics based four-node shell element for general non-linear analysis. *Engineering computations*, 1(1):77–88, 1984.

[104] S. Ahmad, B.M. Irons, and O.C. Zienkiewicz. Analysis of thick and thin shell structures by curved finite elements. *International Journal for Numerical Methods in Engineering*, 2(3):419–451, 1970.

[105] R.L. Taylor and O.C. Zienkiewicz. *The finite element method*. McGraw-Hill, 1989.

[106] E. Reissner. The effect of transverse shear deformation on the bending of elastic plates. *J. appl. Mech.*, pages A69–A77, 1945.

[107] R.D. Mindlin. Influence of rotatory inertia and shear on flexural motions of isotropic, elastic plates. *J. appl. Mech.*, 18:31–38, 1951.

[108] K. Bathe and S. Bolourchi. A geometric and material nonlinear plate and shell element. *Computers & structures*, 11(1-2):23–48, 1980.

[109] K.J. Bathe. *Finite element procedures in engineering analysis*. Prentice-Hall, 1982.

[110] E.N. Dvorkin. Nonlinear analysis of shells using the mitc formulation. *Archives of Computational Methods in Engineering*, 2(2): 1, 1995.

[111] J.P. Judd and F.S. Fonseca. Analytical model for sheathing-to-framing connections in wood shear walls and diaphragms. *Journal of Structural Engineering*, 131(2):345–352, 2005.

[112] C.G. Koh, Y.F. Chen, and C. Liaw. A hybrid computational strategy for identification of structural parameters. *Computers & Structures*, 81(2):107–117, 2003.

[113] G. Monti, G. Quaranta, and G.C. Marano. Genetic-algorithm-based strategies for dynamic identification of nonlinear systems with noise-corrupted response. *Journal of Computing in Civil Engineering*, 24(2):173–187, 2009.

[114] G.C. Marano, G. Quaranta, and G. Monti. Genetic algorithms in mechanical systems identification: state-of-the-art review. *Soft computing in civil and structural engineering*, 2009.

[115] G. Quaranta, G. Monti, and G.C. Marano. Parameters identification of van der pol–duffing oscillators via particle swarm optimization and differential evolution. *Mechanical Systems and Signal Processing*, 24(7):2076–2095, 2010.

[116] F. Ma, C.H. Ng, and N. Ajavakom. On system identification and response prediction of degrading structures. *Structural Control and Health Monitoring: The Official Journal of the International Association for Structural Control and Monitoring and of the European Association for the Control of Structures*, 13(1):347–364, 2006.

[117] A. Togay, Ö. Anil, Ü. Karagöz Işleyen, İ. Ediz, and C. Durucan. Finite-element analyses of light timber-framed walls with and without openings. *Proceedings of the Institution of Civil Engineers-Structures and Buildings*, 170(8):555–569, 2017.

[118] Candeloro F. Petracca, M. and G. Camata. Stko user manual, 2017.

[119] D. Casagrande, S. Rossi, T. Sartori, and R. Tomasi. Analytical and numerical analysis of timber framed shear walls. In *Proceedings of World Conference on Timber Engineering, Auckland, New Zealand*, pages 497–503, 2012.

[120] A. Filiatrault, H. Isoda, and B. Folz. Hysteretic damping of wood framed buildings. *Engineering Structures*, 25(4):461–471, 2003.

[121] V. Pareto. Manuale di economica politica, societa editrice libraria. *Manual of political economy*, 1971, 1906.

[122] N. Richard, L. Daudeville, and F. Prion, H.and Lam. Timber shear walls with large openings: experimental and numerical prediction of the structural behaviour. *Canadian Journal of Civil Engineering*, 29(5):713–724, 2002.

[123] N.N. Carlson and K. Miller. Design and application of a gradient-weighted moving finite element code i: in one dimension. *SIAM Journal on Scientific Computing*, 19(3):728–765, 1998.

[124] M.H. Scott and G.L. Fenves. A krylov subspace accelerated newton algorithm. In *Proc., 2003 ASCE Structures Congress*, 2003.

[125] W. Mmari. Modeling of nailed timber connection: Displacement path dependency in sheathing-to-framing connections, 2017.

[126] Z. Li, Y. Xiao, R. Wang, and G. Monti. Studies of nail connectors used in wood frame shear walls with ply-bamboo sheathing panels. *Journal of Materials in Civil Engineering*, 27(7):04014216, 2014.

[127] ASTM International D1761. Standard test methods for mechanical fasteners in wood., 2006.

[128] H. Krawinkler, F. Parisi, L. Ibarra, A. Ayoub, and R. Medina. Development of a testing protocol for wood frame structures, curee publication. *W-02, California*, 2000.

List of Figures

List of Tables